

**ANALYSIS OF SHOULDER AND KNEE JOINT
MUSCLES USING DEVELOPED CPM MACHINE
AND FINITE ELEMENT METHOD**

Thesis

Submitted in partial fulfillment of the requirements for the degree of

DOCTOR OF PHILOSOPHY

by

METAN SHRINIWAS SIDRAMAPPA



DEPARTMENT OF MECHANICAL ENGINEERING,
NATIONAL INSTITUTE OF TECHNOLOGY KARNATAKA,
SURATHKAL, MANGALORE – 575025

APRIL, 2016

**ANALYSIS OF SHOULDER AND KNEE JOINT
MUSCLES USING DEVELOPED CPM MACHINE
AND FINITE ELEMENT METHOD**

Thesis

Submitted in partial fulfillment of the requirements for the degree of

DOCTOR OF PHILOSOPHY

by

METAN SHRINIWAS SIDRAMAPPA



DEPARTMENT OF MECHANICAL ENGINEERING,
NATIONAL INSTITUTE OF TECHNOLOGY KARNATAKA,
SURATHKAL, MANGALORE – 575025

APRIL, 2016

DECLARATION

I hereby *declare* that the Research Thesis entitled “**Analysis of Shoulder and Knee Joint Muscles using Developed CPM Machine and Finite Element Method**”, which is being submitted to the **National Institute of Technology Karnataka, Surathkal** in partial fulfilment of the requirements for the award of the Degree of **Doctor of Philosophy in Mechanical Engineering**, is a *bonafide report of the research work* carried out by me. The material contained in this Research Thesis has not been submitted to any University or Institution for the award of any degree.

Register Number: **100535ME10P03**

Name of the Research Scholar: **Metan Shriniwas Sidramappa**

Signature of the Research Scholar:

Department of Mechanical Engineering

Place: NITK-Surathkal

Date:

CERTIFICATE

This is to *certify* that the Research Thesis entitled “**Analysis of Shoulder and Knee Joint Muscles using Developed CPM Machine and Finite Element Method**”, submitted by **Mr. Metan Shriniwas Sidramappa** (Register Number: 100535ME10P03) as the record of the research work carried out by him, is *accepted as the Research Thesis submission* in partial fulfilment of the requirements for the award of degree of **Doctor of Philosophy**.

Prof. G.C. Mohankumar

Research Guide

Date:

Prof. Prasad Krishna

Research Guide

Date:

Prof. K. V. Gangadharan

Chairman – DRPC and

Head of the Department

Date:

DEDICATED
TO
MY RESPECTED
PARENTS
AND
TEACHERS

ACKNOWLEDGEMENT

This thesis embodied the results of the last five years' work whereby I have been accompanied and supported by many people. It is an honour and pleasant opportunity to be able to express my gratitude to all of them.

I express my sincere thanks and heartfelt gratitude towards my research supervisors Prof. G.C. Mohankumar and Prof. Prasad Krishna, former Head of the Department of Mechanical Engineering, as both of them are my source of inspiration. First and foremost, I would like to thank Prof. G.C. Mohan Kumar for being my guide and advisor for my research work. Dr. G. C. Mohankumar was a friend, mentor, philosopher and scientist par excellence who gave me valuable insights during the research work. Not only has he been a wonderful mentor in the areas of Finite Element Analysis, musculoskeletal modelling such as shoulder and knee joint and research, but also a great mentor about life in general. It has been an honour and a pleasure to work with you sir. I would like to thank Prof. Prasad Krishna for his invaluable suggestions and constant encouragement throughout my research work which will be etched in my memory forever. His knowledge both in theoretical and practical aspects of Finite Element Analysis and Manufacturing has helped me in my research work and also helped me to learn lot of new things. He is also a great mentor about life in general from whom I learned patience and professionalism. Thank you so much Prof. G. C. Mohankumar and Prof. Prasad Krishna for the time you have invested in me.

I am thankful to Prof. K. V. Gangadharan, Professor and Head, Department of Mechanical Engineering for his wholehearted support and encouragement. I am also grateful to all faculty members of the Department of Mechanical Engineering, NITK, Surathkal for their precious teaching, suggestions, constant encouragement, incubating the learning environment, and family atmosphere.

I am thankful to the members of Research Progress Assessment Committee, Prof. Gopal Mugeraya, Department of Chemical Engineering, Prof. Prakash Raghvendra, Department of Computer Science and Engineering, Prof. T. Laxminidhi, Department

of Electronics and Communication Engineering and Dr. M. R. Doddamani, Department of Mechanical Engineering for their patient hearing to my seminars and for their suggestions, evaluation and constant encouragement.

I express my deep sense of gratitude and heartfelt thanks to the Management, Secretary Mr N.M.Patil, Dr. M.G.Devmane, Director and Principal of Nagesh Karajagi Orchid College of Engineering and Technology Solapur.

I am thankful to Dr.Vyanktesh S Metan for extending his valuable guidance in the shoulder and knee anatomy, muscle behaviour study and allowing the present work to be carried in Dr. Metan Hospital Orthopedic & Neurology Center, India. I am also thankful to Dr. Manisha Talpallikar for extending her valuable guidance in the shoulder and knee physiotherapy, Surface Electromyography study of the muscles and allowing the present work to be carried in Dr. Talpallikar Physiotherapy Center, India.

My special thanks to my friends Dr. Vinayak Patki, Mrs Vrushali Mulay, Mr.Swapnil Panke and Mr.Satish Lakade for helping me in editing the final report, constant support and encouragement. I also thankful to Mr.Samadhan Patil, Mr.Santosh Patil and Mr. Siddheshwar Sakkargi for their valuable contribution during the CPM machine experimentation.

Most importantly I would like to thank my family members especially my parents Mr. Sidramappa and Mrs. Laxmibai ; wife Mrs. Sonal and two sons Aditya and Aryan; brother and sisters who always supported and encouraged me in this endeavour and their support kept me going through hard times and gave me confidence, courage and inspiration.

NITK, Surathkal

(Mr. Shrinivas S Metan)

Date:

ABSTRACT

Shoulder and knee joints pain, injury and discomfort are public health and economic issues world-wide. As per the Indian orthopedic association survey, there are about 50% of the patient visits to doctors' offices because of common shoulder and knee injuries such as fractures, dislocations, sprains, and ligament tears. Shoulder and knee are the most complex, maximum used and critical joints in the human body. The shoulder and knee joint muscle behaviour during different exercises is one of the major concerns to the orthopedic surgeon for analysing the exact healing and duration of the injury. Quantification of mechanical stresses and strains in the human joints and the musco-skeletal system is still a big concern for the researchers. The injury mechanisms and analysis of the post-operative progress is one of the most critical studies for orthopedic surgeons, biomechanical engineers and researchers.

In the present work a classical 3D Finite Element Method (FEM) modelling technique has been used to investigate the stresses induced in the shoulder joint muscles during abduction arm movement and knee joint muscles during flexion leg movement for different range of motion. 3D model provides valuable information for analysing complex bio-mechanical systems and characterization of the joint mechanics. Reverse modelling method was used for generating fast, accurate and detailed contours of the shoulder and knee model. Scanning of the complicated shoulder and knee joint bones were made by 3D scanner (ATOS III) to generate '.stl' file. Accurate and detailed 3D bone geometry of the shoulder and knee joint models was done using CATIA V5 software from the scanned '.stl' file. The higher order geometrical features (curve and surfaces) were designed by filtering and aligning number of cloud points, tessellation of polygonal model, recognition and defining the referential geometrical entities. According to quadratic dependency, a non-homogeneous bone constitutive law was implemented. Different muscles were then added on the shoulder and knee joint models in CATIA V5. 3D models were then imported in '.igs' format into ANSYS workbench for the stress analysis.

A 3D FEM model was developed for the five important shoulder joint muscles, namely deltoid, supraspinatus, subscapularies, teres minor and infraspinatus. The

kinematics for shoulder abduction arm movement was prescribed as an input to finite element simulations and the Von Mises stresses and equivalent elastic strain in the shoulder muscles were plotted. Individual and group muscle analysis was done to evaluate the Von Mises stresses and equivalent elastic strain of the shoulder muscles during the abduction arm movement. During the individual muscle analysis, the Von Mises stresses induced in deltoid muscle was maximum (4.2175 MPa) and in group muscle analysis it was (2.4127MPa) compared to other individual four rotor cuff muscles. During the individual muscle analysis, the equivalent elastic strain induced in deltoid muscle was maximum (3.5146 mm/mm) and in group muscle analysis it was (2.0106 mm/mm) compared to other individual four rotor cuff muscles. The percentage analysis of individual muscles contribution for abduction arm movement predicted by FEM analysis was maximum (46.85%) in the deltoid muscle. The results showed that deltoid muscle was the most stressed muscle in both individual and group muscle analysis.

The Surface Electromyography (SEMG) test was conducted on the shoulder prone subjects using the developed low cost shoulder Continuous Passive Motion (CPM) machine. The percentage analysis of individual muscles contribution for abduction arm movement predicted by SEMG analysis was maximum (48.15%; 46.15% and 47.05%) in the deltoid muscle. Deltoid was the most contracted (stressed) muscle observed during the SEMG analysis amongst the five shoulder muscles. The results showed by both FEM and SEMG methods that deltoid muscle was the most sensitive amongst the five shoulder joint muscles during abduction arm movement.

FEM analysis was done to investigate the Von Mises stresses in two important knee joint muscles such as the rectus femoris and biceps femoris muscle during the flexion leg movement. During the muscle analysis, the Von Mises stresses induced in rectus femoris muscle was the maximum (1.5579 MPa). The results showed that rectus femoris muscle was the most stressed muscle than the biceps femoris muscle during flexion leg movement.

The SEMG test was conducted on the knee prone subjects using the developed low cost knee CPM machine. The average percentage contraction (stress distribution) exhibited by SEMG analysis on the rectus femoris muscle was 70% of the total

muscles contraction. The results by both FEM and SEMG methods showed that rectus femoris was the most stressed muscle during the flexion leg movement.

The present work provides in depth information to the researchers and orthopedicians for the better understanding of the shoulder and knee joint mechanism in human anatomy. It predicts the most stressed muscle in the shoulder joint during the abduction arm movement and in the knee joint during the flexion leg movement at different range of motion.

Key words:

FEM model, Deltoid, Supraspinatus, Abduction, Rectus Femoris, Flexion, Sensitivity Analysis, Surface Electromyography, Von Mises Stresses, Equivalent Elastic Strain.

CONTENTS

	TITLE	Page No.
	ACKNOWLEDGEMENT	
	ABSTRACT	
	CONTENTS	i-v
	LIST OF FIGURES	vi-x
	LIST OF TABLES	xi-xii
	NOMENCLATURE	xiii
	ABBREVIATIONS	xiv
CHAPTER 1	INTRODUCTION	1-13
1.1	PREAMBLE	1
1.2	SHOULDER JOINT ANATOMY	2
1.2.1	Shoulder Joint Muscles	5
1.3	KNEE JOINT ANATOMY	6
1.3.1	Knee Joint Muscles	8
1.4	ELECTROMYOGRAPHY	9
1.5	CONTINUOUS PASSIVE MOTION (CPM) MACHINE	10
1.6	ORGANISATION OF THESIS	12
CHAPTER 2	LITERATURE REVIEW	14-28
2.1	PREAMBLE	14
2.2	HUMAN JOINTS AND MUSCLE ANALYSIS BY 3D FEM MODEL	14
2.3	SHOULDER AND KNEE CPM	21
2.4	MUSCLE ANALYSIS BY SEMG	23

2.5	RESEARCH GAPS	25
2.6	AIMS AND OBJECTIVES	26
2.7	SCOPE OF WORK	27
CHAPTER 3	METHODS AND MATERIALS	29-77
3.1	METHODOLOGY OF THE PRESENT WORK	29
3.2	3D MODELLING OF SHOULDER BONES	32
3.2.1	3D Scanning of Shoulder Bones	32
3.2.2	3D CAD Modelling of Shoulder Bones	35
3.2.3	Assembly and Simulation of Shoulder Joints	37
3.2.4	Contact Constraints	38
3.2.5	Addition of Muscles on Shoulder Joint	39
3.3	FEM ANALYSIS OF SHOULDER JOINT	40
3.3.1	Material Properties	42
3.3.2	Loading Conditions	42
3.3.3	Meshing of the 3D model	44
3.4	3D MODELLING OF KNEE BONES	46
3.4.1	3D Scanning of Knee Bones	46
3.4.2	3D CAD Modelling of Knee Bones	47
3.4.3	Assembly and Simulation of Knee Joints	48
3.4.4	Addition of Muscles on Knee Joint	49
3.5	FEM ANALYSIS OF KNEE JOINT	50
3.5.1	Material Properties	51
3.5.2	Loading Conditions	52
3.5.3	Meshing of 3D Model	53
3.6	CPM MACHINE FOR SHOULDER AND KNEE JOINT	54
3.6.1	Shoulder CPM Machine	54

3.6.1.1	Motor Design (M ₁)	56
3.6.1.2	Electronics Design	59
3.6.1.3	Fabrication of CPM Machine	60
3.6.1.4	Testing on the CPM Machine	64
3.6.2	Knee CPM Machine	66
3.6.2.1	Motor Design	68
3.6.2.2	Electronics Design	70
3.6.2.3	Fabrication of CPM Machine	70
3.6.2.4	Testing on the CPM Machine	71
3.7	MUSCLE TESTING BY USING SEMG ON CPM MACHINE	73
3.7.1	SEMG Test on Shoulder CPM Machine	73
3.7.2	SEMG Test on Knee CPM Machine	76
CHAPTER 4	RESULTS AND DISCUSSIONS: ANALYSIS OF SHOULDER JOINT MUSCLES	78-103
4.1	FEM ANALYSIS	78
4.1.1	Analysis of Deltoid Muscle	78
4.1.2	Analysis of Supraspinatus Muscle	80
4.1.3	Analysis of Subscapularies Muscle	81
4.1.4	Analysis of Infraspinatus Muscle	84
4.1.5	Analysis of Teres Minor Muscles	84
4.1.6	Group Muscle Analysis of Shoulder Joint	85
4.2	CPM MACHINE TEST	90
4.3	MUSCLE ANALYSIS BY SEMG	92
4.4	DISCUSSIONS	95
4.4.1	Comparison of FEM Analysis Results with SEMG Analysis	97

4.4.2	Comparison of FEM Analysis Results with Previous Work	100
4.4.3	Remarks of Orthopedic Surgeons	102
CHAPTER 5	RESULTS AND DISCUSSIONS: ANALYSIS OF KNEE JOINT	104 -116
5.1	FEM ANALYSIS	104
5.1.1	Analysis of Rectus Femoris and Biceps Femoris Muscles	104
5.2	CPM MACHINE TEST	106
5.3	MUSCLE ANALYSIS BY SEMG	108
5.4	DISCUSSIONS	111
5.4.1	Comparison of FEM Analysis Results with SEMG Analysis	112
5.4.2	Comparison of FEM Analysis Results with Previous Work	114
5.4.3	Orthopedic Surgeons Remarks	116
CHAPTER 6	CONCLUDING REMARKS AND SCOPE FOR FUTURE WORK	117 -120
6.1	CONCLUDING REMARKS	117
6.2	MAJOR RESEARCH OUTCOMES	119
6.3	SCOPE FOR FUTURE WORK	120
REFERENCES		121-131
APPENDIX I	Specification of ATOS III 3D Scanner Used for Scanning the Shoulder and Knee Bones	132
APPENDIX II	Cost Sheet for the Shoulder CPM Machine Fabrication	133

APPENDIX III	Shoulder Pain and Disability Index (SPADI)	134
APPENDIX IV	Cost Sheet for the Knee CPM Machine Fabrication	135
APPENDIX V	Knee Pain and Disability Index (KPADI)	136
APPENDIX VI	Shoulder CPM Report	137
APPENDIX VII	SEMG Report of Shoulder Muscles	138-142
APPENDIX VIII	MATLAB Program by Using a Biomedical Model to Quantify Shoulder Load by Dul	143-145
APPENDIX IX	Knee CPM report	146
APPENDIX X	SEMG Report of Knee Muscles	147-148
APPENDIX XI	Shoulder CPM Machine Certification	149
APPENDIX XII	Knee CPM Machine Certification	150
	LIST OF PUBLICATIONS	151
	CURRICULUM VITAE	152

LIST OF FIGURES

Figure No	Title	Page No
1.1	Shoulder Joint Anatomy	3
1.2	Humerus Bone	3
1.3	Clavicle Bone	4
1.4	Scapula Bone	4
1.5	Shoulder Joint Muscles	5
1.6	Femur Bone	6
1.7	Tibia and Fibula Bone	7
1.8	Patella	8
1.9	Knee Joint Muscles	8
1.10	SEMG Machine Setup	10
1.11	Knee CPM ^{lite} Machine	11
3.1	Methodology Used for 3D FEM Analysis of Shoulder Joint Muscles	30
3.2	Methodology Used for FEM Analysis of Knee Joint Muscles	31
3.3	Methodology Used for SEMG Analysis of Shoulder and Knee joint Muscles	31
3.4	Scanning of Shoulder Joint Bones by ATOS III Scanner	34
3.5	3D Scanning Procedure to Generate Scapula Bone	34
3.6	3D Scanning Procedure to Generate Humerus Bone	34
3.7	3D Scanning Procedure to Generate Clavicle Bone	35
3.8	Points and Spline Curves on the Humerus Bone	35
3.9	Points and Spline Curves on the Scapula	36

Figure No	Title	Page No
3.10	Refinement of the Shoulder Bones in CATIA V5	36
3.11	Shoulder Joint Bone Assembly in CATIA V5	37
3.12	Shoulder Joint Planes of Motion	38
3.13	Defining Contact Constraints between Humerus, Clavicle and Scapula	38
3.14	Origin and Insertion Regions of the Shoulder Joint Muscles	40
3.15	Shoulder Adduction and Abduction Arm Movement	42
3.16	Shoulder Model Efficacy for its Position, Orientation, Rotational Movements and Direction of Pull during Abduction Arm Movement	43
3.17	Shoulder Joint Abduction Arm Simulation for 0° to 130° ROM	43
3.18	Shoulder Joint Meshed Model with all Five Muscles	45
3.19	3D Scanning of the Tibia by using ATOS III Scanner	46
3.20	Refinement of the Knee Joint Bones in CATIA V5	47
3.21	Knee Joint Assembly in CATIA	48
3.22	Front View of the Knee Joint with Rectus Femoris and Biceps Femoris	49
3.23	Side View of the Knee Joint with Rectus Femoris and Biceps Femoris	49
3.24	Knee Flexion and Elevation Leg Movement	52
3.25	Knee Joint Flexion Simulation in ANSYS for 0° to 60° ROM	52
3.26	Knee Joint Meshed Model with Rectus and Biceps Femoris Muscles	53
3.27	Open Kinetic Chain for Shoulder CPM Machine	55
3.28	CATIA Model of the Shoulder Arm with Motor M ₁ and M ₂	56
3.29	Schematic Representation of Shoulder Arm of the CPM Machine	56

Figure No	Title	Page No
3.30	Loading Diagram for Motor M_1	57
3.31	Loading Diagram for Torque Measurement	57
3.32	Power Supply Block Diagram and Motor Control Circuit	59
3.33	Rear View of Stepper Motor and PLC Control Unit	59
3.34	Hybrid NEMA make High Torque Motors M_1 and M_2	60
3.35	Block Diagram of Shoulder CPM Machine	61
3.36	Low Cost Shoulder CPM Machine	62
3.37	Shoulder CPM Fabrication from Raw stage to the Finished Product	63
3.38	Shoulder Joint Exercise on Developed CPM Machine	65
3.39	Closed Kinetic Chain Mechanism for the Knee CPM Machine	67
3.40	Control Circuit for Knee CPM Machine	70
3.41	Power Supply Circuit for Knee CPM Machine	70
3.42	Block Diagram of Developed Knee CPM Machine	71
3.43	Low Cost Knee CPM Machine	71
3.44	Set up for Shoulder Muscles Test by SEMG	74
3.45	SEMG Electrode Positions for the Shoulder Joint Muscle Analysis	75
3.46	Set up for Knee Muscles Test by SEMG on CPM Machine	76
3.47	SEMG Electrode Positions for the Knee Joint Muscle Analysis	77
4.1	Maximum Von Mises Stresses in Deltoid Muscle	79
4.2	Maximum Equivalent Elastic Strain in Deltoid Muscle	80
4.3	Maximum Von Mises Stresses in Supraspinatus Muscle	80
4.4	Maximum Von Mises Stresses in Subscapularies Muscle	81
4.5	Maximum Von Mises Stresses in Infraspinatus Muscle	83

Figure No	Title	Page No
4.6	Maximum Von Mises Stresses in Teres Minor Muscle	84
4.7	Equivalent Elastic Strain in Deltoid Muscle during the Group Muscle Analysis	85
4.8	Von Mises stresses in Supraspinatus Muscle during the Group Muscle Analysis	86
4.9	Von Mises Stresses Distribution in the Shoulder Joint Muscles during Individual Muscle Analysis for Abduction Arm Movement	87
4.10	Von Mises Stresses Distribution in the Shoulder Joint Muscles during Group Muscle Analysis for Abduction Arm Movement	88
4.11	Von Mises Stresses Distribution of Deltoid Muscle	88
4.12	Von Mises Stresses Distribution of Supraspinatus Muscle	89
4.13	Equivalent Elastic Strain Distribution in the Shoulder Joint Muscles	89
4.14	Percentage Improvement in the Shoulder ROM on Weekly Basis	91
4.15	Motor Unit Firing Against ROM in Shoulder Muscles	93
4.16	Motor Unit Firing against ROM in Deltoid Muscle during Abduction Arm Movement	94
4.17	Motor Unit Firing against ROM in Supraspinatus Muscle during Abduction Arm Movement	94
4.18	Von Mises Stresses Distribution in the Rotor cuff Muscles and Deltoid during Individual Muscle Analysis	96
4.19	Stress Distribution in the Rotor cuff Muscles and Deltoid during Group Muscle Analysis	97

Figure No	Title	Page No
4.20	Percentage Variation in the Muscle Contractions of Rotor cuff and Deltoid Muscles during Abduction Arm Movement by SEMG at 75°	98
4.21	Percentage Variation in the Muscle Contraction of Rotor cuff and Deltoid Muscles during Abduction Arm Movement by SEMG at 80°	98
4.22	Percentage Variation in the Muscle Contraction of Rotor cuff Muscles and Deltoid Muscle during Abduction Arm Movement by SEMG at 85°	99
4.23	Stress Distribution amongst the Rotor Cuff Muscles during Group Muscle Analysis	101
4.24	Arm Movement during (a) Elevation and (b) Abduction	102
5.1	Maximum Von Mises Stresses at Rectus Femoris Muscle	105
5.2	Von Mises Stresses at Rectus Femoris Muscle during Flexion Leg Movement from 10° to 90°	106
5.3	Percentage Improvement in Knee ROM during Exercise on CPM Machine	107
5.4	Motor Unit Firing against ROM in Rectus Femoris and Biceps Femoris Muscles by SEMG	109
5.5	Motor Unit Firing against ROM in Rectus Femoris Muscle during Flexion Leg Movement	110
5.6	Motor Unit Firing against ROM in Biceps Femoris Muscle during Flexion Leg Movement	110
5.7	Percentage Variation Muscle Contraction in the Rectus Femoris and Biceps Femoris Muscle during SEMG Test	113

LIST OF TABLES

Table No.	Title	Page No
3.1	Types of Planes for Shoulder Joint Movement	37
3.2	Different Laws and Mechanical Properties Used in the Shoulder Model	42
3.3	Summary of Number of Nodes and Elements Generated in Shoulder Muscle Joint FEM Analysis	44
3.4	Different Laws and Mechanical Properties Used in the Knee Model	51
3.5	Summary of Number of Nodes and Elements Generated in Knee Muscle Joint FEM Analysis	53
3.6	Normal Range of Motion for Shoulder Joint Exercise	55
3.7	Normal Range of Motion for the Knee Joint	67
4.1	Von Mises Stresses and Equivalent Elastic Strain on Deltoid Muscle	79
4.2	Von Mises Stresses and Equivalent Elastic Strain on Supraspinatus Muscle	81
4.3	Von Mises Stresses and Equivalent Elastic Strain on Subscapularies Muscle	82
4.4	Von Mises Stresses and Equivalent Elastic Strain on Infraspinatus Muscle	83
4.5	Von Mises Stresses and Equivalent Elastic Strain on Teres Minor Muscle	84
4.6	Von Mises Stresses and Equivalent Elastic Strain on the Deltoid Muscle during the Group Muscle Analysis	85

Table No	Title	Page No
4.7	Von Mises Stresses in MPa on the Rotor Cuff Muscles during Group Muscle Analysis	86
4.8	Test Report of the Shoulder Joint Exercises on CPM Machine	90
4.9	Normal Range of Motion for the Shoulder Joint	91
4.10	Maximum Motor Unit Firing during the Abduction Arm Movement	92
4.11	Shoulder Muscles Contraction during Abduction Arm Movement	93
4.12	Von Mises Stresses Distribution in the Rotor cuff and Deltoid Muscle during Individual Muscle Analysis	96
4.13	Von Mises Stresses Distribution in the Rotor cuff and Deltoid Muscle during Group Muscle Analysis	96
4.14	Equivalent Elastic Strain (mm/mm) in the Rotor cuff and Deltoid during Group Muscle Analysis	97
4.15	Muscles Contraction in the Shoulder Muscle during SEMG Analysis	98
5.1	Von Mises Stresses on Rectus Femoris Muscle	105
5.2	Test Report of the Knee Joint Exercises on CPM Machine	106
5.3	Normal Range of Motion for the Knee Joint Movement	107
5.4	Maximum Motor Unit Firing Angle by SEMG Test on CPM Machine	108
5.5	Rectus Femoris and Biceps Femoris Contraction during Flexion	109
5.6	Maximum Contraction in Rectus Femoris and Biceps Femoris Muscle during SEMG Analysis at Different ROM in five Subjects	112

NOMENCLATURE

F	External force matrix
F_d	Deltoid force
F_s	Supraspinatus force
K	Global stiffness matrix
M	Moment
ϕ_d	Angle made by F_d with Y-axis
ϕ_s	Angle made by F_s with Y-axis
ϕ_{st}	Angle between the trunk line and glenoid line of scapula
T	Torque
T_e	Equivalent Torque
α	Shoulder arm movement angle
μ	Bearing coefficient of friction
σ_b	Maximum bending stress
ω	Angular displacement

ABBREVIATIONS

CAD	Computer Aided Design
CP	Cerebral Palsy
CPM	Continuous Passive Motion
CT	Computed Tomography
EMG	Electromyography
FEA	Finite Element Analysis
FEM	Finite Element Method
KPa	Kilo Pascal
KPADI	Knee Pain and Disability Index
MPa	Mega Pascal
OKC	Open kinematic chain
PLC	Programmable Logic Control
ROM	Range of motion
SA	Sensitivity Analysis
SEMG	Surface Electromyography
SMPS	Switched Mode Power Supply
SPADI	Shoulder Pain and Disability Index
VAS	Visual Analogue Scale

CHAPTER 1

INTRODUCTION

1.1 PREAMBLE

The injury and distress related with the shoulder and knee joints are one of the major issues worldwide. The function of these joints and the stress developed during their movement is a major concern to an orthopedic surgeon; to study precisely the injury and thereafter to analyse the post-operative progress of the injury. The muscle behavior is one of the major concerns to analyze the exact healing progress of the patient during different exercise. Human joint muscle is soft, flexible and is having hyper elastic properties, which changes with respect to the muscle activity. Measurement and understanding of the pain (i.e. stresses induced) in the human joints and muscles are important in several areas such as, rehabilitation engineering, biomechanics, bionics, human robotics and others. This understanding of the human joints and muscles permit to develop bio-inspired control strategies or tools to be implemented in new ways such as to explore new therapies in disabled people, disabilities affecting the human motor system after the surgery, individual and group muscles behaviour in the human joints. Though a lot of work is in progress on the shoulder and knee joint stress analysis and its behavior, still the exact stresses developed and its behavior is a major concern for the orthopedic surgeons.

The work on the behavior of shoulder and knee joints by use of FEM model is in progress from late nineties. The first biomechanical model for shoulder joint was developed by Dul in 1988 to quantify the joint muscle load. To investigate the stability of Glenohumeral joint for determining muscular forces and stresses, recent model with inverse dynamic theory with Finite Element models were used (Lacroix et al., 2000, Murphy et al., 2001). A CT scan dataset of the different bones of human anatomy were meshed in Hypermesh and after adding mechanical properties to them, the static and dynamic conditions were performed along with the simulation (Astier et al., 2007). A finite element model was effectively utilized to study the sensitivities of

tibio-menisco-femoral joint contact behavior to variations in knee kinematics (Yao et al., 2008). To analyze the stresses and contact pressure peaks, knee FEM model was developed (Ingrassia et al., 2013). FEM model's applicability for real time analysis for knee joint muscle has been explained in detail with the knee joint case study (Lukáš et al., 2014). The 3D CAD knee joint model was created on the basis of visible human project CT scans to analyze the stress state and contact pressures performed in the knee bending position. The results showed that the maximum stress did not exceed the yield strength (90 MPa) of the material (Zach et al., 2015).

Similarly analysis of muscle behavior using Electromyography (EMG) test is a trend followed by many researchers. Wired EMG tests were carried to analyze the force direction and magnitude in shoulder joint (Henk et al., 1997). Behavior of deltoid and trapezius muscles in tension and fatigue were conducted using surface electromyography (SEMG) (Liu et al., 2001). A model for estimation of isometric joint torque using SEMG signals was developed (Amirreza et al., 2011). Analysis of shoulder and neck fatigue was made using surface EMG (Suman et al., 2013). EMG based muscle synergy analysis was performed for the knee flexion / extension and lower limb muscle forces (Dao., 2015).

1.2 SHOULDER JOINT ANATOMY

Shoulder is one of the most critical joint with maximum degrees of freedom. It is an elegantly multifaceted system of bones, joints and muscles that together allows almost infinite number of movements. The shoulder joint allows us to move our hands wherever necessary to perform predefined task. To perform any task; strength, flexibility and stability of the shoulder joints has to be balanced. The flexibility and stability of the shoulder joint during large range of motion is provided by dynamically controlled system of muscles and ligaments. The shoulder complex is the functional unit that results in the movement of the arm with respect to the trunk. The unit consists of the clavicle, scapula and humerus; the articulations linking them and the muscles that move them. It is formed where the humerus fits into the scapula like a ball and socket joint. Fig 1.1 illustrates the orientation of three bones of the shoulder

joint. The shoulder bones orientation and alignment is one of the important inputs for building a CAD model in CATIA.

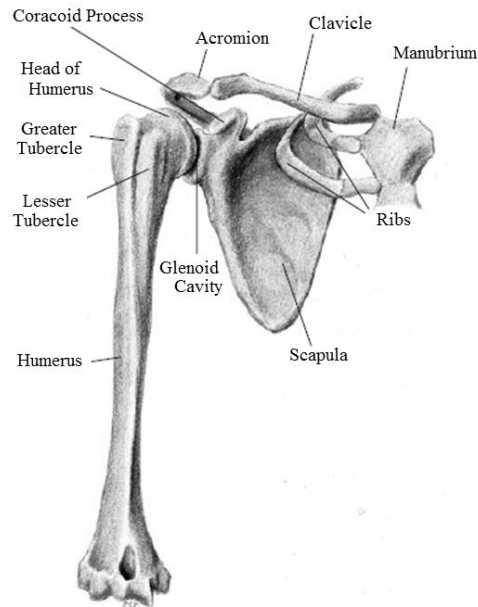


Fig. 1.1 Shoulder Joint Anatomy

Humerus is the longest bone of the upper limb. It has an upper end, a lower end and a shaft. The upper one-third of the anterior border forms the lateral lip of the inter tubercular sulcus. The lower half of the anterior border is smooth and rounded. The anterolateral surface between the anterior borders the upper half of this surface is covered by deltoid. The deltoid muscle originates from the humerus (Romanes, 2012).

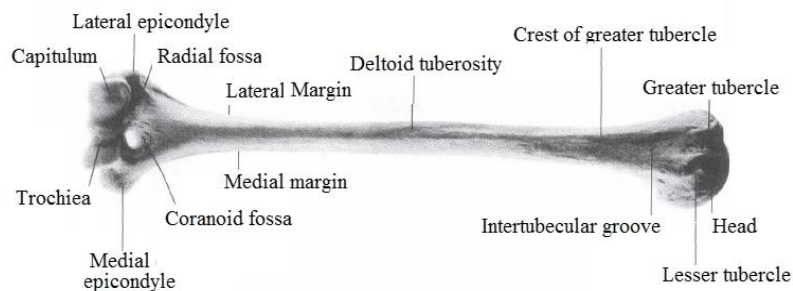


Fig. 1.2 Humerus Bone

Fig. 1.2 shows the elements of Humerus bone. The geometry of the humerus is complicated and is difficult to model it directly in CATIA. This is because, the upper end is rounded to form the head, the lower end is expanded from side to side and

flattened from backwards and the head is directed medially and backwards (Romanes, 2012).

Clavicle is a short bone in the shoulder joint. It supports the shoulder and enables the arm to swing clearly away from the trunk. The clavicle transmits the weight of the limb to the sternum. The bone has a cylindrical part called the shaft and two ends, lateral and medial. It is the only long bone that lies horizontally and which has two primary centers of ossification. The Clavicle shown in Fig. 1.3 has a flat lateral end with a quadrilateral medial end. The inferior surface is grooved longitudinally in its middle one-third, which is difficult to model in CATIA (Romanes, 2012).

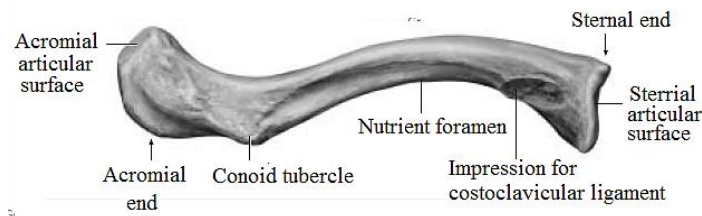


Fig. 1.3 Clavicle Bone

Scapula is a thin bone placed on the posterolateral aspect of the thoracic cage. The scapula has two surfaces, three borders, three angles and three processes. Scapula bone is shown in Fig 1.4.

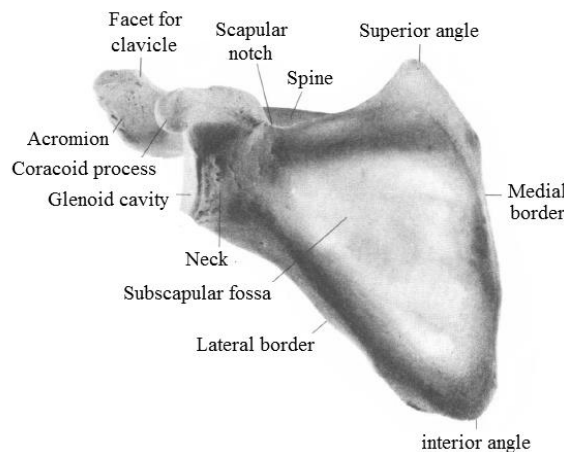


Fig. 1.4 Scapula Bone

The different rotor cuff muscles attached to the scapula includes teres minor, subscapularies, infraspinatus, and supraspinatus. These muscles are responsible for

the internal and external rotation of the shoulder joint, along with humeral abduction and adduction (Romanes, 2012).

1.2.1 Shoulder Joint Muscles

Although ligaments protect and surround the shoulder joint, most of its stability comes from the powerful muscles and tendons of the rotator cuff. There are twenty muscles crossing the shoulder, and these muscles must coordinate their activation and force production in such a way that it has to generate the joint motion while maintaining stable base support for the arm. The rotator cuff consists of four major muscles such as supraspinatus, infraspinatus, subscapularies, and teres minor. Each of these muscles has its origin on the scapula and enclosures around the head of the humerus. The tendons of these muscles support the humerus while the contraction of the muscles rotates, adducts, or abducts the humerus. The deltoid muscle located superior to shoulder joint works with the supraspinatus muscle to elevate and lower the arm at the shoulder.

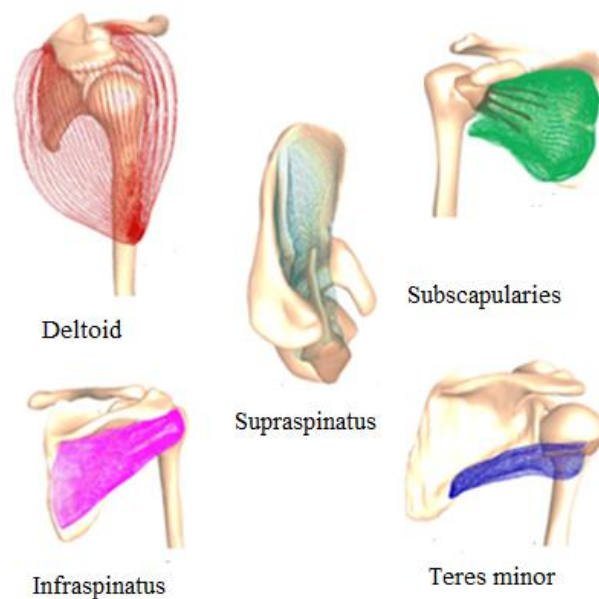


Fig. 1.5 Shoulder Joint Muscles

Although the joint is held together by these extensive ligament and muscle attachments, certain types of forces can weaken the shoulder joint easily. With this complex structure the upper limbs perform tedious tasks such as throwing a ball, lifting of the objects, playing musical instruments and writing. Fig. 1.5 shows the 3D fiber routes for each shoulder joint. Shoulder pain, injury and discomfort are often

caused by the unbalancing of these muscles in the shoulder joint. Some of the common shoulder injuries include dislocation, chronic instability, rotator cuff tears, and impingement. Children shoulder joints are susceptible to dislocations from sudden jerks of the arm, as the muscles are not fully developed (Webb et al., 2014).

1.3 KNEE JOINT ANATOMY

Knee is the one of the most complex and extensively used joints in the human body. The knee joint basically consists of four bones; femur (thigh bone), tibia (shin bone), fibula (calf bone) and patella (kneecap). These bones are held together by a complex muscle system that move the knee joint. Stability of the knee joint is a critical aspect which is provided by the muscles and ligaments. The anterior and posterior cruciate ligament prevents the femur from sliding backward or forward on the tibia. Side to side sliding of the femur is prevented by medial and lateral collateral ligaments (Veeger et al., 2007).

Femur is the longest and strongest bone in the human body. It is the only long bone in the thigh, which includes a diaphysis, the shaft and two extremities that articulate with adjacent bones in the hip and knee.



Fig. 1.6 Femur Bone

The head of the femur has two third of a sphere and a small groove, connected through the ligament to the acetabula notch. The area between head and neck is used to connect different muscles to the femur. The femur bone body is cylindrical,

somewhat flattened and is slightly arched. The femur bone is convex in front, and concave at back. The lower extremity of the femur is larger than upper extremity. Fig.1.6 shows the front section of femur, the contour of which is complex and uneven, so it becomes difficult to model directly the femur bone in CATIA V5.

The fibula is a leg bone positioned on the lateral side of the tibia, which is connected at the top and bottom side of tibia. Its shaft is slender, long, non-uniform having an anterior surface and narrow in its upper part. The lower part of the fibula is having a triangular facet. Different muscles are attached to the fibula, which supports and give strength to different knee bones. The contour of fibula is not so difficult to 3D model in CATIA V5. The assembly of the tibia and fibula is shown in Fig.1.7.

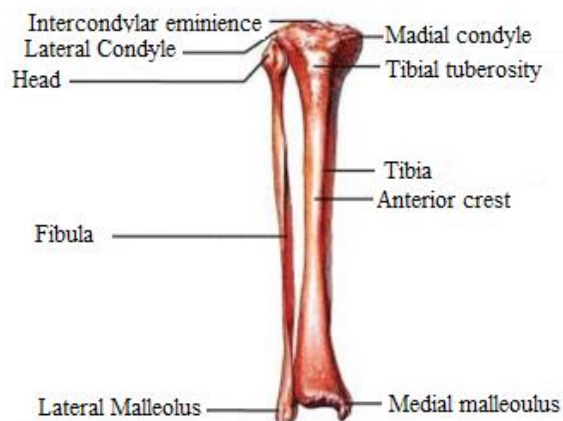


Fig. 1.7 Tibia and Fibula Bone

The tibia is a stronger and longer bone than fibula which is also known as shining bone. It is located in the lower leg and is connected with the fibula. The upper extremity of the tibia is enlarged in the transverse plane with the medial and lateral condyle. The shaft of the tibia is triangular in cross-section and forms three borders which form three surfaces. The lower extremity of the tibia is much smaller than the upper extremity. It is one of the most fracture prone bones in the knee joint.

The patella is also known as knee cap and is the weakest bone in the knee joint assembly. It is about circular in cross section and different muscles are connected to it. The stability of the knee cap is one of the major concerns and is prone to injury because of its frontier location. The front section of patella is shown in Fig.1.8.

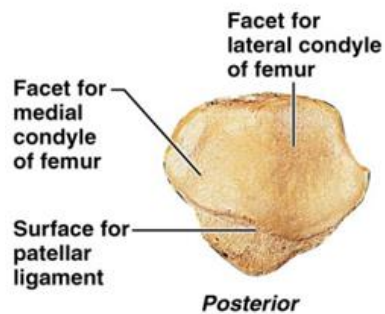


Fig. 1.8 Patella

1.3.1 Knee Joint Muscles

Knee bones are connected together by a very complex muscle system that moves the joint. Stability of the knee joint is a critical aspect which is provided by the muscles and ligaments. The sliding backward or forward of the femur on the tibia is prevented by the anterior and the exterior cruciate ligament. The medial and lateral collateral ligaments prevent the femur from sliding side to side. Fig.1.9 shows the knee joint muscles.

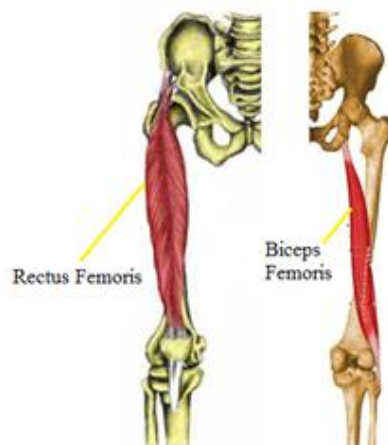


Fig. 1.9 Knee Joint Muscles

The complex muscles are divided into two parts quadriceps femoris, biceps femoris, along with popliteus, soleus and ilio-tibial band. Quadriceps muscle is further divided into four separate muscles such as rectus femoris, vastus lateralis, vastus medialis and vastus intermedius. Rectus femoris is the major muscle, which occupies the center of the thigh. Anteriorly the rounded tendon of the rectus femoris muscle flattens immediately above the patella, and forms the anterior lamina which is inserted

separately at the anterior of the head of tibia. Biceps femoris is located at the posterior side and is one of the sensitive muscles for hamstring (Last, 1948). The rectus femoris is the initiator of the flexion movement and biceps femoris is the initiator of the elevation movement problem (Brooke et al., 1997). To evaluate the rectus femoris and biceps femoris muscles role during the leg movements FEM model may be developed.

1.4 ELECTROMYOGRAPHY (EMG)

Electromyography (EMG) is the study of muscle function by recording the electrical signals that muscles emanate during its stimulation. The EMG activity of voluntary muscle contractions is related to the tension in the muscle. The functional unit of the muscle contraction is a motor unit, which comprised of a single alpha motor neuron and all the fibres it innervates. In EMG, electric signals are passed in the muscles through stimulator and are recorded by electrodes. After these signals are amplified and further processed the output is displayed on the monitor (Konrad, 2005). Basically there are two types of EMG studies based on the type of electrodes used which are surface and fine wire.

Fine wire electrodes require a needle for insertion into the belly of the muscle to measure the muscle contraction. Fine wire electrodes are used to test small muscles which would be impossible to detect with a surface electrode due to cross-talk and also to test the deep muscles behaviour. But the insertion of the needle causes discomfort and can causes tightness in the muscle.

The surface electrodes are divided into two groups such as active electrode and passive electrodes. In active electrodes, a built-in amplifier is used at the electrode site to improve the impedance and no gel is required for these electrodes as they increase the noise ratio. Passive electrodes are used to detect the EMG signal without a built-in amplifier, making it important to reduce all possible skin resistance. It requires conducting gel and extensive skin preparation. The advantages of surface electrodes are that there is minimal pain with application. SEMG recordings provide a safe, easy and non-invasive method that allows objective quantification of the energy of the

muscle (Konrad, 2005). SEMG recordings from human skeletal muscle offer a simple and reliable educational tool to the medical practitioners and researchers to analyze the behavior of muscles for a particular action. It is not necessary to penetrate the skin and record from single motor units to obtain useful and meaningful information regarding muscles (Cram and Kasman, 2005). SEMG is closely related to muscles contraction and is an indicator of the associated actions. For an amputee, SEMG of the residual muscles becomes an obvious choice for natural control of the prosthetic hand (Dinesh et al., 2013). Researchers have reported success in the use of single and multiple channels SEMG recording for controlling the prosthetic hand (Tenore et al., 2009). Fig 1.10 shows the SEMG set up to be used for the muscle analysis for shoulder and knee joint.



Fig. 1.10 SEMG Machine Setup

Results generated by SEMG should be easily accessible so that the exact functioning of the muscles can be known. The output of SEMG is a graph obtained by taking the time on abscissa (or number of motor unit firing turns) and amplitude on the ordinate. Normally the time is in microseconds and the amplitude is in millivolts. This graph interprets the contraction behavior of the muscle during the exercise.

1.5 CONTINUOUS PASSIVE MOTION (CPM) MACHINE

CPM machine is widely used as a part of rehabilitation following the knee and shoulder surgery. There is evidence that its use following the post operation can lead

to a reduction in hospital observation, analgesic requirements and an increase in early range of motion. After extensive joint surgery, attempts to move the joints cause pain and as a result, the patient is unable to move the joint. Due to this the tissue around the joint becomes stiff and scar tissue is formed resulting in limited Range of Motion (ROM) and often may take months of physical therapy to recover that motion. Passive range of motion means that the joint is moved without the patient's muscular power being used. Due to use of CPM machine joint receives nutrition, venous flow increases and deterioration of cartilage is prevented. In addition, pain is decreased, range of motion is maintained and recovery is accelerated. Fig.1.11 shows a knee CPM^{lite} machine for knee post-operative exercise for flexion and extension (London et al., 1999).

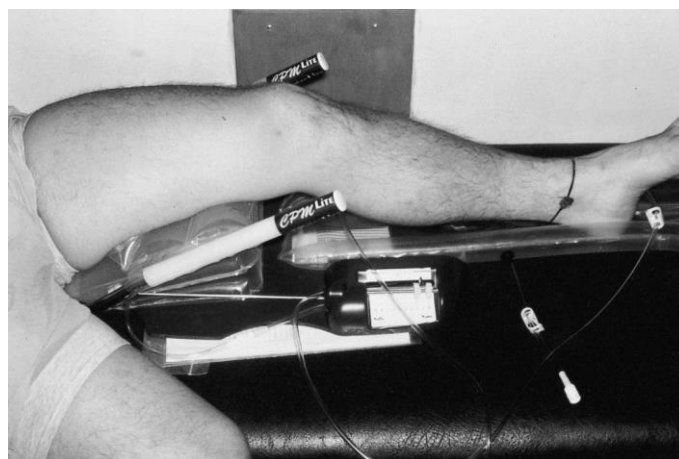


Fig. 1.11 Knee CPM^{lite} Machine

In India knee and shoulder related problems compared to other joint problems are severe and more in number. Continuous passive motion started immediately after surgery seemed to be an effective method both for allowing complete and quick recovery of the range of motion of the ankle and for reducing the risk of early degenerative joint disease (Pasquale et al., 2009). The use of continuous passive motion in the rehabilitation of patients following knee surgery is limited in most countries by the initial cost of the machines (London et al., 1999, Yili et al., 2005, Farhad et al., 2009, Bradley et al., 2009).

1.6 ORGANISATION OF THE THESIS

The current research work is presented systematically in different chapters as follows. The thesis consists of six chapters.

First Chapter starts with an introduction to the problem considered in the present study. Shoulder and knee joint anatomy along with its bones and muscles are explained in brief. The use of CPM machine and its importance in the present rehabilitation process is explained. The wire and surface electrode EMG technique and its use in muscle behavior analysis in modern physiotherapy centers is elaborated.

The **Second Chapter** contains a detailed literature review of the shoulder and knee muscle analysis using FEM and SEMG analysis. The literature review of the knee and shoulder CPM machine for post-operative treatment is also explained in brief. The gaps identified through the literature survey provided the scope for the present research. The problem definition, aims and objectives of the present thesis have been set.

The **Third Chapter** contains 3D model generation of the shoulder and knee joint by using CATIA software. The 3D shoulder and knee models generation from scanning of the bones in ATOS III scanner to its post-processing in the ANSYS APDL is elucidated. The Von Mises stresses and equivalent elastic strain behavior of the shoulder and knee joints by applying the material properties, the loading conditions, defining elements type and size to the 3D FEM model is explained in detail. Design and development of the shoulder and knee joint CPM machine is explained in detail. The procedure for conducting different post-operative exercises on the developed CPM machine to regain original range of motion is explained in brief. The use of surface electromyography (SEMG) method to analyze the muscle contraction during abduction and flexion exercise on the developed CPM machine is elaborated in brief.

The **Fourth Chapter** contains the detailed analysis of shoulder muscle during abduction arm movement by using FEM as well as SEMG analysis. The plots of the Von Mises stresses and the equivalent elastic strain (mm/mm) are explained in brief along with the sensitivity analysis of shoulder joint muscles. The results of SEMG analysis of the shoulder muscles are tabulated and plotted. The discussion about the shoulder FEM analysis and the SEMG results are also briefed. The comparison of the

results of 3D FEM models by SEMG tests and with the trends of previous work is elaborated in detail.

The **Fifth Chapter** contains the detailed analysis of knee muscle during flexion exercise using FEM and SEMG analysis. The plots of the Von Mises stresses are explained in brief. The results of SEMG analysis of the knee muscles are tabulated and plotted to understand the rectus femoris and biceps femoris muscles behavior during the flexion leg movement. The discussion about the knee FEM analysis and the SEMG results are also briefed. The comparison of the results of 3D FEM models by SEMG tests and with the trends of previous work is elaborated in detail.

The **Sixth Chapter** presents objective conclusions made from the present study. The scope for the future work is also stated in this chapter.

CHAPTER 2

LITERATURE REVIEW

2.1 PREAMBLE

Human joint muscle behavior is one of the most critical investigations for the orthopedic surgeons, biomechanical engineers and the researchers. The study of muscle behavior has been done by various methods such as SEMG technique, force analysis by biomechanics and the latest one carried out through FEM technique.

This chapter includes the literature on the analysis of the shoulder and knee joint muscles to identify the muscle stresses by the FEM and SEMG analysis, the development of CPM machine applied to Biomedical Engineering study and use of CPM machine after post-operative treatment. The research gaps are identified and mentioned in this chapter. Based on the research gaps made in the literature survey, the problem of the current research work has been defined and detailed objectives are identified.

2.2 HUMAN JOINTS AND MUSCLE ANALYSIS BY 3D FEM MODEL

Though a lot of work on the shoulder joint stress analysis and its behavior is in progress for the last three decade, but actual stress developed in the shoulder joints and muscles is a big concern for the orthopedic surgeons. Dul (1988) has developed a two-dimensional biomechanical model of the shoulder joint to quantify shoulder muscle load and joint load during elevation arm movement. The maximum retention time of muscle endurance during arm elevation was also estimated. This was the first attempt by any researcher to work on the shoulder muscle behavior of the human joint. The model was used to analyze the maximum force generated at the workplace in the Glenohumeral joint, deltoid and supraspinatus muscles during upper arm elevation. The input variable to the model was the elevation angle between the upper arm and a vertical line. The supraspinatus and deltoid muscle forces were expressed in

percentage of their maximum force. As the shoulder arm angle increases from zero to maximum the muscle force escalates and at 80° of the arm elevation, deltoid and supraspinatus muscles reaches to the maximum effort of 22% and 25% respectively. These trends are used for the comparison of the present FEM model.

Liu et al. (1997) analysed the role of different shoulder rotor cuff muscles and deltoid muscle during the elevation and the moment of the arm was measured. It was observed that anterior deltoid and middle deltoid are responsible for the abduction arm moment during full range of motion. The posterior deltoid has internal and external rotation moment for the full range of motion. Lacroix et al. (1997) observed stress distribution along the glenoid surface by developing a 3D model. The analysis was done in two different sets of abduction angles: 60° and 90°; high and low conformity and constrains. Lee et al. (1998) has developed a 2D FEM knee model for the trans-femoral amputees to estimate the stresses in the muscles. The maximum stresses recorded were 27.4 KPa at the medial side of the adductor Magnus.

Lacroix et al. (2000) has developed a three dimensional model of the scapula using computed tomography (CT) data for geometry and material property definition. The scapula model was keeled and inserted into glenoid surrounded by a 1mm layer of bone cement to determine the stresses in the cement layer and surrounding bones for glenoid replacement components. Douglas et al. (2000) studied both extramedullary and intramedullary humeral morphology by using CT data and three-dimensional computer modeling. Garner et al. (2001) developed the mathematical model of the upper limb from the visible human male. CT images were used to construct high resolution images of the muscles and bones. Murphy et al. (2001) used a computer based glenohumeral joint FEM model for the dynamic loading up to 180° in flexion and abduction exercise. FEM analysis was done for normal and the rheumatoid arthritis cases to determine the muscular forces in flexion and abduction. It was observed that the cement mantle in the offset-keel was much less stressed than the Glenohumeral joint.

Büchler et al. (2002) developed a shoulder FEM model to compare the biomechanics of normal and osteoarthritic shoulder. The soft tissues on the shoulder bones were modeled by considering the shoulder stability aspect. 3D computed tomography was

used to generate the shoulder bone geometry and then the rotator cuff muscles were added to the shoulder model. It was observed that the Von Mises stress distribution at posterior part of glenoid region in normal shoulder was less as compared with the osteoarthritic shoulder. Tammy et al. (2002) developed a 3D model for the knee joint which was used to identify the variables in the selection of meniscal replacement. FEM analysis was one of the good tools to analyze the solid contact behavior of the knee joint. The knee joint model was comprised of the femur, tibia, femoral condyles and tibial plateau. CT images were generated and then exported for FEM analysis. During FEM analysis three different mesh sizes 1mm, 2mm and 5mm were used. The study reveals that contact behaviour of the knee joint is sensitive to rotational constraints placed on the joint.

Eriko et al. (2004) proposed a 3D FEM model to analyze the bone loss around the implants bones. Nine bone models were created, axial and buccolingual forces were applied independently to this super structured model. The study revealed that bone stresses were higher in vertical resorption whereas the cortical bone was much less stressed. Gupta et al. (2004) has developed a 3D FEM model of the scapula by using CT scan data. Their study revealed that the maximum principal stresses generated in the cement mantle were below its failure strength. Gupta and Helm (2004) studied the stress distribution pattern of the scapula during abduction arm movement. 3D FEM model of the scapula with shell solid modelling approach was used to find out the musculoskeletal shoulder force of the muscles, ligaments and joints. Force analysis of a biomechanical musculoskeletal model of the upper extremity was done during 15° of the shoulder arm rotation. The model estimated the muscle forces and joint moments for the given pattern of muscle activations.

Blemker et al. (2005) developed a 3D finite element knee and shoulder models for analyzing the behavior of complex muscle. The limitations of the muscle geometry using series of line segment model were overawed by this model. The model accurately predicted the muscle geometry changes till 55° of hip flexion range of motion as compared to magnetic resonance images. Jeffrey et al. (2005) described the strategies for 3D FEM modelling of knee ligaments mechanics with a whole joint model and individual ligaments. The authors proposed that sensitivity studies should

be performed for both experimentally measured and assumed model inputs. These results will directly imply the importance of one of the inputs than the others in the analysis. Maurel et al. (2005) developed a 3D finite element model of scapula to understand the loosening phenomenon around glenoid prostheses by using CT scans. The results were validated with the vitro experiments carried out on the scapula.

Pena et al. (2006) developed a 3D FEM model of knee joint to investigate the maximum principal stress on the knee muscle under anterior and posterior load conditions. Under rotary load condition the role of ligament and menisci in the stability of the knee joint were also investigated. Blemker et al. (2006) has developed a 3D FEM model of rectus femoris and vastus muscle by using magnetic resonance (MR) images. By using lumped-parameter models and FEM models the fibre excursions were compared. The rectus femoris complex architecture was studied in detail. Mohsen et al. (2007) developed a 3D FEM model of the human buttocks to compute the Von Mises stresses during sitting posture. The Von Mises stresses developed were in the range of 55 to 65 KPa. Ellis et al. (2007) has developed a 3D FEM model of the inferior glenohumeral ligament complex (IGHL) to determine the optimal mesh density for the FEM analysis. Simple translation test was done in the frontal direction on a cadaveric shoulder for 60°abduction. The geometries of the relevant structures for FEM model was created by extracting the volumetric CT data. The sensitivity study was conducted for the subject-specific modeling of the IGHL mechanics.

Astier et al. (2007) developed a 3D shoulder model to study the biomechanics of the shoulder in different configurations. The CT scan database was used to construct a 3D shoulder bone and Hypermesh software was used for the analysis. Thollon et al. (2008) developed a FEM model of the upper extremity in order to study the biomechanics of the shoulder in different configurations such as dynamic loading cases and joint rehabilitation. Model was used to investigate intramedullary nailing capabilities, to understand nail interactions and capabilities to ensure proper bone rehabilitation process. The simulation demonstrated local damage effect at bone nail interface which can induce complications and was observed clinically during rehabilitation process. Jiang et al. (2008) developed a finite element model to study

the sensitivities of tibio-menisco-femoral joint contact behavior in the knee kinematics. Magnetic resonance images were captured to obtain the kinematics of tibia and femur. Then the kinematic boundary conditions were applied in FEM and the results were verified by comparing the model-predicted reaction force during MR image based experiment.

Iwamoto et al. (2009) developed 3D FEM model to find out the performance of shoulder muscles in the pre-impact injury. Two series of experimental tests were conducted to validate the results. The study revealed that muscle activity in pre-impact injury had significant effects on the motion and stress distribution of the arm bones. Melisa et al. (2010) has worked on a shoulder muscoskeletal model associated with manual wheel chair activity of living subjects. Optimization technique was used to estimate the joint contact forces associated with the joint muscles. Level propulsion, ramp propulsion, and a weight relief lift conditions were the inputs used to measure the upper extremity kinematics. Validation of the model was done by a mean absolute error calculation. Though the level propulsion was identified but the observations were not conclusive with the frequency consideration in the propulsion. Kluess (2010) has showed that the FEM method is the most preferred method for the stress and strain analysis of the bones, joints and muscles. The load bearing implants in the orthopedic field with a real time model was used to analyze the stress in the different human bones.

Gulshan et al. (2010) proposed a 3D FEM model of the glenoid to demonstrate the capability of the glenoid bone remodeling produced by changing prosthesis design features. The twelve FEM prosthesis models were individually combined to simulate the surgical implantation with the glenoid models. The initial results demonstrated the capability and potential of adaptive glenoid bone remodeling simulation. Magnus et al. (2010) proposed the methodology for creating a FEM model of wrist joint which is one of the most complex composite articulations joint in the human anatomy. Marko et al. (2011) presented and compared the application of two modeling techniques for creating a geometrical model of the human tibia. The study revealed that the application of this method can be extended to other bones in the human body. Vitković et al. (2012) proposed different methods for creating human bone and

fixators by geometrical models by the reverse engineering technique. These CAD models were used in a web application for the preoperative planning.

Dew et al. (2012) has measured the rectus femoris muscle thickness of thirteen youth by cerebral palsy (CP). The average thickness of the muscle was in the range of 11mm to 28 mm. Alexandre et al. (2012) developed a FEM model of a prosthetic shoulder consisting of three bones and rotor cuff muscles. Shoulder joint muscle thickness (2mm, 4mm, and 6mm) conformity test was carried by gradually crushing the glenoid surface. The different stress values such as cement stress, contact pressure and shear stress were found by abducting the shoulder joint. It was observed that the optimum thickness to avoid stress concentration and joint stuffing was 4mm. Daniel et al. (2012) studied the effect of mechanical loading during the post-operative changes in the shoulder joint bones. 3D finite element models of a scapula with and without cement less glenoid component were created and strain energy density for different loading conditions was evaluated. The study revealed that irrespective of the interface condition, the local bone resorption was the maximum in some regions along the bone–implant interface.

Ingrassia et al. (2013) used a FEM Knee model to analyze the stress and contact pressure peaks between femoral and tibial plates. The model was developed by 3D laser scanning, CAD modeling and then exporting it to FEM environment for knee joint analysis. The polyethylene (PE) component was inserted between the femoral and tibial plates during the analysis. Chandreshwar et al. (2013) developed a statistical shape and alignment modeling (SSAM) approach to characterize the intersubject variability in the knee joint. This study used the relative position of the knee structures through a loaded simulator activity to find the relationship between the variation in shape and relative alignment of the knee joint.

Ashutosh et al. (2014) has developed a 3D Knee joint model to analyze the Von Mises stresses at the different load conditions and weights. Scanning of the knee bones were done to get the correct dimensions and profile of the bones. The 3D model was generated in Pro-Engineer Wildfire 4.0 modelling software. The FEM analysis was done in ANSYS software to get the Von Mises stresses at different loads. Adouni et al. (2013) computed lower extremity muscle forces and knee joint stresses-strains by

using a knee joint FEM model. The knee model was constructed from the CT images of three bones (femur, tibia, and patella) and the soft tissue bounding to these bones. The results of the model driven by gait data were compared with the data on the normal controls.

Webb et al. (2014) has developed a 3D shoulder joint model to examine the functions of the deltoid and rotor cuff muscles during abduction, internal and external rotation. The abduction fibre moment arms by using three-line segment approximation of deltoid predicted that the anterior and posterior deltoid have moment arms that vary greatly with abduction angle compared to other muscles. The results revealed from this work are used for comparing the results of the present 3D FEM model. Deltoid abduction moment arms range from 2.5 cm abduction to 1.2 cm adduction. The study revealed that Sensitivity Analysis should be carried out for 3D FEM model muscles to identify the most important muscle for the shoulder arm movement. Lukáš et al. (2014) developed a FEM model for hinges PROSPON oncological knee endoprosthesis. The CT scanned knee bones were imported into a CAD model and then FEM analysis of the knee joint during the flexion leg movement was done.

Schmidutz et al. (2014) studied the two different cementless surface replacement arthroplasty (CSRA) fixation designs were studied 3D FEA as well as the evaluation of contact radiographs from human CSRA retrievals. The FEA model with a reduced bone stock quality was included in the CSRA. Compressive strains were evaluated before and after virtual CSRA implantation. Alexandre et al. (2014) developed a 3D FEM model of total ankle replacement associated with the clinical problems. The results were validated with the experimental setup on eight cadaveric tibias. The maximum strains were observed in the anterior and posterior of the implant keel. Zach et al. (2015) created a 3D CAD knee joint model on the basis of Visible Human Project CT scans to analyze the stress state and contact pressures performed in the knee bending position. The results showed that the maximum stress did not exceed the yield strength (90 MPa) of the material.

2.3 SHOULDER AND KNEE CPM

Von Riemke in 1926 stated that, after the surgery all the joints should be moved from the first day. The movement should be very slow and as much as possible it should be

continuous. Based on a series of investigation, Robert Salter in 1960, experimented on a rabbit knee joint under continuous compression, and invented the concept of the CPM. This knowledge was based on the gate-control theory of pain by Melzack and Wall, which states that with competing afferent sensory stimulation, painful stimuli would be inhibited. The CPM concepts were tested on the subjects since 1978 and were proven to be feasible. Salter hypothesized that CPM would accelerate the healing of articular cartilage and particularly structures, such as the joint capsule, ligaments and tendons (Shawn et al., 2000).

London et al. (1999) developed a new low cost and portable CPM Machine (CPM^{lite}) for the knee joint. Thirty nine subjects were tested on the developed CPM^{lite} machine to get early ROM and reduced hospital stay. Their study showed that use of CPM^{lite} machines is limited in the rehabilitation centres due to the cost of the equipment and concluded that their low cost CPM^{lite} machine compares well with the other existing machines. The significant reduction in cost has forced the large number of rehabilitation centres to use the CPM machine for the cost effective treatment. Shawn et al. (2000) proposed that the CPM should be started immediately after the post-operative treatment. This reduces the scar tissue formation around the joint, due to its immobility after surgery or the injuries. The soft tissue in the human joint should be subjected to tension immediately following the surgery. Their study showed that initial or delayed accumulation of periarticular interstitial fluids should be the focus of the next research and CPM is the key option to reduce this.

Yili et al. (2005) developed a biometric mechanism for human fingers and a finger CPM machine. Moving scope of fingers, finger's force and speed were precisely controlled by using the developed mechanism and the machine. Toby et al. (2007) commented on the use of CPM machine after post-operative treatment by reviewing the 505 papers from different journals. The authors concluded that it was unclear that the use or non-use of CPM post-operative treatment has any benefits. There were numerous methodological weaknesses within the evidence-base study. Shota et al. (2008) developed the CPM device that has two degrees of freedom with the inner / outer rotation and the adduction /abduction. By keeping fixed adduction / abduction

angle, the variation in the inner/outer rotation torque was analyzed on the shoulder CPM.

Pasquale et al. (2009) studied the effect of immediate use of the CPM machine for the surgically treated bimalleolar and trimalleolar fractures. Study was conducted on the two series of twenty two subjects each with different ankle fracture treated surgically. The first series of the subjects were applied immediately on a CPM machine after the surgery for three weeks and the other series were casted with plaster for three weeks. They were evaluated clinically and radio-graphically using the Ankle Hind foot Score System. Their findings were the CPM applied immediately after surgery seemed to be an effective method both for allowing complete and quick recovery of the range of motion of the ankle and for reducing the risk of early degenerative joint disease. Farhad et al. (2009) developed a new and innovative Glenohumeral test rig for the shoulder exercises and shoulder injury prevention, replacement and repair. This study was undertaken to evaluate the forces acting on the glenoid by different ROM of shoulder abduction. The Ranking and weighing table was used for the selection of the curved track turning method and for selection of the mounting module.

Onderko et al. (2013) claimed that CPM has its potential benefits for the post-operative treatment in the articular fracture management. Human studies had shown the improved rate of hemarthrosis clearance with CPM compared with immobilization. Basic science studies showed that the early postoperative care of articular fractures treated with open reduction and internal fixation, a natural extension, would be beneficial by the use of CPM.

Yoon and Choi (2014) developed a CPM machine for the upper part extremity by using pneumatic air. The author stated that the use of motor driven CPM machine had a forceful (ROM) exercise without sensing the patient's compliance. Wrist and finger CPM was developed by using multi air bag system with costly solenoid operated valve. The bi-directional feedback system between the patient and the machine was used for safe ROM and pressure on the joint. The cost of the developed CPM therapy compared to conventional CPM is very high.

2.4 MUSCLE ANALYSIS BY SEMG

Henk et al. (1997) used surface and wire electrode EMG to analyze the static force in the fourteen shoulder muscles during the arm movement. EMG was used for analyzing the maximal force direction in the muscle. It was observed that for every shoulder joint, the force direction was unique and dependent on the structure of the muscle. David et al. (2000) identified the activation patterns of several muscles acting on the shoulder joint during isokinetic internal and external rotation. EMG activity of the rotator cuff, biceps, deltoid and pectoralis major was carried for internal and external rotations. The rotator cuff and biceps muscles were active during these two exercises and were case sensitive. SEMG was preferred over the wired EMG method. Liu et al. (2001) studied the behavior of the deltoid and trapezius muscles by using SEMG under the influence of precision task. The muscle tension and fatigue were reflected by Root Mean Square (RMS) amplitude and changes in the median power frequency. The hand activity was not influenced by the deltoid muscle but it was influenced by the descending part of the trapezius muscle. EMG measurements were performed during isometric muscle contractions. The tests were conducted on ten young, right-hand dominant men aged 20–29, in the sitting position on the same upper limb and spine location. Two parameters of the EMG signal were analyzed: the normalized integrated EMG amplitude and the fatigue index.

Carel et al. (2004) assessed the reliability of force direction dependent EMG parameters in shoulder muscles for future clinical research. The isometric external loading performance on the rotor cuff muscles were measured by SEMG. Shoulder muscle coordination of patients before and after interventions like surgery or physical therapy was evaluated. Dark et al. (2007) compared the rotor cuff muscle pattern with the other shoulder muscles by SEMG technique during the side arm exercise. Fifteen subjects were tested by SEMG to analyses the muscle activities in supraspinatus, infraspinatus, subscapularies, latissimus dorsi, pectoralis major, and posterior deltoid muscles during the arm rotation with the pulley system. The muscle activity was increased systematically in all the muscle during the internal and external rotation exercise. Christopher et al. (2008) evaluated three methods for predicting shoulder muscle forces during shoulder arm movement by SEMG. He compared the results with the calculated muscle force. The three methods used to determine the muscle

parameters were the traditional multiple linear regression, principal-components regression, and a sequential muscle parameter determination process using principal-components regression. The study revealed that no method was superior with respect to all evaluation criteria.

Jaspal et al. (2008) compared the myoelectric amplitude of shoulder muscles during push-up exercise on labile and stable surface. SEMG was recorded on thirty healthy male subjects on the triceps, pectoralis major, serratus anterior and upper trapezius muscles during the push-up exercises. Significant increase in muscle activity was observed in pectoralis major and triceps muscles compared to serratus anterior and upper trapezius muscles. Laura et al. (2009) studied the co-activation of forearm extensor and flexor muscle by SEMG during the tapping of different keys on the keyboard. Two channel SEMG was used on thirteen subjects to monitor fore arm muscle activation. It was concluded that the make-force level over 0.59N were ergonomically inadequate.

Venkatesh et al. (2009) studied the muscle activity of aerobic cyclist on the biceps brachii medial, trapezius medial, latissimus dorsi medial, and erector spinae muscles bilaterally during 30 minutes of cycling. Statistical tests were performed to determine the difference in fatigue by mean power frequency difference method. High fatigue in the back muscles in the low back pain (LBP) group was not found and the data showed the possibility of worsening in their condition due to 30 minutes of cycling. William et al. (2010) investigated the force generation capabilities and muscle contraction responses to a simulated hand scaling subtask by SEMG. Surface electrodes were placed on the deltoid and erector spinae muscles of the shoulder joint. The maximum muscle force generated was on the right deltoid muscle. Amirreza et al. (2011) developed a model for the estimation of isometric joint torque using SEMG signals. It would assist the researchers for identifying the most appropriate model for a specific biomedical application. Torque sensor was used on eleven healthy subjects, as each subject flexed and extended his wrist. SEMG data were gathered for wrist muscles along with the torque data. The muscle and torque behaviour for the given ROM was studied.

Zwaan et al. (2012) used electromyography profiles during gait represent muscle coordination for assessing selective motor control (SMC) of the cerebral palsy

functioning. The extensor synergy and thigh synergy were measured by the EMG profiles during gait analysis. The results supported the sensitive nature of EMG to represent an aberrant motor control in cerebral palsy. Dale et al. (2013) studied the muscle activity at the bowing shoulder of a cellist by SEMG during cello playing. SEMG and fine-wire was used in combination to evaluate muscle load placed on the right shoulder of a professional cellist whilst playing a set of various bowing exercises. It was observed that the supraspinatus muscle in particular maintained higher mean contraction (20% MVC) during all bowing patterns testing.

Dinesh et al. (2013) established a method to identify the finger flexion by using a single channel surface electromyogram (SEMG) recorded from the forearm. The study showed that single channel SEMG provides a suitable basis for identifying finger flexion by volume conduction properties based SEMG analysis. Yoshinari et al. (2013) compared the EMG recorded on the shoulder joint muscles in the same position for different arm movement directions. For recording EMG signals wire electrodes were used for the supraspinatus muscle and surface electrodes were used for the infraspinatus, anterior deltoid, middle deltoid, and posterior deltoid muscles. The supraspinatus muscle showed the higher EMG activities during the elevation arm movement from 0° to 90° of ROM and showed lesser activity during abduction arm movement.

2.5 RESEARCH GAPS

The following concluding remarks are made from the above review of literature and the research gaps are mentioned below.

- 1) Although a large number of research has been reported on the FEM analysis for human joints only a few concentrated on FEM analysis of the shoulder and knee joints. The major focus in shoulder analysis was to analyze the maximum force and stress in the clavicle bone during abduction arm movement. Very few researchers have reported on the muscle analysis during the human joint movement especially in the shoulder joint for abduction arm movement and knee joint for flexion leg movement. Stress analysis of the shoulder and knee joint muscles has not been attempted by previous researchers.

- 2) Sensitivity analysis of the shoulder joint muscles is not carried out by the previous researchers to predict the most stress-sensitive muscle during abduction arm post-operative treatment, so that an orthopedic surgeon can concentrate more on the sensitive muscle during rehabilitation procedure.
- 3) Even though large numbers of researchers have reported on use of CPM machine for the human rehabilitation only a few concentrated on the low cost CPM treatment. So it becomes necessary to work in this area for the cost effective human joint treatment and also large number of rehabilitation center can use the low cost CPM therapy.
- 4) Although large number of research has been reported on the SEMG analysis for human joint muscles but only few concentrated on SEMG analysis for shoulder and knee muscle joints. So it becomes necessary to undertake further research work in these areas. This is the first time that the shoulder and knee muscle analysis is carried out on the post-operative patients to predict the most sensitive muscle during abduction arm movement and flexion knee movement.

2.6 AIMS AND OBJECTIVES

Based on the above literature survey and research gaps identified, the Research Problem has been defined as below.

“Analysis of Shoulder and Knee Joint Muscle Stresses by using FEM and SEMG on the Developed CPM Machine” during abduction arm movement and flexion leg movement.

In order to address the issues found in literature, following objectives are formulated for the present work.

- 1) To analyze the behavior of the shoulder joint muscles during abduction arm movement and knee joint muscles during flexion leg movement using the 3D FEM model.
- 2) Sensitivity Analysis (SA) of the shoulder joint muscles for the Von Mises stresses and equivalent elastic strain during abduction arm movement for the individual and group muscles analysis.

- 3) To design and develop a low cost Shoulder and Knee CPM machine for human rehabilitation.
- 4) To analyze the muscle contraction (stress) in the shoulder joint during abduction arm movement and the knee joint during flexion leg movement by SEMG on the developed CPM machine.
- 5) Comparing the results of FEM analysis of the shoulder and knee muscle with the SEMG test conducted on the developed CPM machines and also with the previous work.

2.7 SCOPE OF WORK

In the present work an effort has been made to analyze the stresses developed in the shoulder muscles during abduction arm movement for the full range of motion by using the Finite Element Method (FEM) model. For shoulder muscle analysis deltoid muscle and four rotor cuff muscles are considered. Out of twenty shoulder muscles assembly, these five muscles play a vital role in stabilizing the shoulder ball socket joint. In the mid ranges of motion the ligaments and capsule are slack, and muscles provide the primary support for joint stability (Lee et al., 2000). Deltoid muscle is involved in the analysis because it is one of the largest shoulder muscles. Deltoid muscle has its origin on the scapula and inserts around the humerus head.

In the present work an effort has been made to analyse the stresses developed in rectus femoris and biceps femoris knee joint muscles during flexion leg movement for full range of motion by using 3D FEM model.

In the present study an attempt has been made to design and develop low cost shoulder and knee CPM machines. The abduction arm movement and flexion leg movement tests were conducted on the developed low cost CPM machines. The developed CPM machine fulfills the basic functional requirements of the knee and shoulder exercise under the observations of the orthopedic surgeon.

In the present study an attempt has been made to analyze the knee and shoulder joint muscles contraction (stress) during different exercises using two nodes SEMG machine. The major advantage of using SEMG is that there is minimal pain with

application of surface electrodes and SEMG is very good for movement applications compared to wired electrodes. They are more reproducible and easy to apply. In the present study the SEMG analysis is done for the abduction arm movement and flexion leg movements, where the shoulder and knee joints are rotated from 0° to 130°. One of the major problems of using the needle electrode is needle insertion causes discomfort and can increase tightness in the muscle and it is difficult to insert the needle or fine wire in the same area of the muscle each time. There use is avoided in the large movement applications. SEMG is a useful tool for investigating the timing and activations of muscle, and is used to quantify the relative contributions of muscles during the joint movement (Dark et al., 2007).

The von Misses stress results by FEM analysis are compared with the SEMG test conducted on the developed CPM machines and also with the previous work (Dul, 1988; and Webb et al., 2014).

The present work will help researchers and orthopedicians for a better understanding of the shoulder and knee joint mechanism and the most sensitive muscle during the abduction arm movement and elevation leg movement at different ROM. The orthopedic surgeons can take the corrective measures and focus their therapy to accelerate the healing process of these muscles by using various medication or physiotherapy techniques.

CHAPTER 3

METHODS AND MATERIALS

3.1 METHODOLOGY OF THE PRESENT WORK

In this study a classical 3D FEM modelling technique has been used to study the behaviour of shoulder joint muscles during abduction arm movement and knee joint muscles during flexion leg movement for different ROM. The 3D FEM method is the preferred method for the stress and strain analysis of bones, joints and load bearing implants in the orthopedic field (Klues, 2010). Musculoskeletal models of the shoulder and knee joint have been used for many investigations in biomedical fields, including muscle architectures and geometries, in osteoarthritis joints and in tibio-femoral contact (Büchler et al., 2002, Tammy et al., 2002, Blemker et al. 2005, Webb et al., 2014). In this study 3D models of the shoulder and knee joint bones are constructed by (ATOS III) 3D scanner. The 3D model refinement is done before exporting it into CATIA V5 software. The 3D shoulder and knee joint assembly has been made in a predefined orientation; alignment and by maintaining proper gap between the bones (Romanes, 2012). Shoulder and knee joint muscles are then added in CATIA V5 software. A non-homogeneous constitutive law is used for bones as well as nonlinear hyper elastic laws are used for rotor cuff muscles. Muscles are considered as an active structure (Blemker et al., 2005, Webb et al., 2014). The kinematics abduction for the shoulder joint and flexion for the knee joint are the inputs given for the FEM analysis in ANSYS software. The 3D FEM analysis is done for five different muscles in the shoulder joint and two muscles in the knee joint. The individual and group muscles analysis is done for stress measurement during abduction arm movement. The muscle behavior has been analyzed for abduction arm movement from 0° to 80° in shoulder joint and for flexion leg movement from 0° to 90° in knee joint. The Von Mises stresses and equivalent elastic strains of the shoulder and knee muscles are plotted.

To compare the FEM results a low cost CPM machine is designed and developed. The testing of the CPM machine is done on fifty shoulder and knee prone cases of different age groups and genders. The SEMG is used for analyzing the shoulder and knee muscles contraction during the exercise on the CPM machine. The SEMG probes were mounted on the deltoid, supraspinatus, teres minor, subscapularies, and infraspinatus muscles of the shoulder joint for abduction arm movement. Similarly the SEMG probes were mounted on the rectus femoris and biceps femoris muscles of the knee joint for flexion leg movement. The SEMG testing was done on the twelve subjects of shoulder joint and eight subjects of knee joint on the developed CPM machine. The output graphs of amplitudes in microvolts against the number of turns are plotted (ROM in degrees). The stress sensitivity analysis of the shoulder and knee muscles has been carried out. The 3D FEM modeling results have been compared with the SEMG test results and with the previous work.

Fig.3.1 shows the methodology used for 3D FEM analysis of shoulder joint muscles.

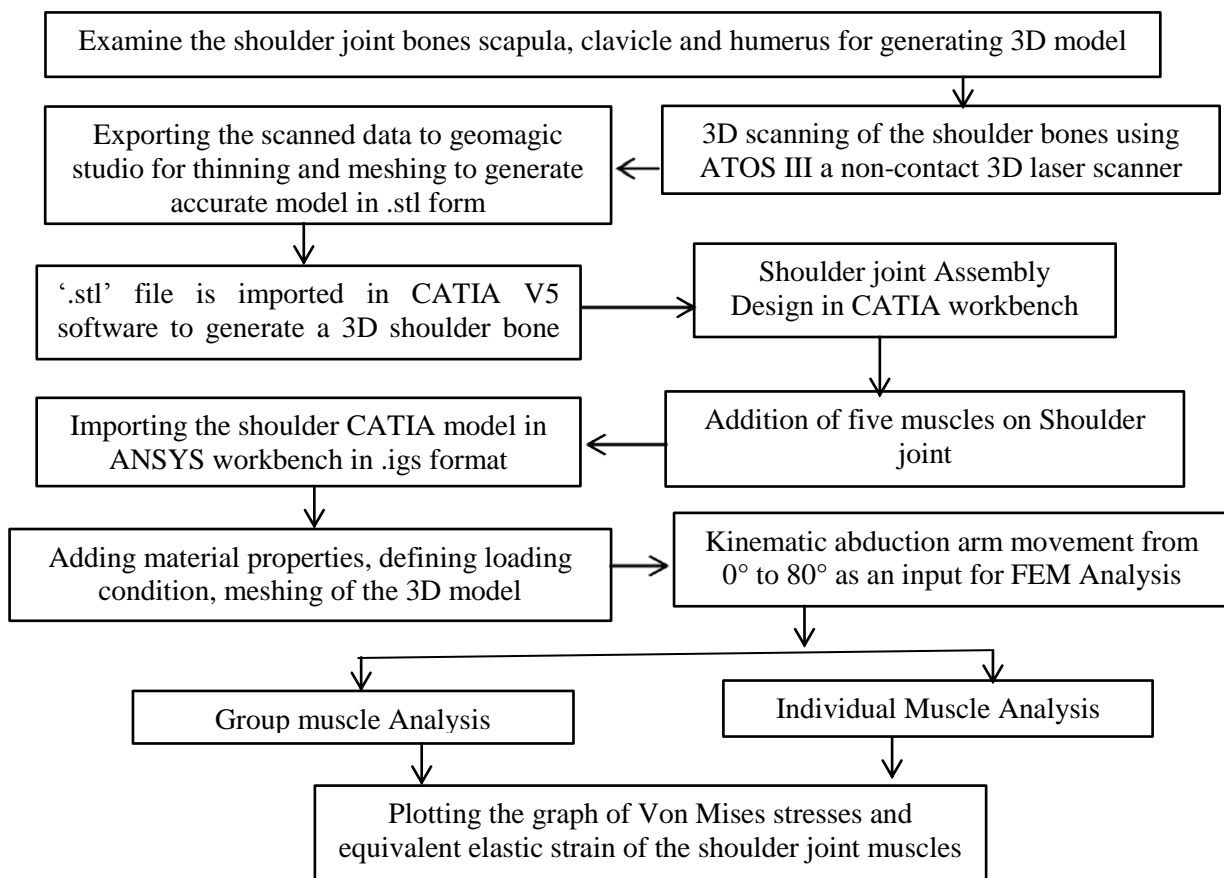


Fig. 3.1 Methodology Used for 3D FEM Analysis of Shoulder Joint Muscles

Fig.3.2 shows the methodology used for 3D FEM Analysis of knee joint muscles.

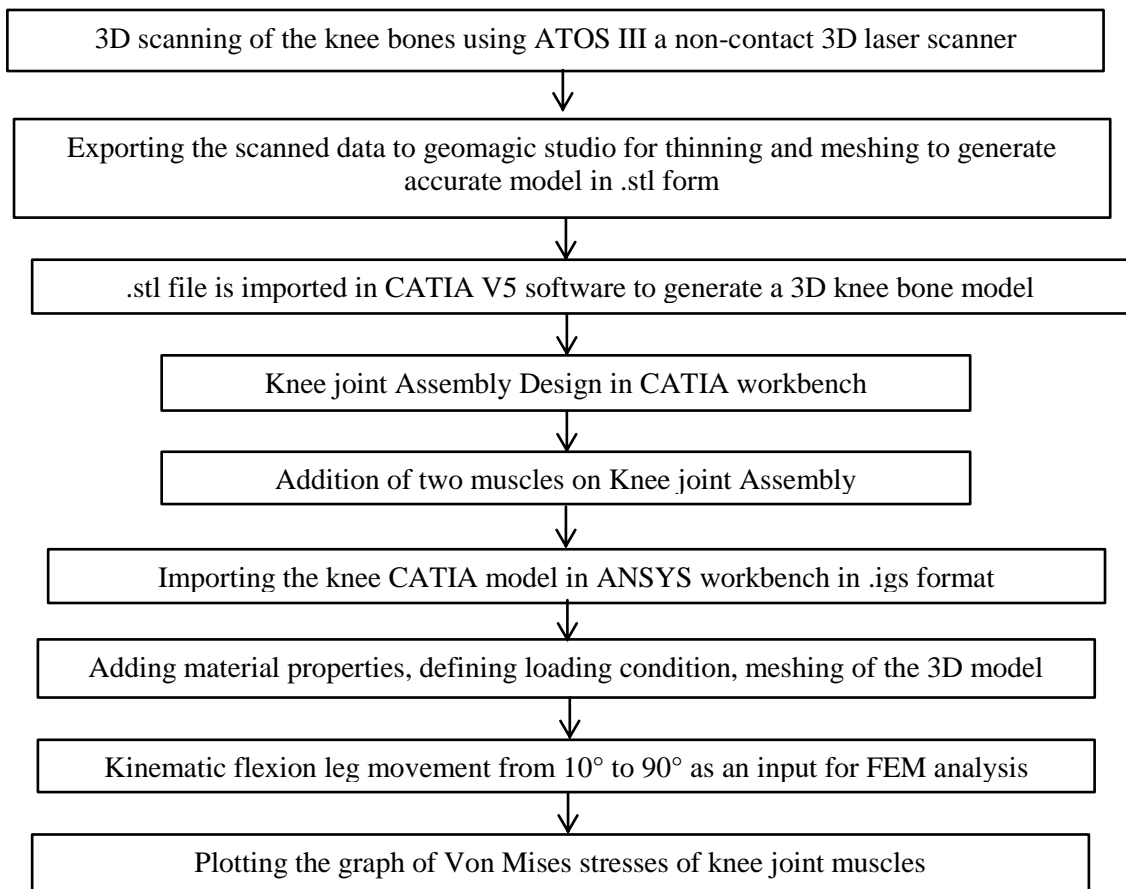


Fig. 3.2 Methodology Used for FEM Analysis of Knee Joint Muscles

Fig.3.3 shows the methodology used for SEMG Analysis of shoulder and knee joint muscles.

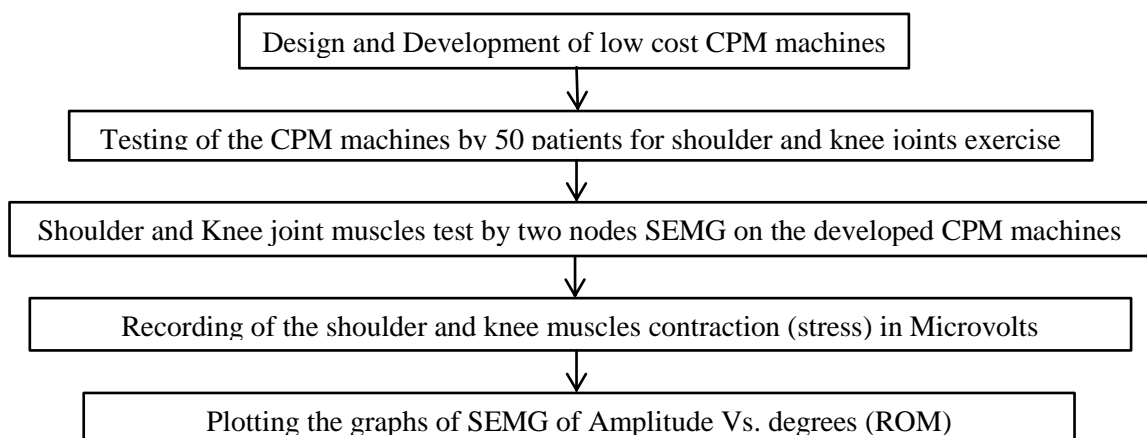


Fig. 3.3 Methodology Used for SEMG Analysis of Shoulder and Knee joint Muscles

3.2 3D MODELLING OF SHOULDER BONES

From the last decade, 3D model techniques are predominately used in different fields such as automobile for component models, in the film industry for animations, aviation industries for surface modelling and medical fields for different body parts models. The science sector uses them for building virtual prototypes for the experimentation work, while the architects use them for demonstrating plans of buildings (Fausto et al., 2002). A 3D model describes an object as a set of points in the 3D space and is joined by various geometric entities such as lines, triangles and curved surfaces. Being a collection of data, 3D models can be created by hand, algorithms or scanning.

The shoulder complex is the functional unit that results in the movement of the arm with respect to trunk. It mainly consists of clavicle, scapula, humerus and different muscles. Shoulder muscles are the complex fibrous structure surrounded by different tissues and blood vessels (Carol, 2009). Accurate topology of all the shoulder bones and muscles is a key to create a valid and accurate 3D shoulder model, which will be useful for an orthopedic surgeon during pre-operative planning. Therefore, it is logical to base the process of geometrical modeling of the shoulder joint on its anatomical and morphological properties (Marko et al., 2011).

3.2.1 3D Scanning of Shoulder Bones

The precise measurement of the bone dimensions, its shape and contours with its position and orientation plays an important role for the accurate prediction and analysis of the human joint movements. A 3D scanner is a device that measures a real-life object by collecting data on its profile to build three dimensional complicated models. Modeling of bones in CATIA software without any background help is very difficult and impractical. The irregular shape of the scapula, clavicle and humerus is difficult to profile directly in CATIA software. The free form modeling option in CATIA does not prove to be much useful, as the dimensions and bone contours vary from person to person with different age groups. Moreover, the minute detailing required during the modeling of ligaments, tendons and muscles is not easy using surface modeling software like CATIA. Several attempts to capture these muscular parts turned out to be a debacle. Thus, 3D scanning of the bones to obtain a point-

cloud is finalized in the present work for the shoulder bone modeling (Marco et al., 1998). 3D scanning set up of four shoulder joint muscle is shown in Fig. 3.4.

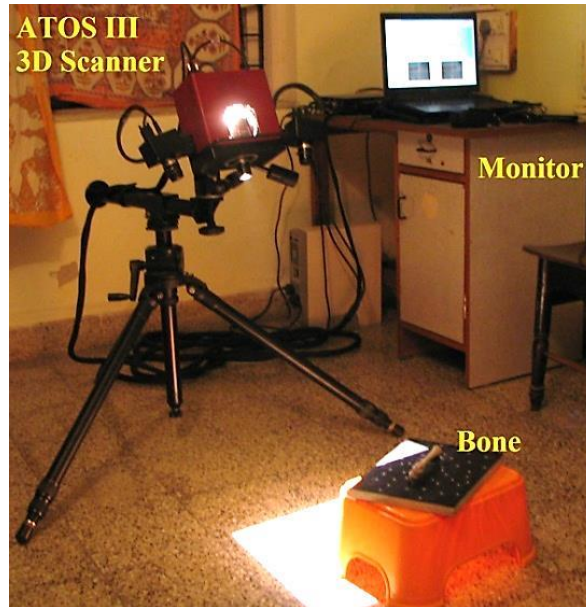
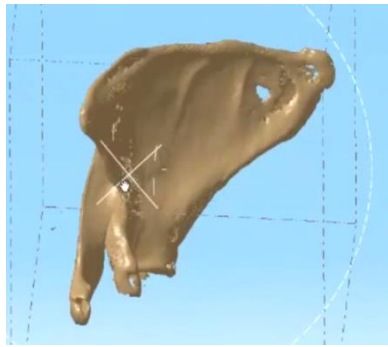


Fig. 3.4 Scanning of Shoulder Joint Bones by ATOS III

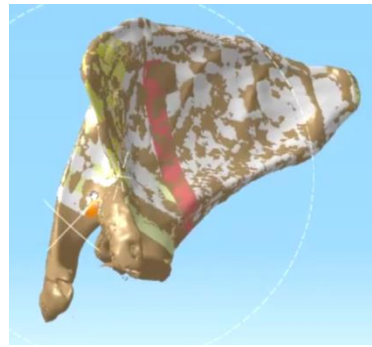
In the present work ATOS III a non-contact 3D laser scanner is used from Arun 3D Labs, Pune, India. The proven two camera technology developed by GOM GMBH was used and delivered four million data points in each measurement to ensure a very dense and highly accurate 3D scanned model. The specifications of ATOS III 3D scanner and the scanning procedure are described in the **Appendix I**.

Reverse modeling is one of the fast and accurate methods to reproduce complicated objects such as shoulder bones. Three shoulder bones scapula, humerus, and clavicle images with the required accuracy and detailed contours were created by using the 3D scanner. The scanned object was then imported into geomagic studio and all points outside the relief area were deleted and various scans were merged into a single data.

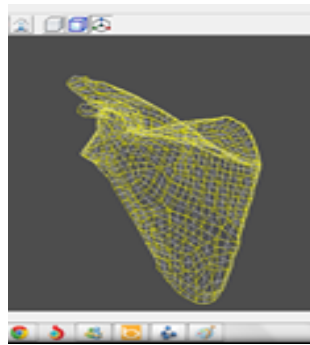
Fig. 3.5 shows the different stages through which the scanned 3D scapula model is created. Thinning of the object was done to reduce the total number of points by deleting surplus points in repeatedly scanned areas. At the same time, the total number of points has to be reduced below four million points which is a critical value for some of the following procedures, especially the reunion procedure following the hole filling ('Merge Polygon Objects').



(a) Scanning Image of Scapula



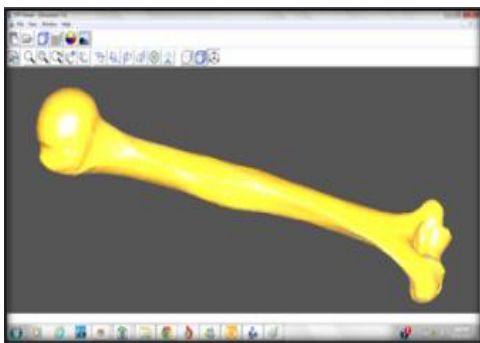
(b) Thinning and Shape Cleaning of Scapula



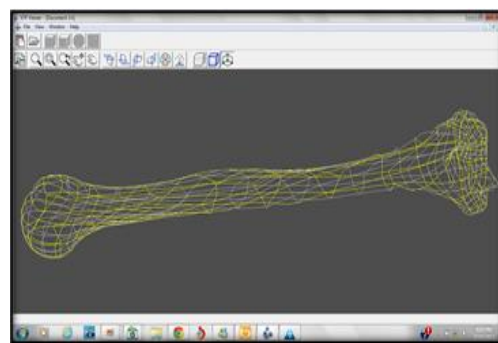
(c) '.stl' File of Scapula

Fig. 3.5 3D Scanning Procedure to Generate Scapula Bone

Fine meshing of scapula was done by generating eight million triangles to get precise contours and topology. To generate an accurate and detailed model shape-cleaning algorithm was used. Finally '.stl' file of scapula was generated by the ATOS III 3D scanner.



(a) Scanning Image of Humerus

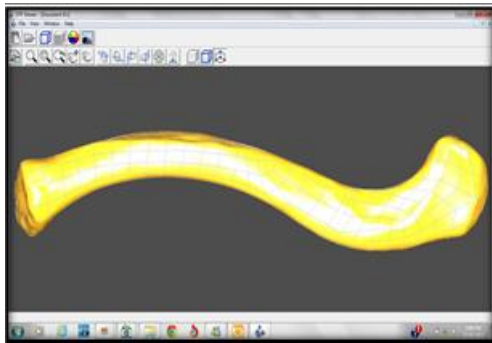


(b) '.stl' Model of Humerus

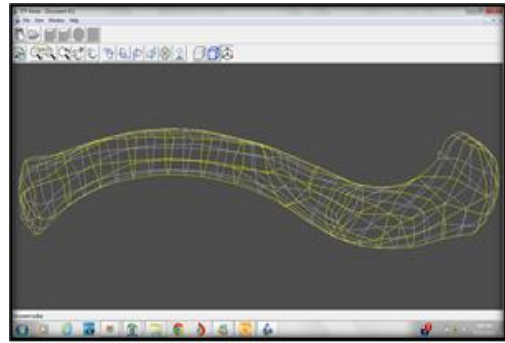
Fig. 3.6 3D Scanning Procedure to Generate Humerus Bone

The '.stl' files generation of humerus and clavicle is shown in Fig. 3.6 and Fig. 3.7. Similar procedure was followed to generate '.stl' file of the humerus and clavicle

bones. A combination of 3D scanning and digital software was used to scan the complicated objects surface and construct an object with sharpened edges such as humerus, clavicle and scapula.



(a) Scanning Image of Clavicle



(b) .stl Model of Clavicle

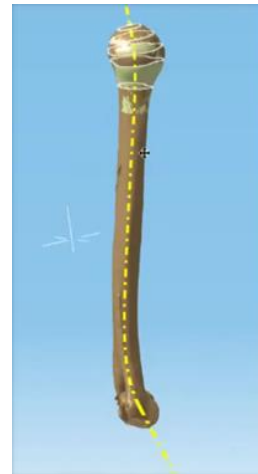
Fig. 3.7 3D Scanning Procedure to Generate Clavicle Bone

3.2.2 3D CAD Modeling of Shoulder Bones

The .stl file was imported in CATIA V5 software to generate a 3D shoulder bone model. Importing the raw data into the CAD system resulted into generation of one or more cloud points (discrete points of the bone, which are scanned by ATOS III scanner).



(a) Front view



(b) Side view

Fig. 3.8 Points and Spline Curves on the Humerus Bone

Fig. 3.8 shows the higher order features added to the Humerus bone. The raw point cloud data, acquired from the 3D body scanner, contained a great deal of noise and redundancy and thus required processing in CATIA V5 (Daniel et al., 2011). In the

next phases of reverse modeling, the geometrical features of higher order (curves and surfaces) were modeled. The overlapping and gap in polynomial model was removed by inserting a large number of triangular planar surfaces in between the cloud points and the minor corrections in the shoulder bone models were also done. By using spline curve, a 3D solid model of the shoulder bones was generated (Marko et al., 2011). Fig. 3.9 shows the scapula by adding points and spline curves in the gaps.

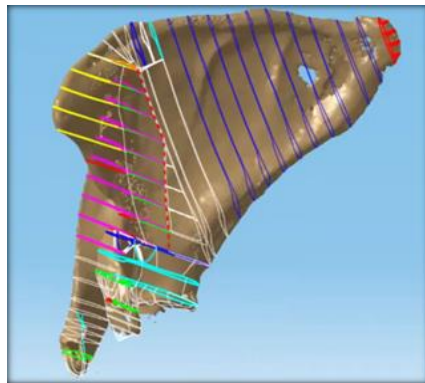


Fig 3.9 Points and Spline Curves on the Scapula

The shoulder bones; clavicle, scapula and humerus were modeled with the intricate details, surface unevenness and with actual contours. The final 3D shoulder bones were ready for assembly after reducing a great deal of noise and redundancy. Fig.3.10 shows final refinement of the shoulder bones before assembly.

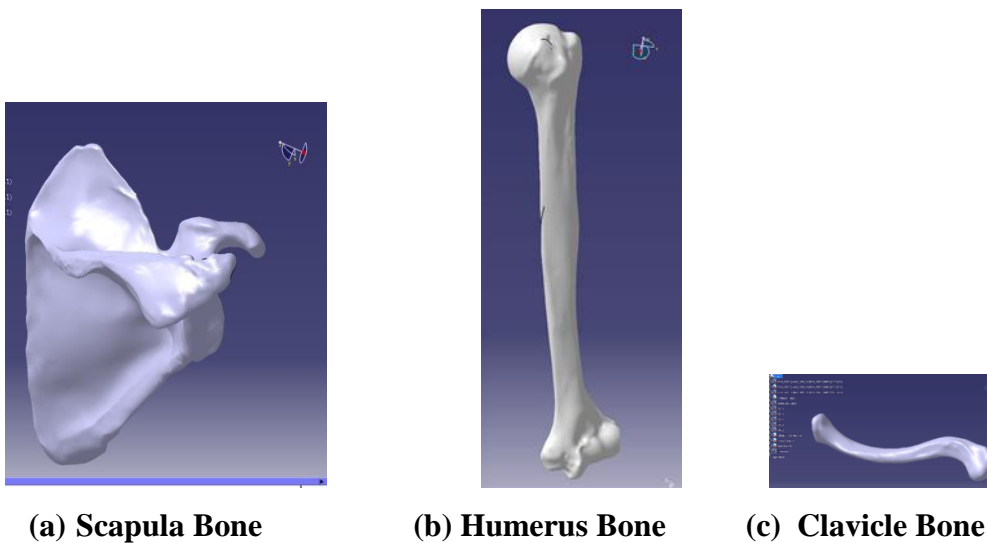


Fig. 3.10 Refinement of the Shoulder Bones in CATIA V5

3.2.3 Assembly and Simulation of Shoulder Joints

The shoulder joint assembly of humerus, clavicle and scapula in pre-defined direction and coordinates, was carried out in Assembly Design Workbench of CATIA V5 software. Fig. 3.11 depicts the shoulder joint assembly in CATIA V5.

The position, orientation, gap between shoulder joints and the axis locations, during abduction arm movement of shoulder were precisely modeled in CAD interface (Van der Helm, 1994). The shoulder can perform six different motions; adduction, abduction, extension, flexion, internal (medial) and external (lateral) rotation. Table 3.1 shows the six shoulder joint assembly movements produced in three different planes.

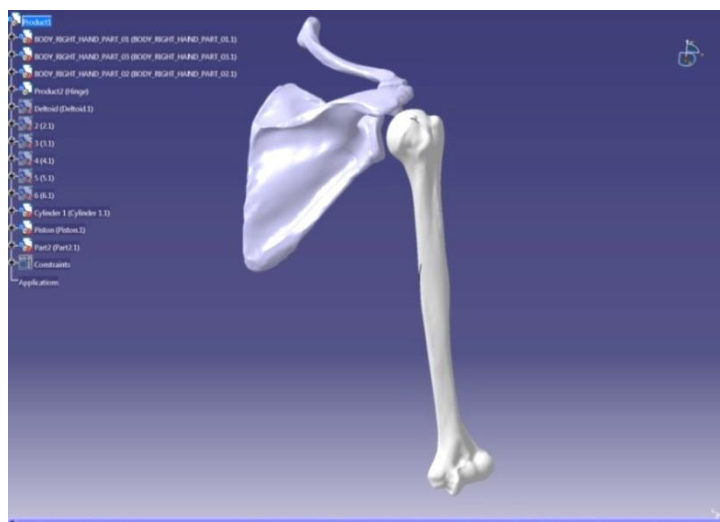


Fig. 3.11 Shoulder Joint Bone Assembly in CATIA V5

Table 3.1 Types of Planes for Shoulder Joint Movement

Plane / Axis of Motion	Physiologic motion	Accessory motion
SAGGITAL	Flexion	Posterior - Inferior
	Extension	Anterior - Superior
CORONAL	Abduction	Inferior
	Adduction	Superior
TRANSVERSE	Internal rotation	Longitudinal-Inferior
	External rotation	Longitudinal-Superior

Each of these movements was restricted by ligaments and moved by the muscles of the shoulder complex. The shoulder has the greatest range of motion amongst any joint in the human body (Hamill and Kuntzen, 2003). The three dimensional view of planes of the shoulder arm movement is shown in the Fig.3.12.

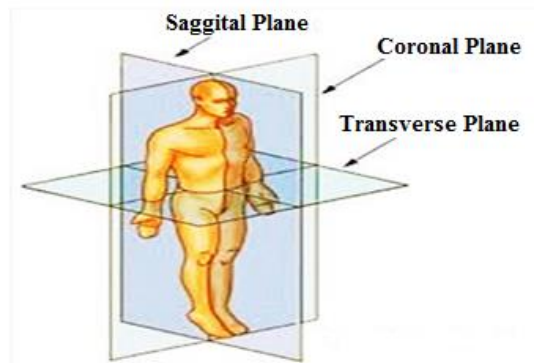


Fig. 3.12 Shoulder Joint Planes of Motion

3.2.4 Contact Constraints

For positioning, orientation and alignment of the three bones, the planes of kinematic motion and the type of contact constraints between scapula and humerus were defined in CATIA interface. The mechanism implying the rotational motion was given to the humerus virtually sliding at surface of glenoid cavity. Fig. 3.13 shows the contact constrains between the humerus and scapula and also the humerus position at 10^0 during abduction arm movement.

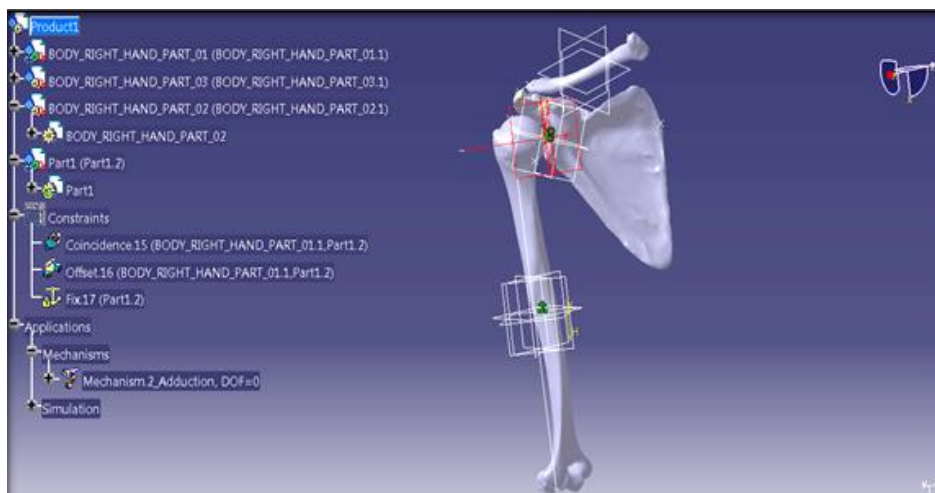


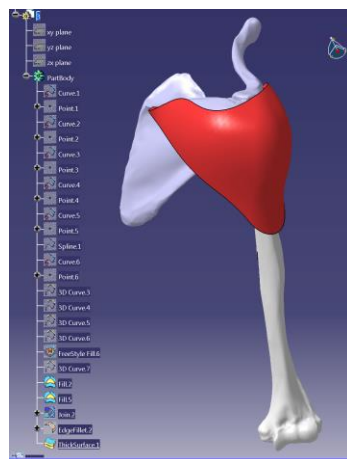
Fig. 3.13 Defining Contact Constraints between Humerus, Clavicle and Scapula

The abduction arm movement was given to shoulder which moves in the frontal plane.

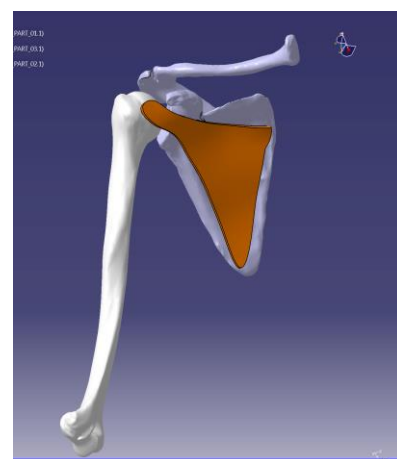
3.2.5 Addition of Muscles on Shoulder Joint

The shoulder model simulation was done to cross-check the interference between humerus, scapula and clavicle bones before adding five muscles to it, during the abduction arm movement from 0° to 130°. Different rotor cuff muscles, namely infraspinatus, supraspinatus, subscapularies, teres minor and deltoid are added on to the shoulder joint. The muscles are modeled as a deformable solid layer that was positioned on the 3D shoulder bones. The initial surface locations of the muscles, its position, and orientation on the shoulder bones were done precisely for developing the correct 3D FEM model (Philippe et al., 2010).

- 1) **Infraspinatus:** The infraspinatus muscle emerges from the medial two-thirds of the infraspinatus fossa, which includes the lower surface of the spine.
- 2) **Supraspinatus:** The supraspinatus emerges from the medial two-thirds of the supraspinatus fossa, which includes the upper surface of the spine.
- 3) **Deltoid:** The deltoid emerges from the lower border of the crest of the spine and from the lateral border of the acromion. The acromial fibers are multipennate.
- 4) **Teres Minor:** The teres minor emerges from the upper two thirds of the rough strip on the dorsal surface along the lateral border.
- 5) **Subscapularies:** The subscapularies emerges from the medial two-thirds of the subscapular fossa. (Romanes, 1986, Anitha, 2010, Webb et al., 2014).



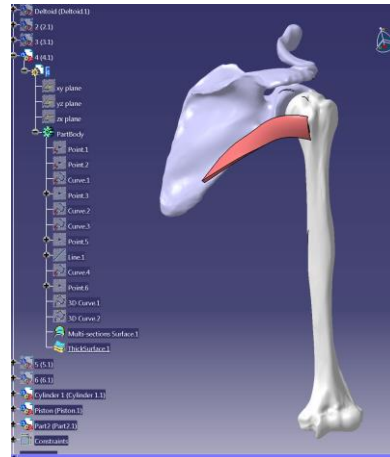
(a) Deltoid Muscle



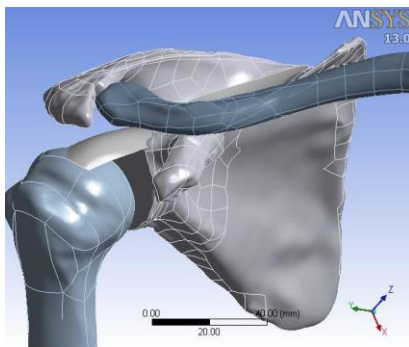
(b) Subscapularies Muscle



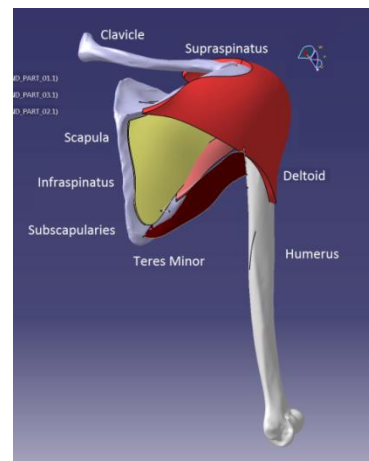
(c) Infraspinatus Muscle



(d) Teres Minor Muscle



(e) Supraspinatus Muscle



(f) Shoulder Muscle Assembly

Fig. 3.14 Origin and Insertion Regions of the Shoulder Joint Muscles

Fig 3.14 shows the origin; insertion region and careful alignment of the five muscles on humerus, scapula and clavicle bones of the shoulder joint (Blemker et al., 2005). Total 58 surfaces were added in humerus to deltoid connection, 28 surfaces in scapula to deltoid and 32 surfaces in clavicle to deltoid. A cup shaped contact between deltoid to shoulder joints was modeled for maintaining the maximum contact in between them.

3.3 FEM ANALYSIS OF SHOULDER JOINT

FEM analysis has significantly upgraded both the standard of engineering designs and the methodology of the design process. The time taken for the engineering products to develop from concept stage to the production line has been significantly reduced by

the use of FEM tool. There are lots of benefits of FEA like improved design, better accuracy and effective prototyping, well insight into critical design parameters, a faster and less expensive design cycle, increased productivity, and increased revenue. ANSYS workbench has robust collection of meshing algorithm and it can be easily integrated with CAD packages for complex geometries.

In the present work FEA Modeling was done by importing the shoulder CATIA model in ANSYS workbench in .igs format. The cleanup tool was used for the corrections of missing data such as edges and corners. The model comprises three major bones and different rotors cuff muscles teres minor, supraspinatus, infraspinatus, subscapularies and the deltoid muscle. The main difficulty in FEA modeling of shoulder assembly was to model it to the level where it should mimic the exact motion of the complex shoulder joint. This was mainly dependent on contact modeling of bones and muscles. Scapula and humerus bones were connected to four rotor cuff muscles and the deltoid. This connection of bone to muscle adds compliance to the pure kinematic motion between the bones, which will further constrains the shoulder joint assembly motion to mimic the real time motion of the shoulder joint. Defining contacts was not that obvious. Difficulties in contact modeling were in its extremely discontinuous force profile which gives abrupt changes in the force. Contact modeling was done in two steps; the contact interface between two bodies was found and then the type of contact between them was defined. Penalty method was used for calculation of contact force in this study. This method allows small penetration, which is a function of its material stiffness. Bigger the stiffness lower is the penetration; more is the abrupt change in the contact force. Lesser stiffness increases the penetration which makes solution never to converge. This is because with too much of penetration, solver applies huge penalty force. This excessive penalty force pushes contact part out of the orbit. Then solver tries to correct it by bisection (applied load is cut to half and tries again), this problem continues with multiple bisections, which never converges, and also too much of contact stiffness also leads to problems with convergence. Tackling this issue was a tricky task, which requires some iterations as in the present case muscle is having much lower stiffness than bones. For this, one has to ensure that two parts should have initial contact, but that should not be excessive. This requires modification of

contact interface, area and initial penetration many a times. The insertion region of the five muscles on humerus, scapula and clavicle were cross checked before exporting it in to the ANSYS APDL solver for the Von Mises stresses and the equivalent elastic strain analysis.

3.3.1 Material Properties

The accuracy of the results obtained in any analysis depends upon its material properties. The different laws and mechanical properties used in the present shoulder model are depicted in table 3.2.

Table 3.2 Different Laws and Mechanical Properties Used in the Shoulder Model (Masami, 2001, Astier et al., 2007, Alexandre et al., 2014)

Element	Type of laws	Poisson's Ratio	Young's Modulus	Density
			MPa	Kg/m ³
Bone	Linear Elastic ,non-homogeneous	0.3	15000	1800
Muscles	nonlinear hyper elastic laws, incompressible	0.45	1.2	1000

3.3.2 Loading Conditions

The efficacy of the Glenohumeral joints model i.e. humerus, clavicle, scapula depends on the positioning, orientation and maintaining proper gap amongst the three bones during abduction arm movement (Van der Helm, 1994).

Fig 3.15 shows the abduction and adduction exercise of the shoulder joint. The axis of rotation of humerus was tested against the interference with scapula and clavicle during the abduction arm movement.

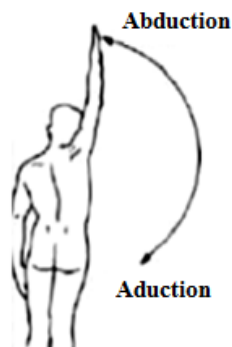


Fig. 3.15 Shoulder Adduction and Abduction Arm Movement

A. Abduction of the arm. Lateral rotation of the scapula is produced by the upper (1) and lower (2) fibres of trapezius, combined with the lower fibres of serratus anterior (3). Abduction at the shoulder joint is produced by supraspinatus (6) and deltoid (5). When deltoid contracts, it tends to pull the humerus upwards against the acromion (9). This is prevented by teres minor (4) which does not interfere with the abduction of the humerus because it is attached to the humerus on the axis of abduction (7). 8 is the axis of scapular rotation.

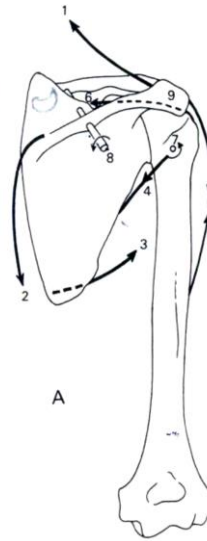


Fig. 3.16 Shoulder Model Efficacy for its Position, Orientation, Rotational Movements and Direction of Pull during Abduction Arm Movement

Fig. 3.16 shows the direction of pull of the various muscles during abduction arm movement. The shoulder bone orientation and alignment was done with utmost care and each bones axis and gap between them was properly maintained (Romanes et al., 1986). Fig. 3.17 shows the shoulder arm abduction simulation from 0° to 130° ROM.

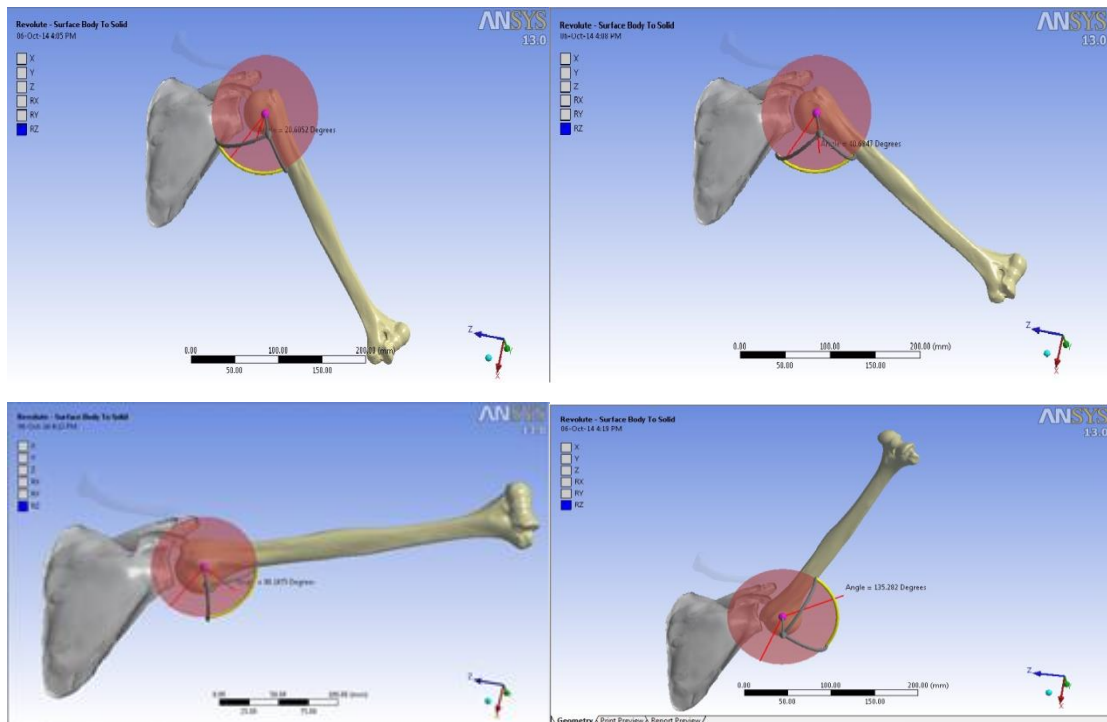


Fig. 3.17 Shoulder Joint Abduction Arm Simulation from 0° to 130° ROM

The analysis is done for the post-operative exercise (abduction) therefore no external load is applied on the model; only self-weight of the arm acting on the joint between humerus and scapula is considered in the analysis. Simulation of the cortical bone humerus with respect to muscles, ligaments and two bones scapula and clavicle is done.

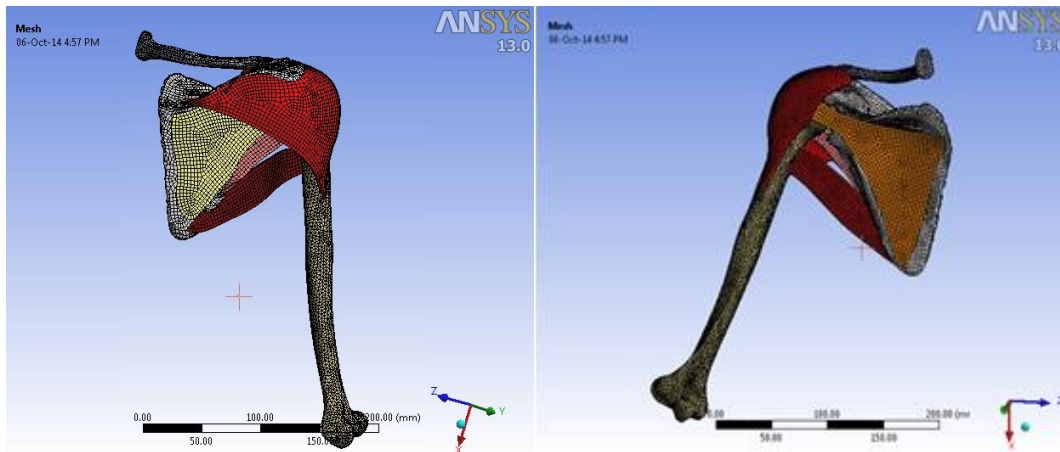
3.3.3 Meshing of the 3D model

Meshing of the model was done after setting the material properties as mentioned in the previous sections. Hexahedral (8 node) and tetrahedral (4 node) 3D solid elements mesh was incorporated in the present model. The mesh requirement for the soft biological tissue that undergoes a large deformation is quite different from the pure mechanical heat transfer and fluid flow problems (Fleishmann et al., 1999). The quality of the tetrahedral mesh has a profound influence on both the accuracy and efficiency of these simulations. So, wherever required the mesh modifications are done by using mapped meshing technique to keep the model within quality criteria. After meshing the bones and muscles the number of nodes and elements generated are depicted in the table 3.3.

Table 3.3 Summary of Number of Nodes and Elements Generated in Shoulder Muscle Joint FEM Analysis

Muscle	Nodes	Elements
Deltoid	33676	23663
Infraspinatus	33167	23115
Subscapularies	33068	23051
Teres minor	32517	22527
Supraspinatus	33392	23363

In this study, iterative process to improve the results was used, until convergence is reached. In the problems with identified exact solutions, evaluating convergence of an FEA is quite forthright. On this ground, three mesh sizes were used, and model is analyzed for von-Mises stresses convergence. To start with (course) economical mesh size of 5 mm was used to mesh the model with mapped meshing. Then, element size is reduced by 2mm and then by 1mm to see the rate of convergence up to least size of 1mm mesh. The meshed shoulder model with all muscles is depicted in Fig. 3.18.



(a) Front End of the Model (b) Rear-End of the Model.
Fig. 3.18 Shoulder Joint Meshed Model with all Five Muscles

The solution is considered to be converged at 1mm mesh size. The percentage variation between von-Mises stress was 8%. But this was not economical mesh size as it took huge computation time. So, another trial with 3 mm mesh size was done and convergence was checked. It gives an optimum combination of convergence with the computation time. It has given the 15% variation with desired results with considerable reduction in computation time. So, 3mm mesh size was used in the present analysis.

First deltoid muscle analysis was done by freezing the other four muscles; the Von Mises stresses and equivalent elastic strain were computed for full range of motion during abduction arm movement. The initial position of the shoulder model for the analysis was taken at vertical downward direction. Then the humerus along with the deltoid muscle was rotated from 10° to 80° at the interval of 10° . The simulation was done in eight steps in eight seconds and each second corresponds to 10° rotations, the motion was chosen to be pure rotation. Five probes were added at five different points in the muscle and the maximum Von Mises stresses and equivalent elastic strain were considered as a final result and are tabulated in the next chapter.

Similarly individual muscle analysis was carried out by freezing the remaining four muscles during the abduction arm movement. Finally the group muscle analysis of the shoulder joint including all the five muscles (rotator cuff muscles and deltoid muscle), was done during the abduction arm movement.

3.4 3D MODELLING OF KNEE BONES

Knee is one of the most complex and maximum used joint in the human body. Stability of the knee joint is a one of the critical aspect which is provided by the muscles and ligaments. Knee joint muscles are the complex fibrous structure surrounded by different tissues and blood vanes (Carol, 2009). Accurate topology of all the knee bones and muscles is a key to create a valid and accurate 3D knee model, which will be useful for the orthopedic surgeon during pre-operative planning. Therefore, it is logical to base the process of geometrical modeling of the human joints on its anatomical and morphological properties (Marko et al., 2011).

3.4.1 3D Scanning of Knee Bones

Similar procedure was adopted to generate a 3D knee joint model. The irregular shape of the femur, tibia, fibula and patella hampers the feasibility of the modeled profile. The free form option in CATIA V5 does not prove to be much useful, as the dimensions and bone contour changed from person to person with different age groups. Moreover, the minute detailing required during the modeling of ligaments, tendons and muscles is not easy using surface modeling. Fig.3.19 shows the scanning process of tibia knee bone by 3D scanner.

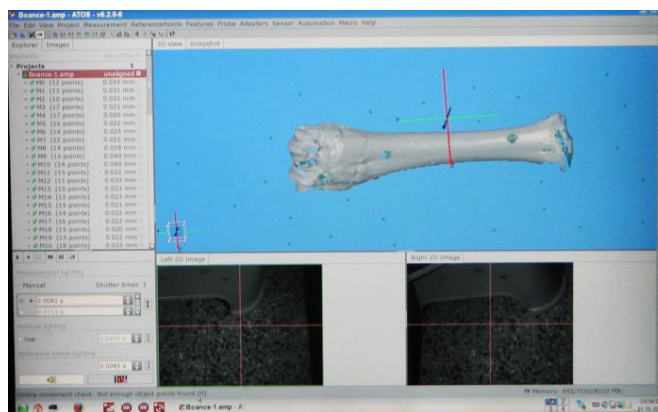


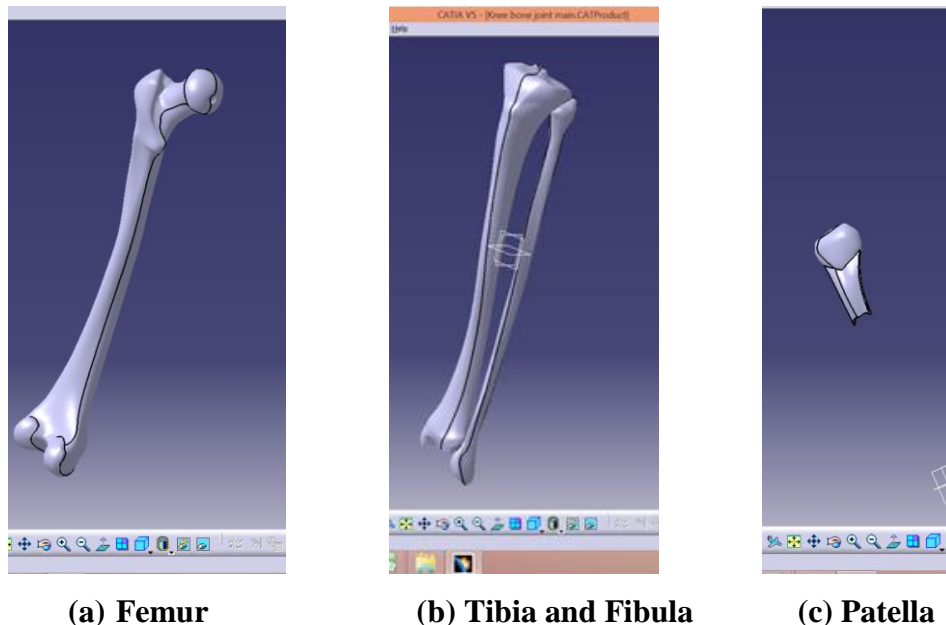
Fig. 3.19 3D Scanning of the Tibia by using ATOS III Scanner

Several attempts to capture these muscular parts in CATIA turned out to be a debacle. Thus, 3D scanning of the bones to obtain a point-cloud is finalized for the knee bone modeling (Marco et al., 1998).

The knee joint bones femur (thigh bone), tibia (shin bone), fibula (calf bone) and patella (kneecap) were scanned by 3D scanner. The scanned object then imported into geomagic studio and all points outside the relief area were deleted and various scans have been merged into single data. Thinning of the object was done to reduce the total number of points by deleting surplus points in repeatedly scanned areas. To generate an accurate and detailed model, shape-cleaning algorithm was used. Finally ‘.stl’ file of scapula was generated. In the present work ATOS III a non-contact 3D lasers scanner was used from Arun 3D Labs, Pune, India. The specifications of ATOS III 3D scanner and the procedure are described in the **Appendix I**.

3.4.2 3D CAD Modeling of Knee Bones

The ‘.stl’ files were imported in CATIA V5 software to generate a 3D CAD model for further analysis. Importing the raw data into the CAD system resulted in to generation of one or more cloud of points in the bones (discrete points of the bone, which are scanned by ATOS III scanner). The raw point cloud data, acquired from the 3D body scanner, contained a great deal of noise and redundancy and thus required processing in CATIA V5 (Daniel et al., 2011). Fig.3.20 shows the refined knee joint bones.



(a) Femur (b) Tibia and Fibula (c) Patella
Fig. 3.20 Refinement of the Knee Joint Bones in CATIA V5

In the next phases of reverse modeling, the geometrical features of higher order (curves and surfaces) were modeled. The overlapping and gap in polynomial model

was removed by inserting a large number of triangular planar surfaces in between the cloud points and corrections in the knee bones were done. By using spline curve 3D solid model of the knee bones were generated (Marko et al., 2011).

The knee bones; the femur, tibia, fibula and patella were modeled with the intricacy, surface unevenness and with basic contours. The final knee joint bones were ready for the assembly after reducing a great deal of noise and redundancy.

3.4.3 Assembly and Simulation of Knee Joints

Assembly of femur, tibia, fibula and patella in pre-defined direction and coordinates, was carried out in Assembly Design Workbench of CATIA V5 software. The position, orientation, gap between knee joints and the axis locations, during flexion leg movement of knee joint we precisely modeled in CAD interface (Van der Helm, 1994). Fig.3.21 shows the final knee joint assembly in CATIA.

The simple rotary motion was given to the knee model to perform flexion leg movement in a single plane. The knee ligaments resist the motion along the single line similar to rubber or rope. Positioning, orientation and alignment of the four bones were precisely done by defining the planes of kinematic motion in CATIA user interface and defining the type of contact constraints between femur, tibia, fibula and patella.

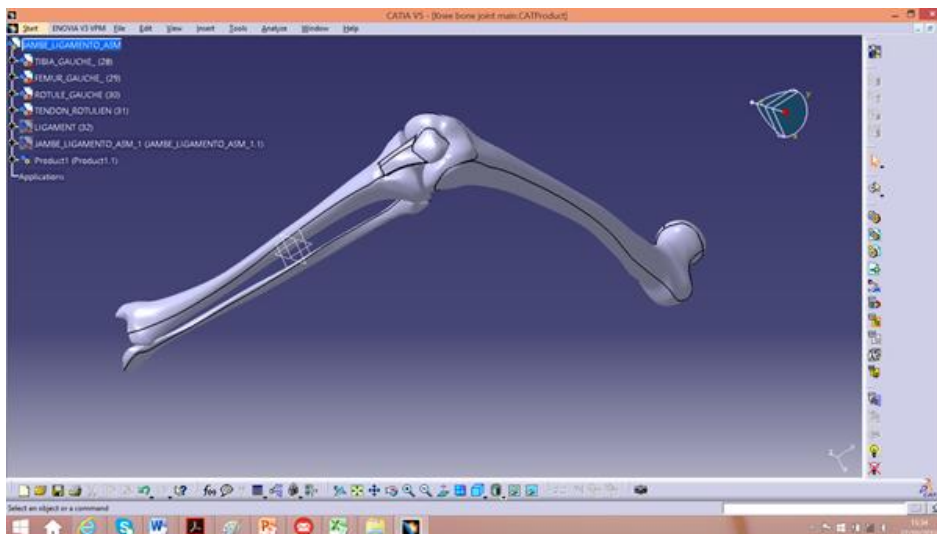


Fig. 3.21 Knee Joint Assembly in CATIA

3.4.4 Addition of Muscles on Knee Joint

The knee model simulation was done to cross-check the interference between femur tibia, fibula and patella bones before adding two muscles to it; during the flexion leg movement from 0° to 120°. Fig 3.22 and Fig.3.23 shows the positions and orientations of the knee joint muscles from front and side view.

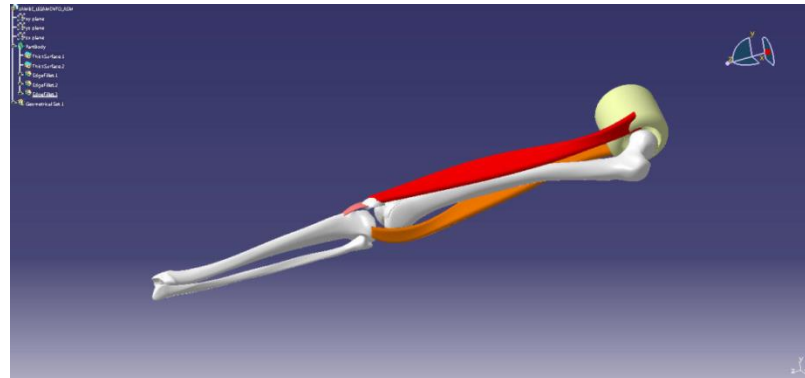


Fig. 3.22 Front View of the Knee Joint with Rectus Femoris and Biceps Femoris

The muscles were modeled as a deformable solid layer, which is positioned on the 3D knee bones. The initial surface locations of the muscles, its position, and orientation on the knee bones were effectively done in developing the correct 3D knee model (Philippe et al., 2010).

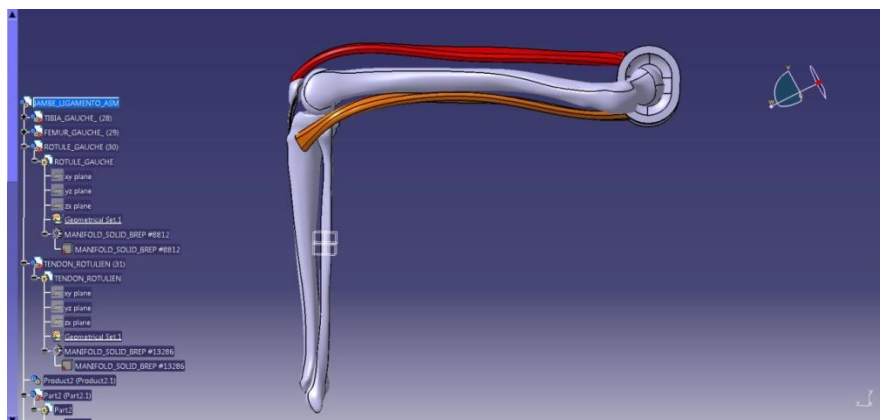


Fig. 3.23 Side View of the Knee Joint with Rectus Femoris and Biceps Femoris

- 1) **Rectus Femoris:** It is situated at the center of the thigh (on the patella); it is cylindrically shaped at the center, its width narrows down at the ends and running straight down to the deep Apo-neurosis.

- 2) **Biceps Femoris:** It originates from the back side of the fibula and passes obliquely downward and lateral across covering the posterior surface of the femur bone to connect on the back end of the hip. It is twisted; cylindrical in shape at the center and its width narrows down at the bones contact.

The origin, insertion region and careful alignment of the two muscles on femur, tibia, fibula and patella were modeled in CATIA interface. Total 11 surfaces were added in patella to rectus femoris connection, 9 surfaces in rectus femoris to the hip connection, 7 surfaces in tibia to biceps femoris connection and 9 surfaces biceps femoris to hip connection. The proper twist and gap was maintained between the knee joints maintaining the maximum contact in between them.

3.5 FEM ANALYSIS OF KNEE JOINT

FEM analysis for the knee muscle is one of the most reliable methods to predict the behaviour of displacements and strain in the human joint using transversely hyper elastic constitutive law. In the present work knee muscle stress analysis is done by using the FEM model during flexion leg movement.

FEA stress analysis was done by importing the knee CATIA model in ANSYS workbench in .igs format and clean up tool was used for the missing data corrections such as edges and corners. The 3D model comprises four major bones femur, tibia, fibula, patella and two muscles rectus femoris, biceps femoris. The major difficulty in FEA modeling of knee assembly was to model it to the level where it should mimic the exact motion of the complex knee joint. This is mainly dependent on the surface contact modeling of bones and muscles. There are two types of contacts, which were modeled for this study.

- 1) **Bone to bone contact:** Femur bone is to be connected to tibia and fibula through patella (knee cap) in such a way that it should mimic the movement of actual knee joint.
- 2) **Bone to muscle contact:** Femur bone is to be connected to rectus femoris muscles and tibia, fibula is to be connected to biceps femoris muscle. This connection of bone to muscle adds compliance to the pure kinematic motion between the bones.

This will further constrain the knee joint assembly motion to mimic the real time motion of knee joint.

But, defining surface contacts between bones and muscles was not that obvious as it is seen. Difficulties in contact modeling were in its extremely discontinuous force profile which gives abrupt change in force. Modeling a contact was done in two steps; the contact interface between two bodies was found and then the type of contact between them was defined. Penalty method was used for calculation of contact force. This method allows small penetration, which is a function of its material stiffness. Bigger the stiffness lower is the penetration and more will be the abrupt change in the contact force. Lesser stiffness increases the penetration which makes solution never to converge. This is because with too much of penetration, solver applies huge penalty force. This excessive penalty force pushes contact part out of orbit. Then solver tries to correct it by bisection (applied load is cut to half and tries again), this problem continues with multiple bisections, which never converges and also too much of contact stiffness also leads to problems with convergence.

Tackling this issue was a tricky task, which requires some iterations as in the present case muscle was having much lower stiffness than bones. For this, one has to ensure that two parts should have initial contact, but that should not be excessive. This requires modification of contact interface, area and initial penetration many a times. The insertion region of the two muscles on femur, tibia, fibula and patella were cross checked before exporting it in the ANSYS APDL solver for the Von Mises stresses analysis.

3.5.1 Material Properties

The accuracy of the results obtained in any analysis depends upon its material properties. The different laws and mechanical properties used in the present knee model are depicted in table 3.4.

Table 3.4 Different Laws and Mechanical Properties Used in the Knee Model (Yunfeng et al., 2012; Adouni et al., 2013; John et al., 2013)

Element	Type of laws	Poisson's Ratio	Young's Modulus MPa	Density Kg/m ³
Bone	Linear Elastic ,non-homogeneous	0.38	12000	1800
Muscles	nonlinear hyper elastic laws, incompressible	0.45	4	1000

3.5.2 Loading Conditions

The knee joint orientation, alignment and the gap between the bones was done with utmost care. As discussed earlier for the 3D muscle-bone model; the detailed FEA modelling, like contact definition and joint definition were defined.

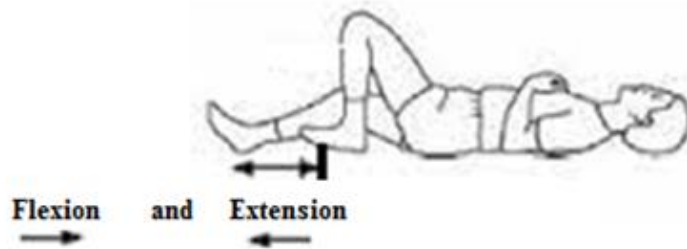


Fig. 3.24 Knee Flexion and Elevation Leg Movement

In the flexion, the leg was moved inwards along the single plane of the body. Normal range of motion for flexion of the knee joint is 0° to 120° . Fig. 3.24 shows the flexion and elevation exercise of the knee joint.

The axis of rotation of tibia was tested against the interference with femur, patella and fibula for flexion, from 0° to 120° as shown in Fig. 3.25.

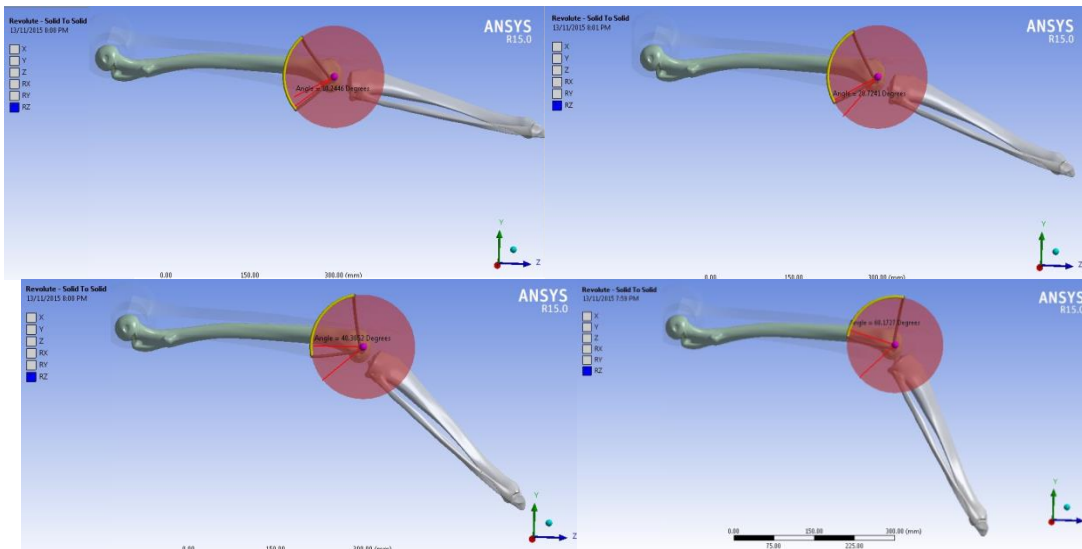


Fig. 3.25 Knee Joint Flexion Simulation in ANSYS for 0° to 60° ROM

The analysis was done for the post-operative exercise (flexion) therefore no external load was applied on the model, only self-weight of the leg acting on the joint between femur, tibia, patella and fibula was considered in the analysis. Simulation of the tibia bone with respect to muscles, ligaments and two bones hip and femur was done.

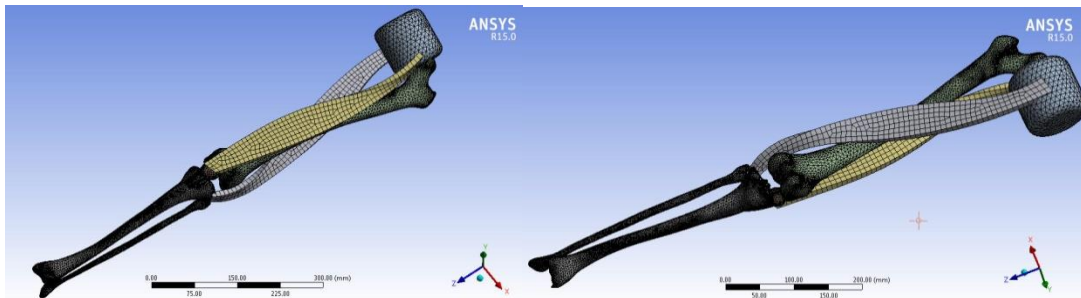
3.5.3 Meshing of 3D Model

Meshing of the model was done after setting the material properties as mentioned in the previous sections. Hexahedral (8 node) and tetrahedral (4 node) 3D solid elements mesh was incorporated in the present model. The mesh requirement for the soft biological tissue that undergoes a large deformation is quite different from the pure mechanical heat transfer and fluid flow problems (Fleishmann et al., 1999). The quality of the tetrahedral mesh has a profound influence on both the accuracy and efficiency of these simulations. The mesh modifications were done by using mapped meshing technique to keep the model within quality criteria. After meshing the bones and muscles the number of nodes and elements generated are depicted in the table 3.5.

Table 3.5 Summary of Number of Nodes and Elements Generated in Knee Muscle Joint FEM Analysis

Muscle	Nodes	Elements
Rectus femoris	375312	249990
Biceps femoris	375312	249990

The meshed knee model with rectus femoris and biceps femoris muscles are depicted in Fig 3.26.



(a) Front End of the Knee Model (b) Back-End of the Knee Model

Fig. 3.26 Knee Joint Meshed Model with Rectus and Biceps Femoris Muscles

Similar to shoulder joint analysis, the mesh convergence for knee joint model was done and the knee model has converged to 3mm mesh size for von-Mises stresses. The Von Mises stresses in the knee muscles was computed for full range of motion during flexion leg movement. The initial position for the analysis was taken as a horizontal plane. Then the tibia along with the knee muscles was rotated inwards along the single plane of the body from 10° to 90° at the interval of 10° . The simulation was done in nine steps in nine seconds and each second corresponds to 10°

rotations and the motion was chosen to be pure rotation in a single plane. The final analysis of the knee joint including rectus femoris and biceps femoris muscles was done for the same angle of rotation to compute the Von Mises stresses.

3.6 CPM MACHINE FOR SHOULDER AND KNEE JOINT

Joint injuries and surgery is one of the difficult conditions in any one's life. It is very difficult to move the joints immediately after the surgery due to aching in the joints. This is due to immobilization and the scar tissue formation around the joint thus the joint becomes stiff. This prolongs the healing time of the tissues around the joints and requires months of physical therapy to regain the original ROM for the patients. CPM therapy is one of the well-known procedures for healing the human joint and to reduce the recovery time. Due to use of CPM machine joint receives nutrition, venous flow increases and deterioration of cartilage is prevented. In addition, pain is decreased, range of motion is maintained and recovery is accelerated (Shawn et al., 2002). CPM machine is one of the applications of the medi-mechatronics branch, in which mechanical engineering devices are controlled by electronics circuits for the medical application.

In the present work an attempt has been made to design, develop and test the low cost shoulder and knee Continuous Passive Motion (CPM) machine for the clinical rehabilitation of injured shoulder and knee joints. By using motorized device the shoulder and knee CPM machine can gradually move the joints in predefined range of motion (ROM). Otherwise, it is not possible for the patients to move the joint actively due to the pain. This motion is called passive because the patient is not using his muscular effort during the exercise on the machine.

3.6.1 Shoulder CPM Machine

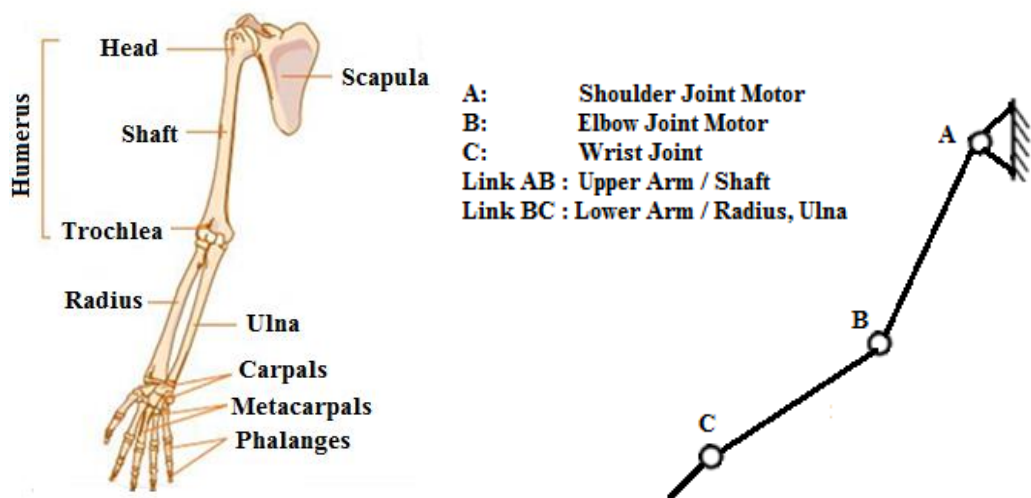
The shoulder joint is one of the most critical joint as it consists of maximum degrees of freedom being a ball and socket nature. Shoulder CPM is used to perform different exercise known as adduction, abduction, extension, flexion, internal (medial) and external (lateral) rotation. Table 3.6 shows normal range of motion of shoulder joint.

Table 3.6 Normal Range of Motion for Shoulder Joint Exercise

Shoulder Exercise	Range of Motion
Abduction/Adduction	0 ⁰ to 175 ⁰
Internal/External rotation	-90 ⁰ to 90 ⁰
Flexion/Elevation	0 ⁰ to 175 ⁰

From the shoulder anthropometric data, the mean values of forearm length (0.25m), upper arm length (0.30m) and weight of the arm (5.25 Kg) were used in the present work for the calculations of the total power required to move the shoulder arm assembly (Holen, 1936; Ronald, 2013).

Though open and closed kinematic chain mechanism are used for the different exercise of the human joints. Open kinematic chain (OKC) is the best approach for the shoulder joint motions as the movement is happening through a single joint (Glenohumeral joint). Open kinetic chain exercises are usually performed in a non-weight bearing position and allows involved limb to move freely on the post-operative shoulder joint. Open kinematic chain analysis was used to find out the motor ratings for the CPM machine. The analogy of shoulder joint skeleton and open kinematic chain is shown in Fig. 3.27.



(a) Shoulder Joint Skeleton (b) Schematic Diagram of Shoulder Machine

Fig. 3.27 Open Kinetic Chain for Shoulder CPM Machine

3.6.1.1 Motor Design (M_1)

The circulatory motion was to be imparted on the shoulder joint, which can be obtained from the open kinematic chain mechanism. In the open kinematic chain mechanism one of the links is connected to the driving unit such as the motor (M_1) to have the rotating motion. This constitutes the higher pair with the other links which gives rise to the rotary motion to the shoulder arm assembly.

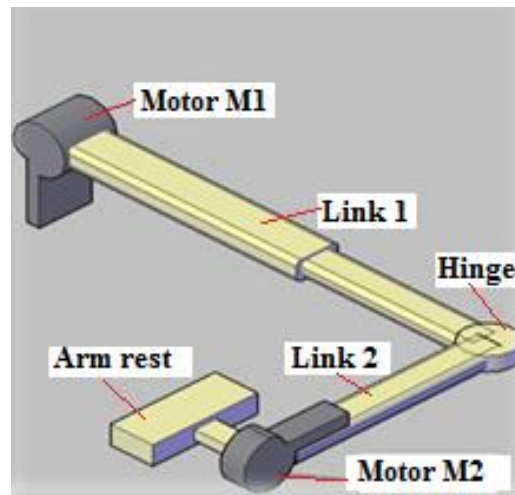


Fig. 3.28 CATIA Model of the Shoulder Arm with Motor M_1 and M_2

Fig. 3.28 shows the CATIA 3D model of the shoulder arm of shoulder CPM machine. Motor M_1 helps in adduction and abduction range of motion. The dead weight of the arm was 52 N and the weight of all the linkages from upper arm link (L_1) to fore arm link (Link L_2) and motor M_2 was 27.45 N; so the total weight of the shoulder arm assembly acting on the motor M_1 will be 79.45N. These weights were uniformly distributed over the upper and forearm assembly.

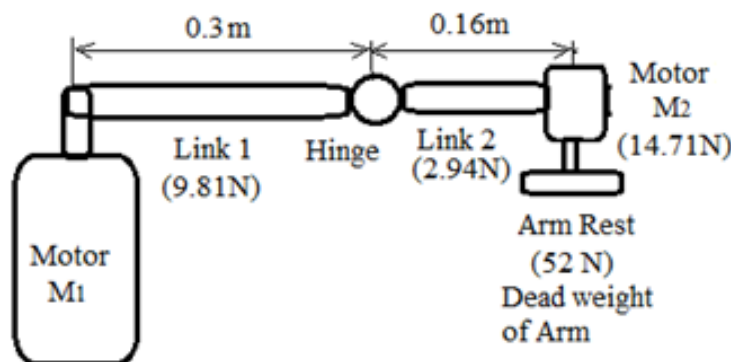


Fig. 3.29 Schematic Representation of Shoulder Arm of the CPM Machine

Fig.3.29 shows the schematic representation of shoulder arm of the CPM machine. The schematic representation of the shoulder arm assembly with upper arm and lower arm linkages is as shown in Fig.3.30. The bending moment and the torque were calculated to find the equivalent torque for the selection of motor M_1 .

Bending Moment (M)

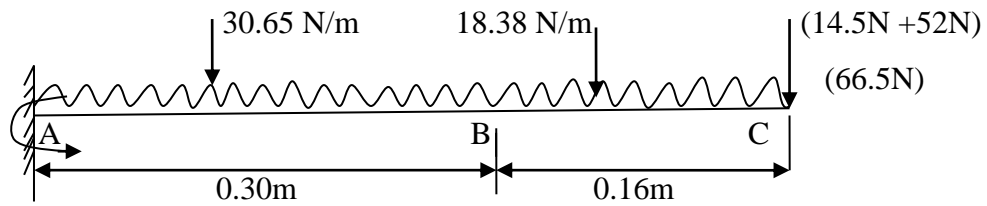


Fig. 3.30 Loading Diagram for Motor M_1

Taking moment about point A

$$30.65 \times \frac{0.3^2}{2} + (18.38 \times 0.16) \times \left(0.3 + \frac{0.16}{2}\right) + 66.5 \times 0.46 - M_A = 0 \quad [3.1]$$

$$M_A = 34.66 \text{ Nm.}$$

The bending moment about point A is $M = 34.66 \text{ Nm}$.

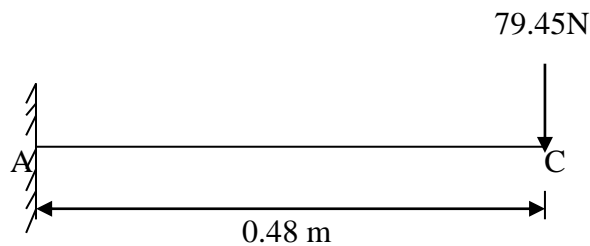


Fig. 3.31 Loading Diagram for Torque Measurement

Torque (T)

As the maximum load is acting at the motor M_2 , for safer design the maximum torque is considered at the load point C, as shown in Fig.3.31.

$$T = \text{Load} \times \text{Perpendicular distance} \quad [3.2]$$

$$T = (79.45 \times 0.48) = 38.04 \text{ Nm}$$

The equivalent torque is given by

$$T_e = \sqrt{M^2 + T^2} \quad [3.3]$$

$$T_e = \sqrt{34.66^2 + 38.04^2}$$

$$T_e = 51.46 \text{ Nm}$$

The motor power is given by

$$P = \frac{2\pi \cdot N \cdot T}{60} \quad [3.4]$$

Where, N= rpm (revolution per minute) of the motor shaft.

T=Torque required to take the load (Nm)

$$P = \frac{2\pi \times 6 \times 51.46}{60}$$

$$P = 32.33 \text{ W}$$

In order to practice standardization, from the manufacturer's catalogue, the next suitable motor available is of 40 Watt power. Selecting a motor of 40 Watt maintains the available factor of safety to 1.25.

The bending failure of the shaft for static load condition

$$\sigma_b = \frac{M}{Z} \quad [3.5]$$

$$\sigma_b = \frac{(\text{Shaft Length} \times \text{Total Weight of the arm})}{\frac{\pi}{32} d^3}$$

From the stepper motor catalogue diameter of the shaft was 10 mm and shaft length was 20 mm and the total weight of the shoulder arm assembly is 79.25 N.

$$\sigma_b = \frac{20 \times 79.45}{\frac{\pi}{32} 10^3}$$

$$\sigma_b = 16.18 \text{ N/mm}^2$$

The tensile yield strength of ASIS 304 is 215 N/mm^2 . Therefore the motor shaft was safe for bending. Now the Factor of Safety with respect to bending failure is 13.28 and for medical instruments the factor of safety is in the range of 6 to 10.

The ergonomic aspects of the chair were also taken in to consideration as the machine is used for the post-operative treatment. The comfort of the patient during the post-operative treatment exercise was taken care by proper cushioning of the injured arm,

adjustable fore arm and shoulder arm to accommodate different arm size, adjustable back rest.

3.6.1.2 Electronics Design

The hardware part of the machine is mainly consists of circuit, the power supply PCB, programmable logic control (PLC), motors and electronic components used in the different circuits. The software part consists of the PLC programming.

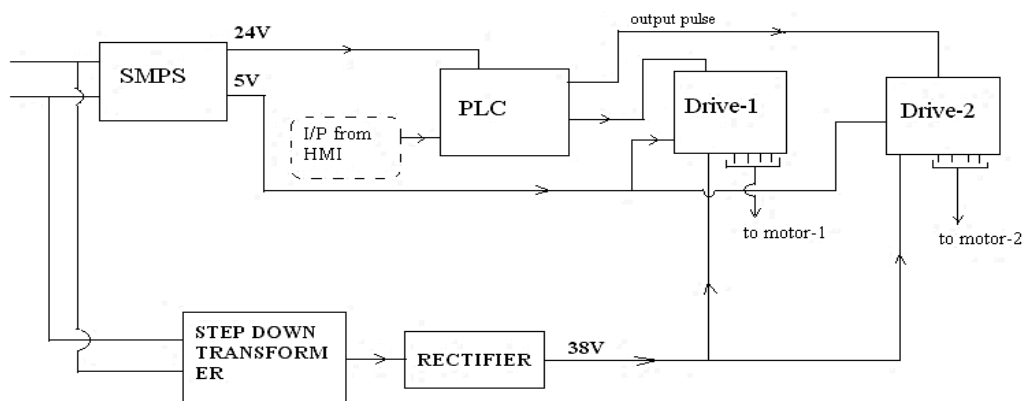


Fig. 3.32 Power Supply Block Diagram and Motor Control Circuit

A switched mode power supply (SMPS) was used in the CPM machine for supplying power to the PLC through the transformer. It incorporates a switching regulator to convert electrical power efficiently. The power supply diagram and motor control circuit is as shown in the Fig.3.32.

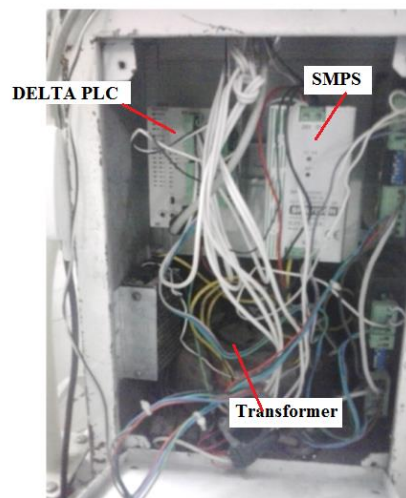


Fig. 3.33 Rear View of Stepper Motor and PLC Control Unit

Motor circuit and its control are very important and difficult aspect of the electronics design of the CPM machine. Stepper motors can be easily controlled with PLC; however logic and drive electronics are little bit complex.

Fig.3.33 shows rear view of stepper motor PLC control unit which consists of PLC system, basic functional components of processor unit, memory, power supply unit, input/output interface section, communications interface and the programming devices. Two brushless hybrid stepper motors M_1 and M_2 were used to control the shoulder arm movement as shown in Fig.3.34. The brushless stepper motors were used in the present CPM machine for the smooth and precise movement of the shoulder arm assembly.



Fig.3.34 Hybrid NEMA Make High Torque Motors M_1 and M_2

The stepper motors M_1 and M_2 can be operated in open loop cycle and are easily controlled by the PLC. The use of stepper motors has reduced the cost of the machine by saving the costly sensors use in the system. The hybrid stepper motor M_1 was used to move the entire shoulder arm assembly in one plane (abduction/adduction, Flexion/extension) or in two different planes (internal rotation and external rotation). The unique feature of this motor is that; it can be used at high torque with a precise control at the smaller step angles 1.8° .

3.6.1.3 Fabrication of CPM Machine

The shoulder CPM consists of the following main components backrest, armrest, adjustment for horizontal adduction or abduction, holding tube for height adjustment, holding tube for upper arm length adjustment, locking screw for adjustment of elbow angle, locking screw for adjustment of forearm length, two motors, elbow support,

forearm support and locking pin. Fig. 3.35 shows a shoulder CPM block diagram consisting of all important components in it.

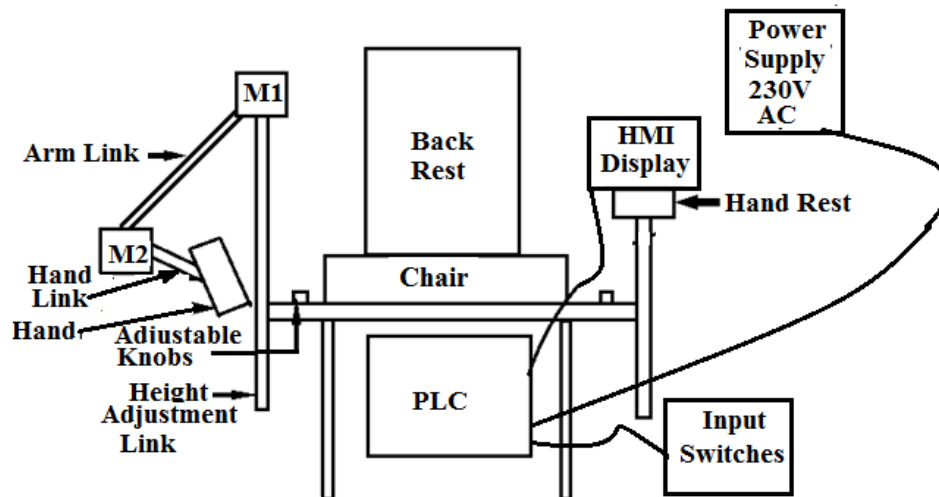


Fig. 3.35 Block Diagram of Shoulder CPM Machine

- a) **Backrest:** The back rest was supported by the natural curve of the spine and 45 mm wide to accommodate the subjects with large variation in size. The backrest is made up of mild steel material on which cushion is pasted by adhesive and covered with resin cloth.
- b) **Holding tube for length adjustment (upper arm):** The vertical upward and downward movement of the holding tube is made to adjust the patients upper arm length of shoulder joint. The material used for the holding tube is carbon steel.
- c) **Seat width and depth:** The seat is made wide and thick enough to support different sized patient to seat comfortably. It is 50 cm wide, 60cm length and 4 cm thick. Leather is used as a cushioning material on the seat of the CPM machine.
- d) **Armrests:** It allows the patient to rest his arm comfortably on the shoulder arm assembly and to keep the shoulder in the relaxed position during the shoulder arm exercise. Its length is 25 cm and 10 cm wide. The forearm rests freely and is sheltered with the cushion.
- e) **Motor (M_1) and (M_2):** Two stepper motors are used to permit fully isolated movements to the arm; i.e. the motors can individually be turned on or off.

M_1 effects adduction, abduction, flexion and extension. M_2 effects internal and external rotation of the arm. Stepper motors are used for actuating the shoulder arm assembly.

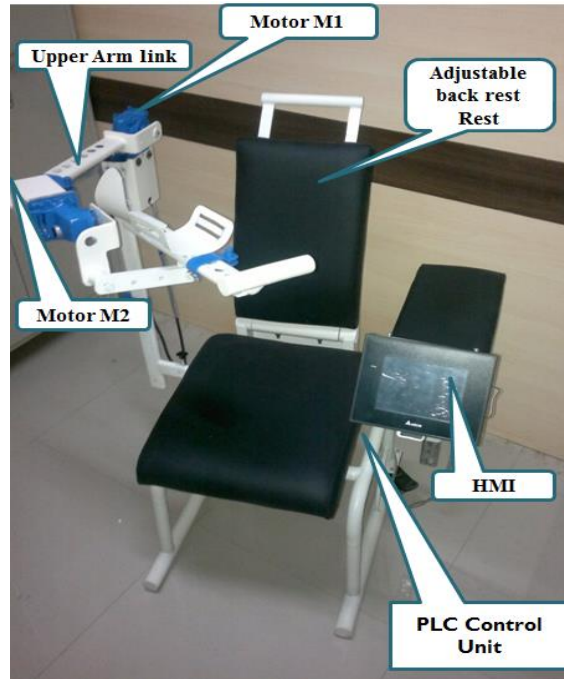


Fig. 3.36 Low Cost Shoulder CPM Machine

- f) **PLC Controller:** Delta PLC DVP 28SV 11T, 28SV PLC with a 28 pointers in column 16 inputs and 12 outputs was used as a control device. The inputs to PLC are given through the human machine interface (HMI).

Fig. 3.36 shows a developed low cost shoulder CPM machine consisting of all important components in it. The total fabrication cost of the machine is 99000/- Rs, (\$1650) (**Appendix II**). The manufacturing cost of the machine is reduced to 40% without compromising its functionality. In the present work CPM machine has been used for performing different shoulder exercises for the muscle contraction analysis using the SEMG. The maximum rehabilitation centers in India can afford this CPM machines, which will reduce the cost of the CPM therapy and ultimately the shoulder injured patients will get benefited. The machine has fulfilled all the requirements of the shoulder therapy such as abduction, adduction, elevation, flexion, internal rotation and external rotation.



(a) Motor casings, holding tubes and rollers



(b) Welding of the plates



(c) CPM chair base and holding tubes



(d) Shoulder arm rest



(e) Rear top view of CPM machine



(f) First run of CPM machine

Fig. 3.37 Shoulder CPM Fabrication from Raw stage to the Finished Product

Fig. 3.37 shows a developed low cost shoulder CPM machine from raw stage to the finished product. The CPM machine was first tested on the normal shoulder for two weeks to crosscheck its functionality and consistency for different shoulder arm exercises. Then the trial was conducted under the supervision of an orthopedic surgeon on the shoulder pain patients. After proving its reliability and satisfying the shoulder physiotherapy requirements, the CPM machine was put to effect on the post-operative patients. Total fifty subjects were exercised on this CPM machine for different shoulder arm exercises. The development of low cost CPM machine is one of the important findings of the present work. The Orthopedic surgeon has approved this machine for the shoulder exercise (**Appendix XI**). This machine is an important part of a physiotherapy center in Dr. Metan Hospital Orthopedic & Neurology Center, Solapur, India.

3.6.1.4 Testing on the CPM Machine

In this study, fifty asymptomatic subjects of different age group and gender, having shoulder pain or undergone shoulder surgery; were tested on the shoulder CPM machine in Dr. Metan Hospital Orthopedic & Neurology Center, India. Subjects were exercised on CPM machine through series of motions for different exercises, such as adduction, abduction, flexion, elevation, internal rotation and external rotation for 2 to 3 weeks. The improved range of motion and reduced pain after the two weeks of CPM treatment are the main outcome measures.

Procedure:

As per the instructions from the orthopedic surgeon, the scales of different exercises were set. The therapy prescription such as type, frequency, and duration of the therapy; goals of therapy; and safety precautions were considered while exercising on the machine. The procedure carried out for different exercises on the developed shoulder CPM machine is explained as follows.

- 1) On the first day subject was trained to use the CPM by the physiotherapist, giving self-demonstration and a trial run.
- 2) Subject was made to sit on the CPM chair, accordingly the height of the arm rest was adjusted, so that the motor M_1 would be in line with the shoulder joint. The precaution was taken that forearm link and upper arm link were kept parallel to

the shoulder forearm and upper arm of the subject during the exercise. This made the subject feel comfort during the exercise.

- 3) The physiotherapist and the orthopedist have decided the dose and duration of the treatment.
- 4) As per instructions of physiotherapist, the required exercise was selected on the control panel and the upper limit of ROM was set for the exercise. The number of iterations was given as per the need of the therapy. Emergency switch was given to the subjects, in case of excess pain. In case of power failure during the exercise the battery backup was provided for uninterrupted exercise.
- 5) Once the subject got comfortable and knowledgeable with the first exercise cycle, then the same cycle was repeated. The angle was increased on daily basis to attain normal ROM, depending upon the patient's pain.
- 6) The exercise was conducted for two weeks and the ROM progress was noted and discussed with the subject.

The CPM machine was conceded throughout a series of motions from 30° to 175° at the progression of 5° , until a normal range of motion is achieved. Subject's progress report was generated and one of the sample reports is explained in the result section. In the report a gradual increase in ROM and pain scale is measured on daily bases. Fig. 3.38 shows the shoulder joint exercise on developed shoulder CPM machine in Dr. Metan Hospital Orthopedic & Neurology Center, Solapur, India.



Fig. 3.38 Shoulder Joint Exercise on Developed CPM Machine

The shoulder pain was evaluated by Visual Analogue Scale (VAS) pain technique. One of the VAS methods, Shoulder Pain and Disability Index (SPADI) was used to assess the pain in the shoulder during the exercise (**Appendix III**). This self-administered questionnaire uses 13 questions, five of which deal with the severity of pain on various arm movements, the pain being assessed by using VAS. The remaining eight questions deal with functional impairment of the shoulder, assessed with a VAS ranging from 0 (no difficulty) to 10 (so difficult that I need help). An overall score was calculated for the 13 questions as a whole. The same procedure to evaluate the shoulder pain was used by few researchers (Yesim et al., 2013, Huskisson et al., 1976). Higher scores indicate a greater level of pain and disability (Biçer et al., 2010).

The ROM was directly set on the HMI display for the different exercise. The motor speed was varied from 1 rpm to 3rpm depending upon the subject's response to the recovery. The displaced angle in radian per second is given by

$$\omega = \frac{2 \cdot \pi \cdot N}{60} \quad [3.6]$$

$$\omega = \frac{2 \cdot \pi \cdot 1}{60}$$

$$\omega = 0.105 \text{ rad/sec}$$

As 1 rad/ second is equal to 57.29 degrees, the angle displaced per second is 6° for 1 rpm of the motor. The angle per second can be given in the steps of 6° by changing the motor RPM.

3.6.2 Knee CPM Machine

The knee is a multipart joint with many mechanisms, making it susceptible to the lot of knee injuries. Though many knee injuries can be successfully treated with simple measures but other injuries may require surgery to correct. After an extensive surgery, due to immobilization of the knee joint scar tissues may get formed and healing may get prolonged to regain its normal ROM. In the recent years, knee CPM is effectively used for different surgical procedures for restoring the normal knee function and ROM (Ngoc-Bich et al., 2013). The developed knee CPM is to perform two different exercises known as hyperextension and full knee flexion as shown in table 3.7.

Table 3.7 Normal Range of Motion for the Knee Joint

Knee Exercise	Range of Motion in Degrees
Hyperextension	120° to 0°
Full knee Flexion	0° to 120°

The knee anthropometric data, the mean values of upper leg (thigh) length (0.60m), lower leg (calf) length (0.50m) and weight of the leg (156.96 N ; 16 Kg) was used in the present work; for the calculations of total power required to reciprocate the leg by using CPM machine (Holen, 1936).

Though open and closed kinematic chain mechanism are used for the different exercise of the human joints. Closed kinematic chain is the best approach for the knee joint motions, as the leg movement is happening in a single plane through a single joint i.e. knee joint. A four bar mechanism was used to translate the leg into hyperextension and flexion. The advantages of using four bar linkage are; it allows the joint to be offset slightly from the center, avoids interference and more freedom for the adjustment of the links in the machine. Closed kinematic chain analysis can be used to find out the motor ratings for the CPM machine. The knee skeleton outline gives all the geometrical information necessary for determining the relative motion of the links as shown in Fig. 3.39.

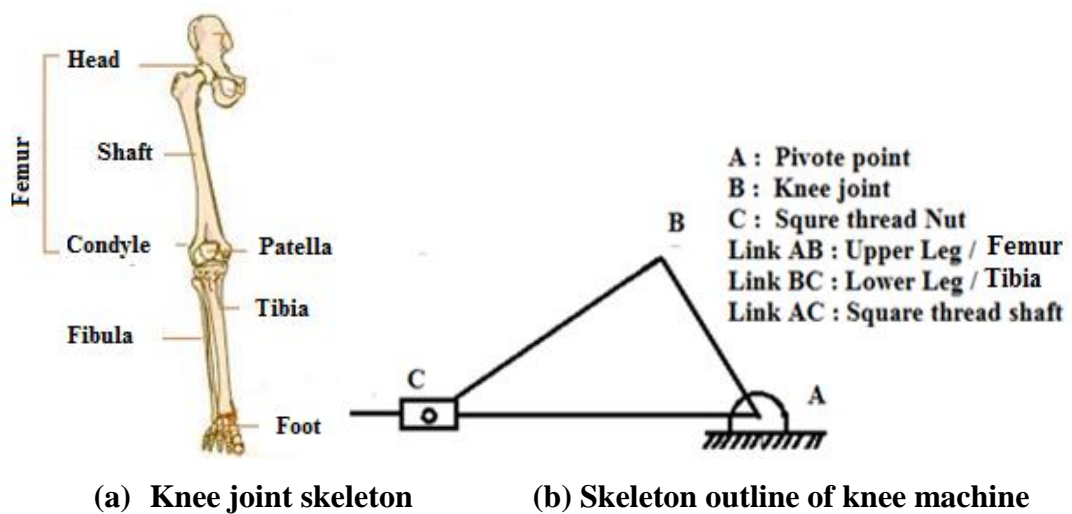


Fig. 3.39 Closed Kinetic Chain Mechanism for the Knee CPM Machine

A power screw is a mechanical device used to convert rotary motion into linear motion and to transmit the power. Square thread screw and nut assembly is used; as there will be no side thrust on the nut and also the efficiency of square thread is high.

3.6.2.1 Motor Design

From the kinematics analysis, as the force value was very less; therefore static loading is considered in the present design calculations. Leg weight was 156.96 N (16 kg) and the weight of the platform structure, plate and cushion assembly was 68.67 N (7 kg), so the total weight of the assembly on the bearings and nut was 225.63N. Considering Factor of Safety 1.5, the total load on the bearing was 338.5N (345N).

The Power absorbed by the bearings to overcome the friction.

Load on bearings is, $W_s = 345 \text{ N}$ (Normal Reaction R_n).

The mean diameter (D_p) of the bearing is 25mm and the bearing friction (μ) is 0.35, Friction force is given by

$$F = \mu \times R_n \quad [3.7]$$

$$F = 120.75 \text{ N}$$

The frictional torque is given by

$$T_f = \frac{F \times D_p}{2} \quad [3.8]$$

$$T_f = 1.50 \text{ N m}$$

Translating velocity of the bearing is 0.0018 m/s.

The angular velocity is given by

$$\omega = \frac{V}{\frac{D_p}{2}} \quad [3.9]$$

$$\omega = \frac{0.0018}{0.0125}$$

$$\omega = 0.144 \text{ rad/s}$$

Hence, the power lost in overcoming the friction will be

$$P_1 = T_f \times \omega \quad [3.10]$$

$$P_1 = 1.5 \times 0.144$$

$$P_1 = 0.216 \text{ W}$$

Power required overcoming the load.

The velocity of slider nut is given by

$$V = \frac{\pi \times D_p \times N}{60} \quad [3.11]$$

$$V = 0.015 \text{ m/s}$$

Power is given by

$$P_2 = F_{st} \times V \quad [3.12]$$

$$P_2 = 345 \times 0.015$$

$$P_2 = 5.175 \text{ W}$$

Total power required is

$$P = P_1 + P_2 = 5.391 \text{ W}$$

There will be some power losses at the screw-nut, gears and different joints. Therefore, considering the screw-nut efficiency (η) equals to 70% and the gear train efficiency (η) equals to 80%.

Actual Power required (P_a) is

$$P_a = \frac{5.391}{0.8 \times 0.7} = 9.627 \text{ W}$$

As the motor is one of the important elements (the heart) of the CPM machine to drive the screw and nut assembly, the factor of safety is taken as 2.5 (Shigle, 2003).

Therefore power required to drive the nut was 24.06 W. The next standard motor available in the market was of 30 Watt; therefore standard motor selected was an a.c. synchronous, having power rating 30 Watt with 60 rpm. One of the unique features of the stepper motor is that irrespective of any load variation it operates at constant rpm and the efficiency is high at low speeds.

Similarly different components screw, nut and the coverings of the machine were designed and checked for the failure test.

3.6.2.2 Electronics Design

A simple electronic circuit was used for the automatic forward / return movements and for the smooth functioning of the CPM machine. Synchronous motor rotates in clockwise and anticlockwise direction by operating 12V relays RL₁ and RL₂ respectively. Open contact relays were used for this purpose as shown in Fig. 3.40. Regulated power supply of +5V @ 500mA is developed by using a full wave rectifier, capacitor filter and three terminal IC voltage regulator 7805 as shown in Fig. 3.41.

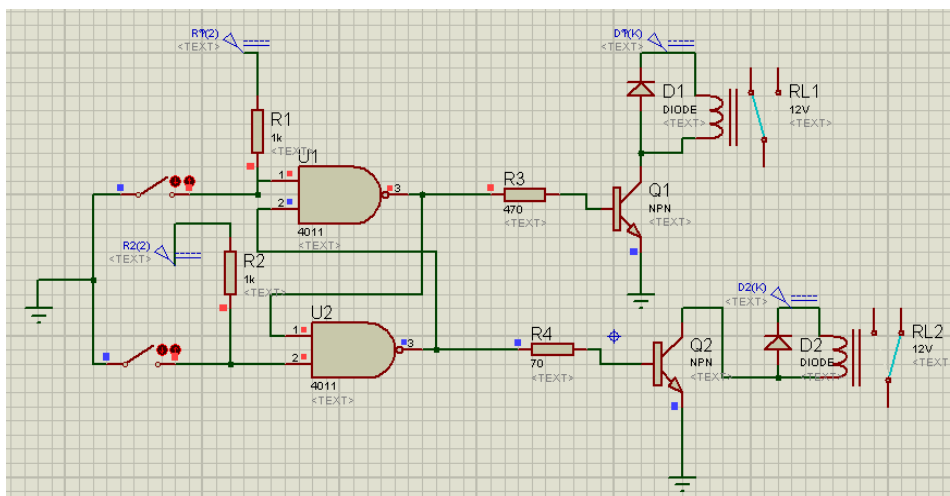


Fig.3.40 Control Circuit for Knee CPM Machine

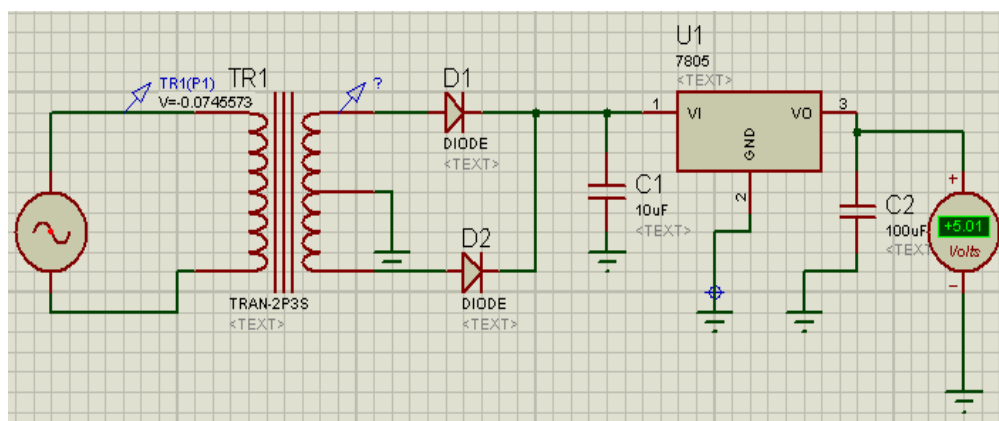


Fig.3.41 Power Supply Circuit for Knee CPM Machine

3.6.2.3 Fabrication of CPM Machine

Fig. 3.42 shows a schematic representation of the knee CPM machine. The CPM machine is fabricated with all the prerequisite of the knee joint flexion and hyper extension exercise. CPM machine body is made up of M.S. sheet (18 gauges) and

used for housing gear train, motor, screw and nut and electronic circuitry of the machine. Lead screw is used to drive to the nut and is made up of M.S. steel material. As the efficiency of square thread is more, there will be no side thrust on the nut and motion of the nut will be smooth and uniform therefore the square thread and nut assembly is used in the present work. Material used for nut is cast iron. Two plastic spur gears with gear ratio 4:1 are used for smooth operation and low speed requirement. Number of teeth's on the driving gear mounted on the motor shaft is 12 and the number of teeth on the driven gear mounted on the lead screw is 48.

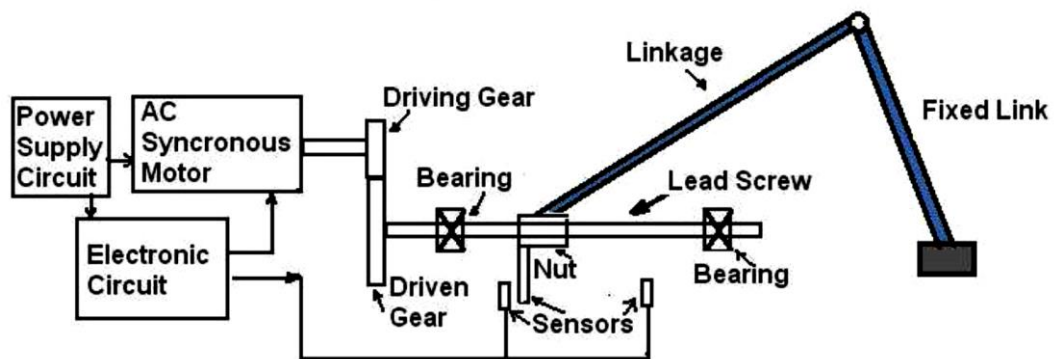


Fig. 3.42 Block Diagram of Developed Knee CPM Machine

The shin rest (linkage) is made of M.S. It is mounted on a C type support, to get the required oscillatory motion to the patient's lower leg. Leather cushioning is provided on both the linkages for the comfort of the patients during the CPM exercise. Fig 3.43 shows the developed low cost CPM machine. The total cost of the knee CPM machine is Rs 10000/- (200 \$). (**Appendix IV**)



Fig. 3.43 Low Cost Knee CPM Machine

3.6.2.4 Testing on the CPM Machine

In present study, 50 asymptomatic subjects of different age group and gender, having knee pain or undergone knee surgery; are tested on the knee CPM machine in

Dr. Metan Hospital Orthopedic & Neurology Center, India. Subjects were exercised on CPM machine through series of motions for flexion and extension exercises for 2 to 3 weeks. The improved range of motion and reduced pain after the two weeks of CPM treatment were the main outcome measures (Ring et al., 2005).

Procedure:

As per the instructions from the orthopedic surgeon, the scales of different exercises are set. The therapy prescription such as type, frequency, and duration of the therapy; goals of therapy; and safety precautions are considered while exercising on the CPM machine (Scott et al., 2007).

The procedure to carry out different exercise on the developed knee CPM Machine is explained below.

- 1) On the first day subject was trained to use the CPM by the physiotherapist, by giving self-demonstration and a trial run.
- 2) Subject was allowed to sit on the knee CPM machine; accordingly the leg was adjusted and strapped on the upper and lower leg linkages, so that the subject should feel comfort during the exercise. The precaution was taken that the upper and lower leg was fully seated on the linkages and the leg belt was properly strapped. A small gap may create a lot of pain during the exercise.
- 3) The physiotherapist and the orthopedist have decided the dose and duration of treatment.
- 4) As per instructions of physiotherapist, the required exercise was selected on the control panel and the limit switches were set to adjust the ROM. The number of iterations was also set. Emergency switch was given to the subjects, in case of excess pain. In case of power failure during the exercise the battery backup was given for uninterrupted exercise.
- 5) Once the subject got comfortable and knowledgeable with the first exercise cycle, then the same cycle was repeated. The angle was increased on daily basis to attain normal ROM, depending upon the patient's pain.
- 6) The exercise was conducted for two weeks and the ROM progress was noted and discussed with the subject.

The CPM machine was conceded throughout a series of motions from 0° to 120° at the progression of 5° until a normal range of motion is achieved (Jesse et al. 2009). Subject's progress report was generated and one of the sample reports is explained in the result section. In the report a gradual increase and pain scale is measured on daily basis.

The shoulder pain in the patients was assessed by Visual Analogue Scale (VAS) pain score. Knee function is assessed by using the Knee Pain and Disability Index (KPADI) (**Appendix V**). This self-administered questionnaire uses 13 questions, 5 of which deal with the severity of pain on various leg movements, the pain being assessed by using VAS. The remaining 8 questions deal with functional impairment of the knee, assessed with a VAS ranging from 0 (no difficulty) to 10 (so difficult that need help). An overall score was calculated for the 13 questions as a whole. The same procedure to evaluate the knee pain was used by few researchers (Raja et al. 1992, Jinks et al., 2002 Burckhardt and Jones, 2003). Higher scores indicate a greater level of pain and disability (Biçer et al., 2010).

3.7 MUSCLE TESTING BY USING SEMG ON CPM MACHINE

In the present study SEMG activity was recorded of the shoulder and knee joint muscles during different exercises. The volume contraction properties of the tissues were used to measure the strength of the muscle activity (Dinesh et al., 2013). The aim of this procedure was to analyze the most sensitive muscle during abduction shoulder exercise and flexion knee exercise.

The standard protocols for SEMG testing were used in the present work. The current protocol included the cleaning of the target area, placing the electrodes, required tasks in order to collect and register the electrical signal and interpretation of the electromyography signal parameters (Klyvia et al., 2012).

3.7.1 SEMG Test on Shoulder CPM Machine

In present study, twelve asymptomatic subjects of different age group and gender were tested with (DELSYS two nodes) SEMG on the shoulder CPM machine in Talpallikar Physiotherapy Center, Sholapur. Subjects were exercised on CPM

machine during abduction arm movement for continuous 10 days at the interval of 2 days. The SEMG testing cost for each muscle analysis was also high, as the study was conducted in the private research institute. Fig. 3.44 demonstrates the SEMG set up on shoulder prone subject during abduction arm movement.

Two electrodes were mounted on the deltoid, supraspinatus, infraspinatus, teres minor and subscapularies of shoulder joint during the abduction arm movement. Due to pain the movement gets restricted, which causes shortening (contraction) of the muscle and the motor unit firing was observed during the abduction arm movement. After taking readings on the five muscles on the two subjects, the amplitude of the muscle contraction was observed to be very small; as the test was conducted during the passive motion of the subject. It was observed that deltoid and supraspinatus motor unit firing were measurable (in micro volts) compared to other three muscles.

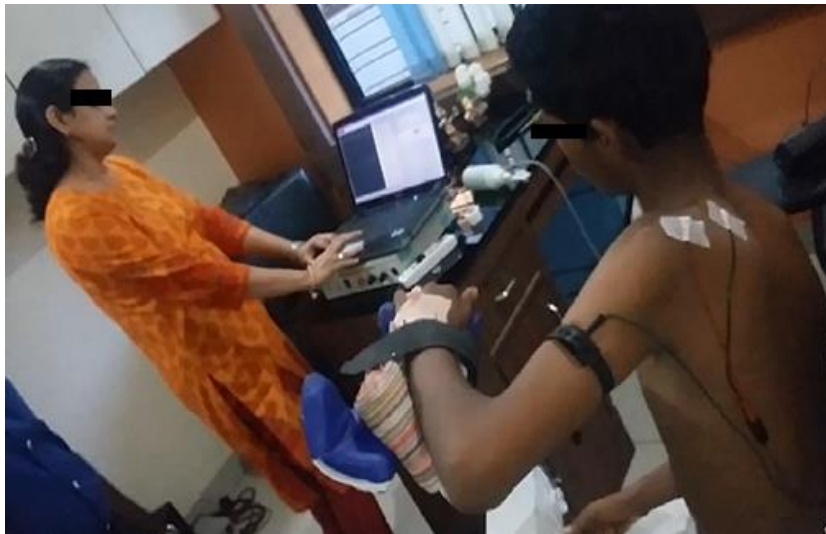


Fig. 3.44 Set up for Shoulder Muscles Test by SEMG

The procedure followed during the SEMG recordings on the subjects by CPM machine is described below.

- 1) Subject was made to sit on the CPM machine chair; accordingly the height of the arm rest was adjusted and the motor M_1 was kept in line with the shoulder joint; so that the subjects feel comfortable during the exercise.
- 2) The subject was first exercised on the shoulder CPM machine without adding SEMG machine.

- 3) The electrodes were mounted along the longitudinal midline of the desired muscle at different locations of the shoulder joint; deltoid, supraspinatus, infraspinatus, teres minor and subscapularies muscles as shown in Fig.3.45.
- 4) SEMG machine was switched ON and motor unit firing were collected as the subject produced a series of contractions for each of the movements during abduction arm movement.
- 5) For each trial the subject has produced three- four second contractions of the same movement, every time starting from and returning to rest.
- 6) The trial was taken 3 times for each exercise and the readings were noted at the highest muscle contraction and the angle was recorded.

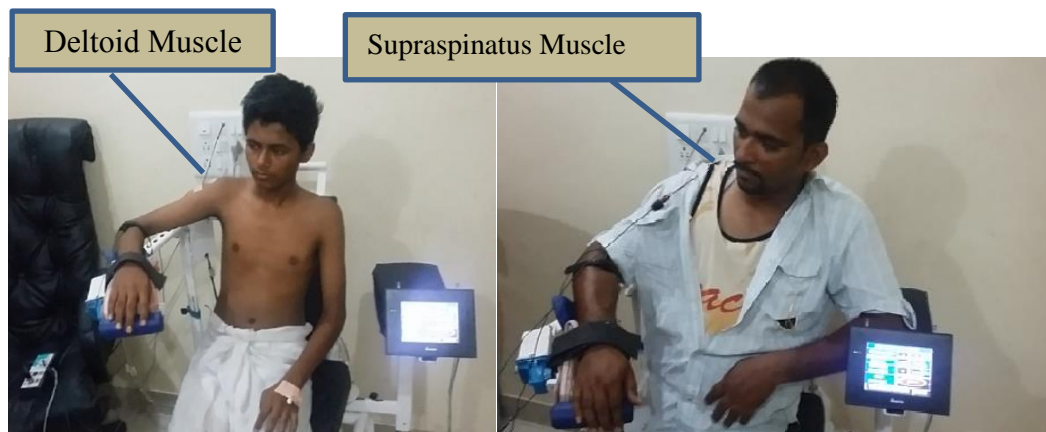


Fig. 3.45 SEMG Electrode Positions for the Shoulder Joint Muscle Analysis

- 7) At five different muscle locations the electrodes were applied and the SEMG recording was done for each muscle.
- 8) The output graph of SEMG was amplitude in Microvolts against the number of turns (ROM in degrees). The maximum muscle contraction occurs at certain angle of the shoulder joint rotation during the CPM exercise and the position (angle) where the maximum contraction (stress) occurred was noted for further analysis. Reports were generated for remaining shoulder muscles by the same procedure.

Portable two Channel SEMG System made from Medicaid was used for the muscle analysis (Liu et al., 2001, Dinesh et al., 2013). Each channel is connected to a Noraxon AgCl gel dual electrode that picked up signals from the muscles. The results

were tabulated for the maximum amplitude in microvolts of different muscles at a particular ROM.

3.7.2 SEMG Test on Knee CPM Machine

In present study, eight asymptomatic subjects of different age group and gender were tested with (DELSYS two nodes) SEMG on the knee CPM machine in Talpallikar Physiotherapy Center, Solapur, India. Subjects were exercised on the knee CPM machine during flexion and extension exercises for continuous 10 days at the interval of 2 days. Fig.3.46 shows the SEMG set up on the developed CPM machine.



Fig.3.46 Set up for Knee Muscles Test by SEMG on CPM Machine

Two electrodes were mounted on the rectus femoris and biceps femoris on the knee joint during the exercise. The maximum motor unit firing (the muscle gets contracted) was observed during the flexion exercise.

The procedure followed during the SEMG recordings on the subjects by CPM machine is described below.

- 1) The CPM machine lower leg (shin) and thigh length were adjusted as per the subjects knee joint position; so that the subject should feel comfort during the exercise.
- 2) The subject was first exercised on the knee CPM machine for small ROM without SEMG.

- 3) Then the electrodes were mounted along the longitudinal midline of the desired muscle at different locations of the knee joint; rectus femoris and biceps femoris as shown in Fig.3.47.
- 4) SEMG machine was switched ON and recordings were collected as the subject produced a series of contractions for each of the movements during flexion.
- 5) For each trial the subject has produced three - four second contractions of the same movement, every time starting from and returning to rest.



Fig. 3.47 SEMG Electrode Positions for the Knee Joint Muscle Analysis

- 6) The trial was taken three times for each exercise and the readings were noted at the highest muscle contraction and the angle was recorded.
- 7) At two different muscle locations the electrodes were applied and the SEMG recordings were done.
- 8) The output graph of SEMG was amplitude in Microvolts against the number of turns (ROM in degrees). The maximum muscle contraction occurs at certain angle of the knee joint rotation during the CPM exercise and the position (angle) where the maximum contraction (stress) was noted for further analysis.

Portable two Channel SEMG System made from Medicaid is used for the muscle analysis. (Liu et al., 2001, Dinesh et al., 2013). Each channel was connected to a Noraxon AgCl gel dual electrode that picked up signals from the muscles. The results are tabulated for the maximum amplitude at a particular ROM.

CHAPTER 4

RESULTS AND DISCUSSIONS: ANALYSIS OF SHOULDER JOINT MUSCLES

The previous chapter conferred about the different steps implemented to generate 3D FEM model for the shoulder joint. The post-processing shoulder model was done in the ANSYS APDL software. The SEMG test conducted on twelve patients during abduction arm movement was also discussed at length. The present chapter discusses the results of the 3D FEM analysis. Results of FEM analysis have been compared with the shoulder muscles test conducted by SEMG on a shoulder CPM machine and also with the previous work.

4.1 FEM ANALYSIS

The post-processing of a 3D shoulder model was done in the ANSYS APDL software to find the maximum stressed muscle during abduction arm movement. Static analysis was done, the results of Von Mises stresses and an equivalent elastic strain were plotted and analyzed (Philippe et al., 2010). The individual and group muscles analysis of four rotor cuff muscles and deltoid muscle of the shoulder joint was done. The maximum stressed muscle during abduction arm movement was analyzed and discussed in detail.

4.1.1 Analysis of Deltoid Muscle

Single deltoid muscle was modelled on the shoulder bone from the lower border of the crest of spine and the lateral border of acromion. Pure rotational motion in a single plane about the shoulder joint was an input for the FEM analysis during the abduction arm movement. The shoulder arm was simulated in eight steps from 10° to 80°. Probes were added at five different locations in the deltoid muscle. The results obtained by FEM analysis for Von Mises stresses and equivalent elastic strain is presented in table 4.1.

Table 4.1 Von Mises Stresses and Equivalent Elastic Strain on Deltoid Muscle

Rotation Angle (ROM)	Von Misses Stresses (MPa)	Equivalent Elastic Strain (mm/mm)
10°	0.6401	0.5334
20°	1.4146	1.1788
30°	2.2940	1.9116
40°	2.4822	2.0685
50°	3.0711	2.5593
60°	3.5690	2.9742
70°	3.8718	3.2265
80°	4.2175	3.5146

The deltoid muscle gets contracted as the shoulder joint is rotated from 0° to 80° during abduction arm movement. This is due to the muscle mass, which always gets broken down and being synthesized with different rates during the movement of the arm. If the rate of breaking and synthesizing of the muscle mass is maintained (equal) then there will be no stresses induced in the shoulder muscles. If this rate is not maintained then the net effect will results in the tissue formation around the joint which induces the stresses in the shoulder muscle.

As the abduction arm movement angle increases from 0° to 80°; the breaking down of the muscle mass increases and is maximum at 80° thus maximum Von Mises stresses is induced in the shoulder muscle.

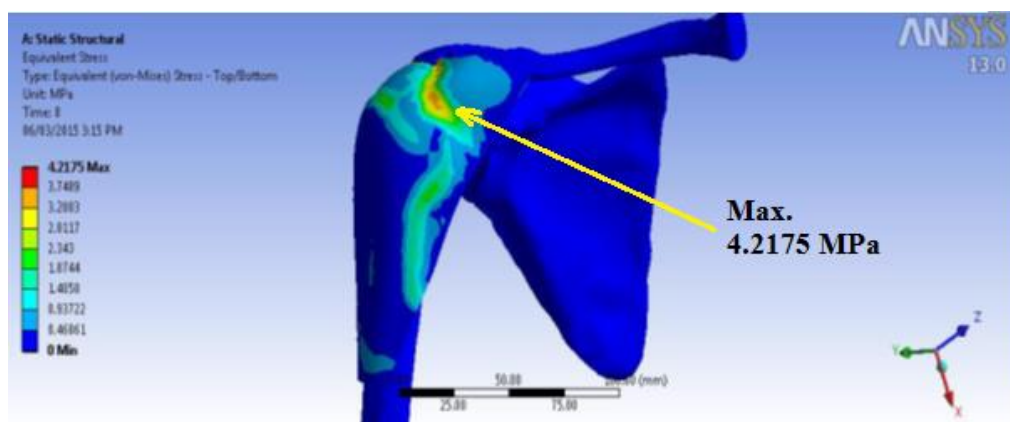


Fig. 4.1 Maximum Von Mises Stresses in Deltoid Muscle

Fig. 4.1 shows the maximum Von Mises stresses in the deltoid muscle during abduction arm movement. Maximum stress in deltoid muscle was found to be 4.2175 MPa at 80° ROM.

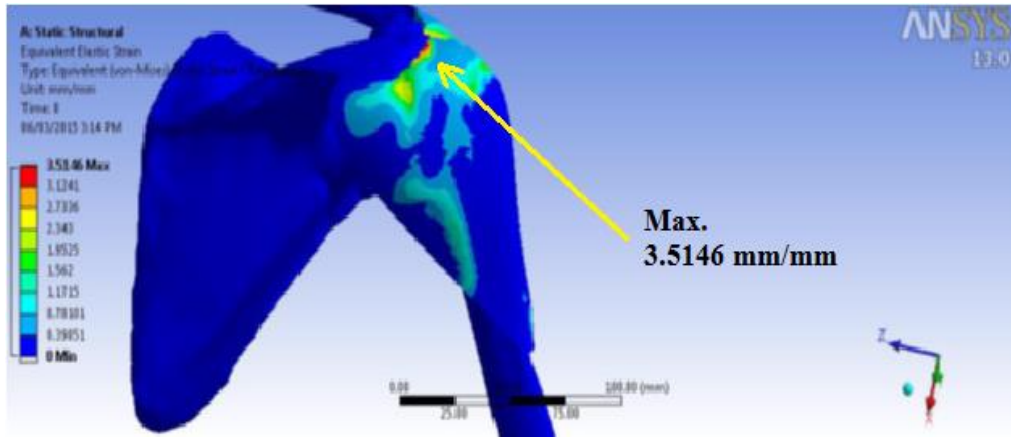


Fig. 4.2 Maximum Equivalent Elastic Strain in Deltoid Muscle

Fig. 4.2 shows the maximum equivalent elastic strain in the deltoid muscle during abduction arm movement. Maximum equivalent elastic strain in the deltoid muscle was found to be 3.5146 mm/mm at 80° ROM.

4.1.2 Analysis of Supraspinatus Muscle

Single supraspinatus muscle was modelled on the shoulder bone from the medial two-thirds of the supraspinatus fossa including the upper surface of the spine. The same procedure was adopted (like deltoid muscle) for the FEM analysis to find out the Von Mises stresses and an equivalent elastic strain. The results obtained for supraspinatus muscle by FEM analysis are presented in the table 4.2.

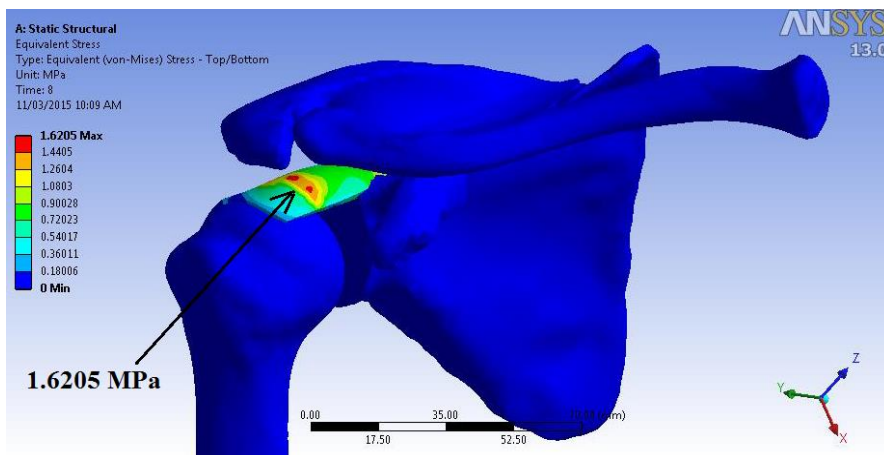


Fig. 4.3 Maximum Von Mises Stresses in Supraspinatus Muscle

Table.4.2 Von Mises Stresses and Equivalent Elastic Strain on Supraspinatus Muscle

Rotation Angle ROM	Von Misses Stresses (MPa)	Equivalent Elastic Strain (mm/mm)
10°	0.1822	0.1518
20°	0.4426	0.3689
30°	0.7246	0.6038
40°	0.9906	0.8255
50°	1.2219	1.0183
60°	1.3665	1.1387
70°	1.4552	1.2126
80°	1.6205	1.3504

Fig. 4.3 shows the Maximum Von Mises stresses in the supraspinatus muscle during abduction arm movement. As the abduction arm movement angle increases from 0° to 80°; the breaking down of the supraspinatus muscle mass increases and is maximum at 80°. Thus maximum Von Mises stresses is induced in the supraspinatus muscle. Maximum stress in supraspinatus muscle was found to be 1.6205 MPa at 80° ROM. Maximum equivalent elastic strain in supraspinatus muscle was found to be 1.3504 mm/mm at 80° ROM.

4.1.3 Analysis of Subscapularies Muscle

Single subscapularies muscle was modelled on the shoulder bone from the medial two-third of the subscapular fossa.

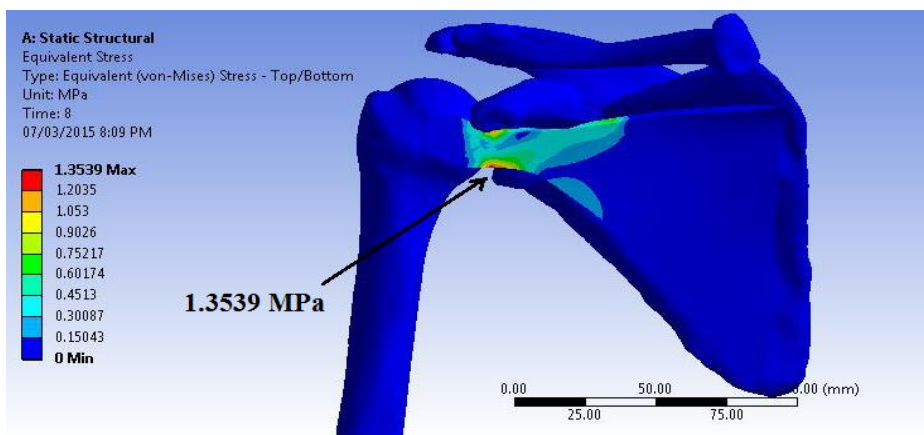


Fig. 4.4 Maximum Von Mises Stresses in Subscapularies Muscle

The same procedure was adopted (like deltoid muscle) for the FEM analysis to find out the Von Mises stresses and an equivalent elastic strain and the results obtained are presented in table 4.3.

Table.4.3 Von Mises Stresses and Equivalent Elastic Strain on Subscapularies Muscle

Rotation Angle ROM	Von Misses Stresses (MPa)	Equivalent Elastic Strain (mm/mm)
10°	0.1882	0.1568
20°	0.3650	0.3042
30°	0.5271	0.4393
40°	0.6966	0.5805
50°	0.9296	0.7747
60°	1.0896	0.9080
70°	1.1910	0.9924
80°	1.3539	1.1283

As the abduction arm movement angle increases from 0° to 80°; the breaking down of the subscapularies muscle mass increases and is maximum at 80°. Thus maximum Von Mises stresses is induced in the subscapularies muscle at 80°.

Fig. 4.4 shows the Maximum Von Mises stresses in the subscapularies muscle during abduction arm movement. Maximum stress in subscapularies muscle was found to be 1.3539 MPa at 80° ROM. Maximum equivalent elastic strain in subscapularies muscle was found to be 1.1283 mm/mm at 80° ROM.

4.1.4 Analysis of Infraspinatus Muscle

Single infraspinatus muscle was modelled on the shoulder bone from the medial two-thirds of the infraspinatus fossa, including the lower surface of the spine. The same procedure was adopted (like deltoid muscle) for the FEM analysis to find out the Von Mises stresses and an equivalent elastic strain and the results obtained are presented in table 4.4.

Fig. 4.5 shows the Maximum Von Mises stresses in the infraspinatus muscle during abduction arm movement.

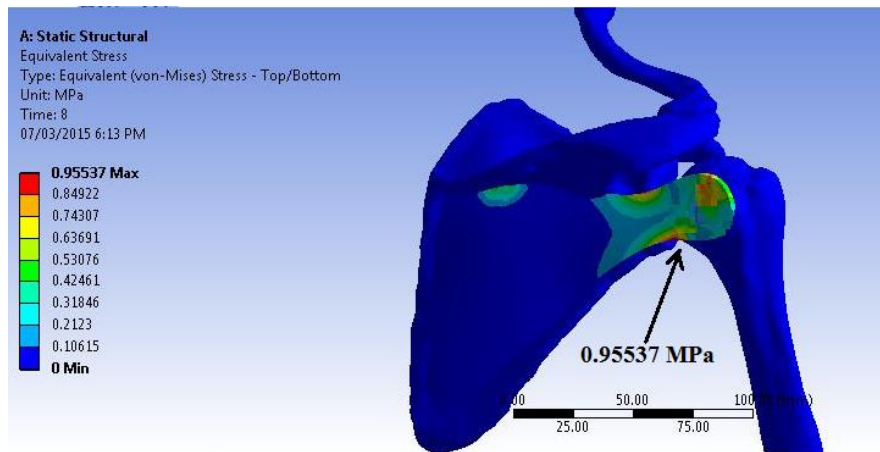


Fig. 4.5 Maximum Von Mises Stresses in Infraspinatus Muscle

Maximum stress in supraspinatus muscle was found to be 0.9553 MPa at 80° ROM. As the abduction arm movement angle increases from 0° to 80°; the breaking down of the infraspinatus muscle mass increases and is maximum at 80°. Thus maximum Von Mises stresses gets induced in the infraspinatus muscle at 80°.

Table.4.4 Von Mises Stresses and Equivalent Elastic Strain on Infraspinatus Muscle

Rotation Angle ROM	Von Misses Stresses(MPa)	Equivalent Elastic Strain (mm/mm)
10°	0.1322	0.1101
20°	0.2407	0.2006
30°	0.3632	0.3026
40°	0.5197	0.4331
50°	0.6053	0.5044
60°	0.7129	0.5941
70°	0.8320	0.6933
80°	0.9553	0.7961

Maximum equivalent elastic strain in infraspinatus muscle was found to be 0.7961 mm/mm at 80° ROM.

4.1.5 Analysis of Teres Minor Muscle

Single teres minor muscle was modelled on the shoulder bone from the upper two thirds of the rough strip on the dorsal surface along the lateral border. The same

procedure was adopted (like deltoid muscle) for the FEM analysis to find out the Von Mises stresses and an equivalent elastic strain. The results obtained are presented in table 4.5.

Table.4.5 Von Mises Stresses and Equivalent Elastic Strain on Teres Minor Muscle

Rotation Angle ROM	Von Misses Stresses (MPa)	Equivalent Elastic Strain (mm/mm)
10°	0.0806	0.0672
20°	0.3027	0.2523
30°	0.3611	0.3009
40°	0.4198	0.3498
50°	0.6093	0.5078
60°	0.5559	0.4633
70°	0.8012	0.6676
80°	0.8544	0.7120

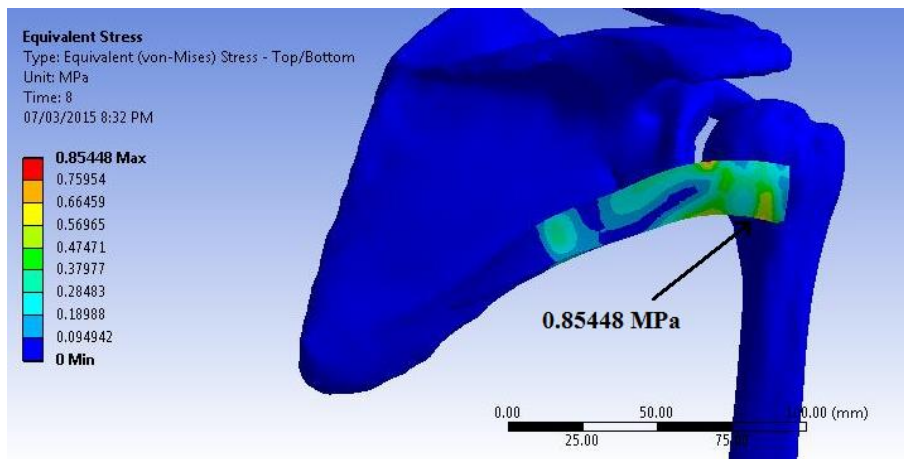


Fig. 4.6 Maximum Von Mises Stresses in Teres Minor Muscle

Fig. 4.6 shows the Maximum Von Mises stresses in the teres minor muscle during abduction arm movement. Maximum stress in teres minor muscle was found to be 0.8544 MPa at 80° ROM. As the abduction arm movement angle increases from 0° to 80°; the breaking down of the teres minor muscle mass increases and is maximum at 80° thus maximum Von Mises stresses gets induced in the teres minor muscle.

Maximum equivalent elastic strain in teres minor muscle was found to be 0.71206 mm/mm at 80° ROM.

4.1.6 Group Muscle Analysis of Shoulder Joint

All the four rotor cuff muscles supraspinatus, subscapularies, infraspinatus, teres minor and deltoid muscle were modelled on the shoulder bone at their ideal locations. The same procedure was adopted (like deltoid muscle) for the FEM analysis to find out the Von Mises stresses and an equivalent elastic strain. The results obtained are presented in table 4.6.

Table 4.6 Von Mises Stresses and Equivalent Elastic Strain on the Deltoid Muscle during the Group Muscle Analysis

Rotation Angle (ROM)	Von Misses Stresses (MPa)	Equivalent Elastic Strain (mm/mm)
10°	1.5900	1.325
20°	1.6932	1.411
30°	1.7713	1.4761
40°	1.9209	1.6007
50°	2.0002	1.6668
60°	2.1163	1.7636
70°	2.2331	1.8609
80°	2.4127	2.0106

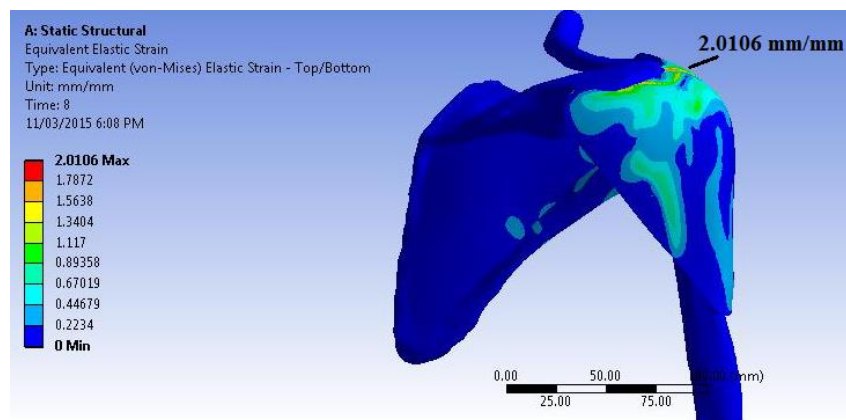


Fig. 4.7 Equivalent Elastic Strain in Deltoid Muscle during the Group Muscle Analysis

Fig. 4.7 shows maximum equivalent elastic strain at the deltoid muscle during the group muscle analysis for abduction arm movement. Maximum strain in deltoid muscle was found to be 2.0106 mm/mm at 80° ROM. Maximum Von Mises stresses in the deltoid muscle was found to be 2.4127 MPa at 80° ROM. Table 4.7 shows the maximum Von Mises stresses at the supraspinatus, infraspinatus, teres minor and subscapularies muscles during the group muscle analysis for abduction arm movement.

Table 4.7 Von Mises Stresses in MPa on the Rotor Cuff Muscles during Group Muscle Analysis

Rotation Angle (ROM)	Supraspinatus	Infraspinatus	Teres Minor	Subscapularies
10°	0.1540	0.1870	0.1850	0.1440
20°	0.3215	0.3012	0.2021	0.3214
30°	0.4892	0.4023	0.2501	0.4236
40°	0.6234	0.5832	0.3214	0.5972
50°	0.7501	0.6364	0.3701	0.7321
60°	0.8728	0.7821	0.4301	0.8235
70°	1.1254	0.9387	0.4827	0.9924
80°	1.2160	1.0474	0.5482	1.0830

Fig. 4.8 shows the maximum Von Mises stresses at the supraspinatus muscle during the group muscle analysis for abduction arm movement.

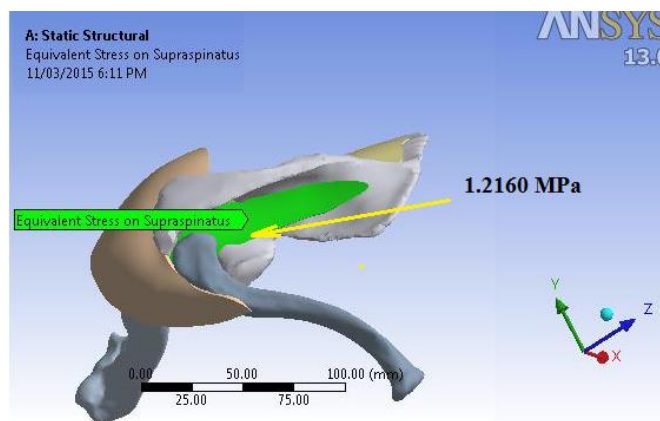


Fig. 4.8 Von Mises stresses in Supraspinatus Muscle during the Group Muscle Analysis

4.1.7 Sensitivity Analysis of Shoulder Joint Muscle

The FEM analysis was done by adding five individual muscles and then adding five muscles in a group, on the shoulder joint. This was done to analyze the individual muscle performance as well as its function in the group muscle analysis during the abduction arm movement. FEM shoulder model analysis was used to quantify the most sensitive muscle during the abduction exercise for the given ROM.

Fig. 4.9 shows the behavior of muscles and their Von Mises stress values during the abduction arm movement for individual muscle analysis.

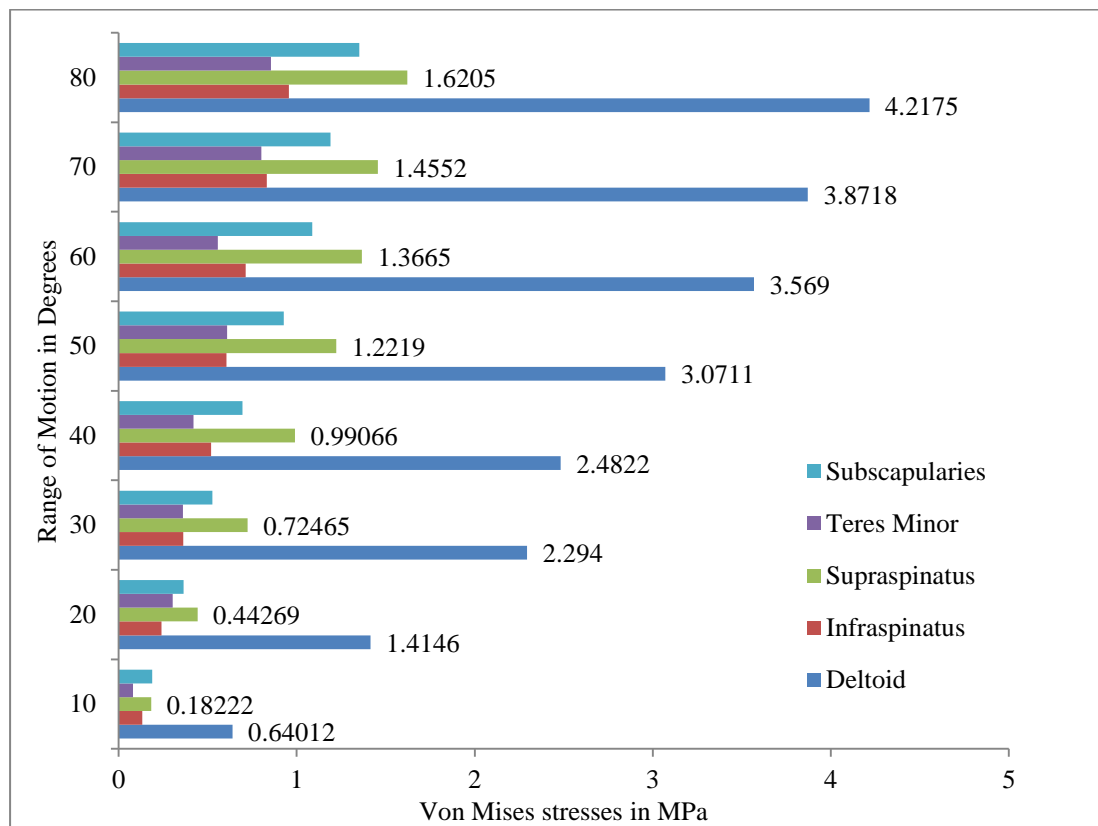


Fig. 4.9 Von Mises Stresses Distribution in the Shoulder Joint Muscles during Individual Muscle Analysis for Abduction Arm Movement

Fig. 4.10 shows the behavior of muscles and their stress values during the abduction arm movement of group muscle analysis.

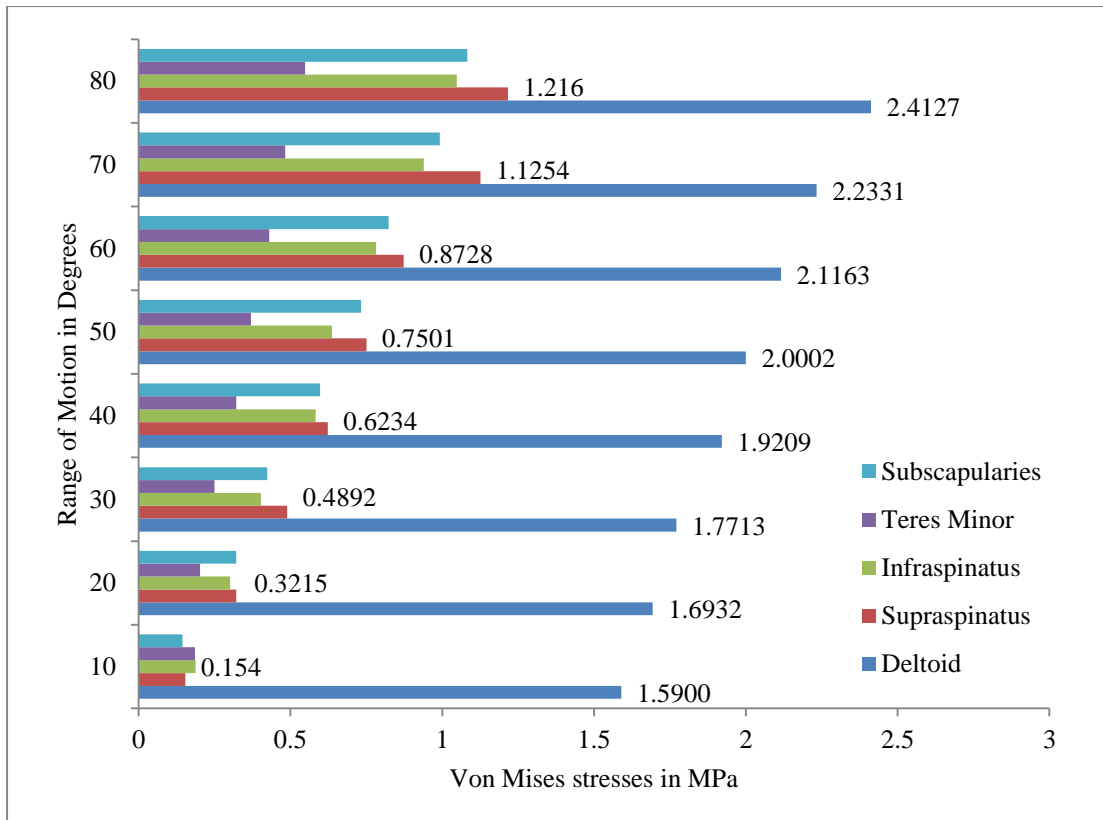


Fig. 4.10 Von Mises Stresses Distribution in the Shoulder Joint Muscles during Group Muscle Analysis for Abduction Arm Movement

Fig. 4.11 shows the Von Mises stresses distribution of the deltoid muscle for different ROM during abduction arm movement.

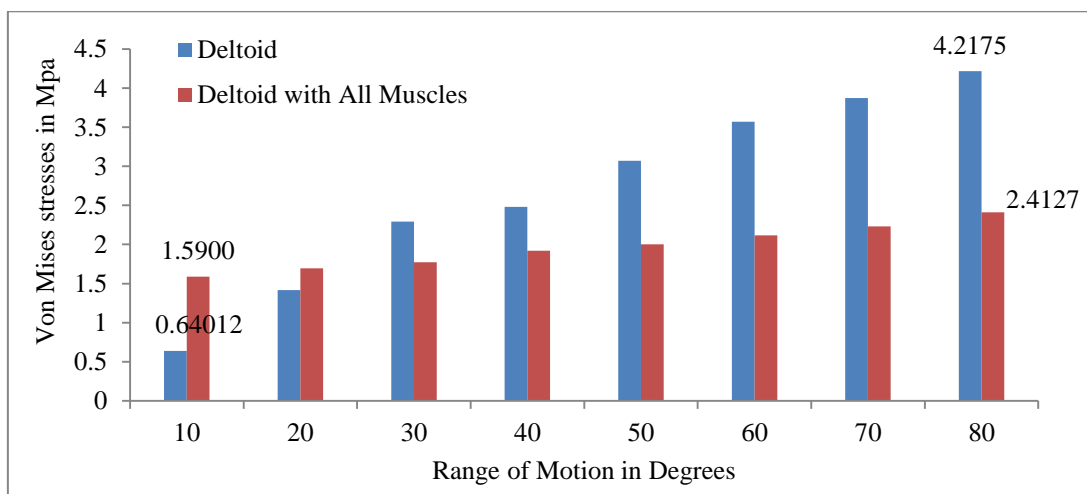


Fig. 4.11 Von Mises Stresses Distribution of Deltoid Muscle

Maximum Von Mises stresses in deltoid muscle during individual muscle analysis was 4.2175 MPa and in a group muscle analysis was 2.4127 MPa. Fig. 4.12 shows the Von Mises stresses distribution of the supraspinatus muscle for different ROM.

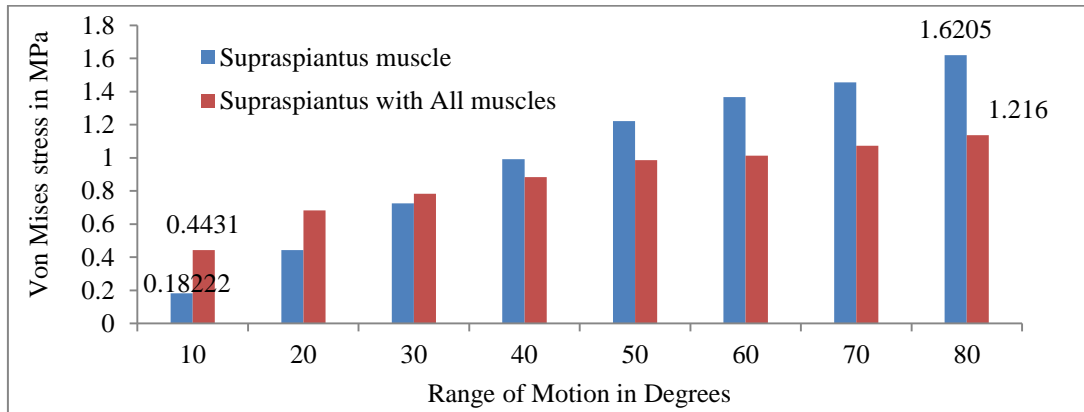


Fig. 4.12 Von Mises Stresses Distribution of Supraspiantus Muscle

Maximum Von Mises stresses in the supraspinatus muscle during individual muscle analysis was 1.6205 MPa and in a group muscle analysis was 1.216 MPa respectively.

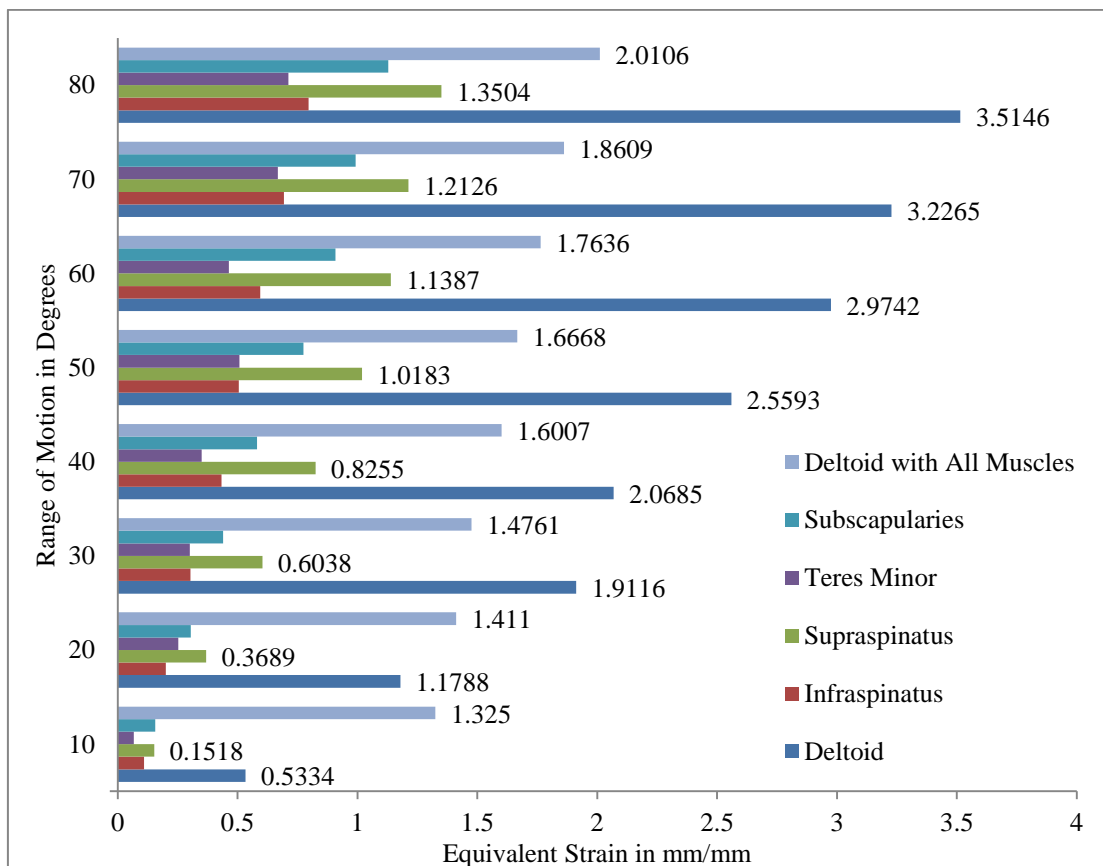


Fig. 4.13 Equivalent Elastic Strain Distribution in the Shoulder Joint Muscles

Fig.4.13 shows an equivalent elastic strain values in the shoulder muscles during the abduction arm movement.

The deltoid muscle was found to be the most sensitive muscle during abduction arm movement in both the cases i.e. individual and group muscle analysis. The result revealed that supraspinatus was the most sensitive muscle after the deltoid muscle, during abduction arm movement in both the cases individual and group analysis. Deltoid is the key muscle to be focused in case of injuries or after postoperative treatment for the abduction arm movement. Orthopedic surgeons can enhance the strength of the deltoid muscle with different treatment methods to maintain the normal ROM.

4.2 CPM MACHINE TEST

Fifty asymptomatic shoulder prone patients of different genders and age groups were tested on the developed CPM machine. The CPM machine was passed through series of motions for different exercises such as adduction, abduction, flexion, elevation, internal rotation and external rotation for 2 to 3 weeks. The test was conducted under the observation of the orthopedic surgeon. Table 4.8 shows an increase in the ROM of patients during two weeks of shoulder exercises on the developed shoulder CPM machine. A test report is presented in the **Appendix VI**.

Table 4.8 Test Report of the Shoulder Joint Exercises on CPM machine

Exercise	Range of Motion in Degrees														
	Day	01	02	03	04	05	06	07	08	09	10	11	12	13	14
IR	45	45	50	55	60	60	65	65	70	70	75	75	80	80	88.8
ER	40	40	45	45	45	50	50	55	55	60	65	65	70	70	77.7
Abduction	70	70	75	75	75	80	80	85	85	90	90	95	95	100	57.1
Adduction	60	65	65	70	70	75	75	80	80	85	85	90	95	100	57.1
Flexion	75	75	80	80	85	90	95	95	100	100	105	105	110	115	65.7
Elevation	75	75	80	80	85	85	90	95	100	100	105	110	115	115	65.7
Pain Scale	8	8	7.5	7.5	7	7	7	6.5	6.5	6	5.5	5.5	5	5	50

(IR= Internal Rotation; ER = External Rotation)

% R is the percentage recovery of the patient and is calculated with respect to the normal range of motion as shown in table 4.9.

Table. 4.9 Normal Range of Motion for the Shoulder Joint

Shoulder Exercise	Range of Motion in Degrees
Abduction/Adduction	0 to 175
Internal/external rotation	- 90 to 90
Flexion/elevation	0 to 175

Fig. 4.14 shows the subjects improvement in the ROM on weekly basis after exercising on the developed shoulder CPM machine. This data will be useful for the orthopedic surgeon for understanding the progress of the subject on daily basis and accordingly prescribe the physiotherapy treatment to achieve normal ROM. This percentage improvement is not compared to the normal range of motion.

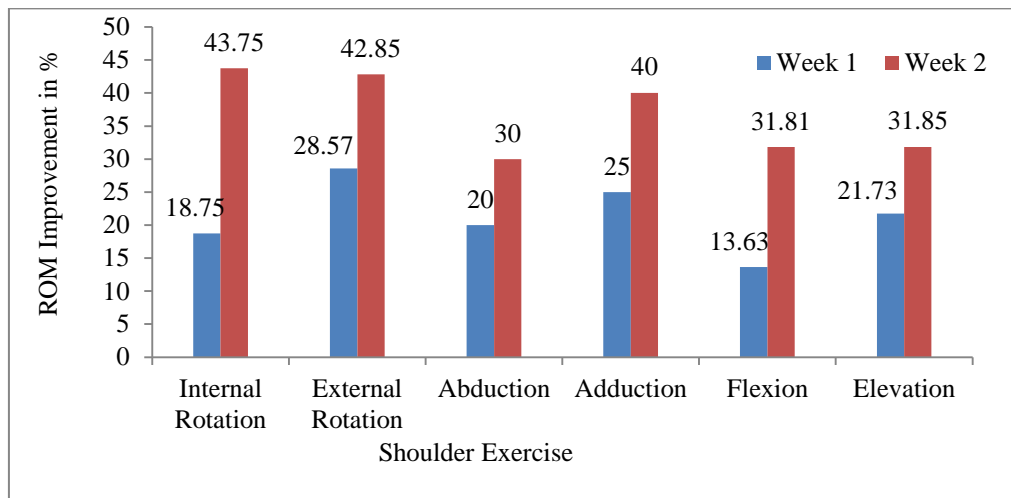


Fig. 4.14 Percentage Improvement in the Shoulder ROM on Weekly Basis

Orthopedic Surgeons Remarks: After two weeks of shoulder exercise on the CPM machine the subject’s pain and range of motion improved by 65% to 88% as compared to normal range of motion. Three months back the patient has undergone a surgery of supracondylar fracture (humerus), he needs further two to three weeks of shoulder therapy on the CPM machine. The progress is satisfactory.

The reports attested that low cost CPM machine is full proof, comfortable and functioned satisfactorily for the shoulder arm exercises. The cost of the CPM exercise is also less and affordable to the common patients. This tested CPM machine was

further used to analyze the shoulder muscle behavior using SEMG on different shoulder prone patients.

4.3 MUSCLE ANALYSIS BY SEMG

Twelve asymptomatic shoulder prone subjects of different genders and age groups were tested using SEMG on the developed CPM machine. The SEMG machine was passed through a series of motions for abduction arm movement for five days. The test was conducted under the observation of a Neurophysiotherapist surgeon in Talpallikar Physiotherapy center, Solapur, India.

Table 4.10 shows the maximum amplitude of motor unit firing angle occurred in deltoid muscle at different ROM during abduction arm movement by SEMG.

Table 4.10 Maximum Motor Unit Firing during the Abduction Arm Movement

ROM in degrees for maximum amplitude display					
Movements	Day 1	Day 3	Day 5	Day 7	Day9
Abduction	60°	70°	75°	85°	95°
Adduction	65°	70°	80°	85°	90°
Pain scale	7	6.5	6	5.5	5

The maximum motor unit firing occurred at the different ROM in the shoulder muscles during abduction arm movement by SEMG machine was studied. The shoulder movement was very slow and continuous as the patients were under post-operative treatment; suffering from the pain and injuries. As the exercise was done for the passive motion, the motor unit firing range was kept small. Due to pain the movement gets restricted, which causes shortening (contraction) of the muscle. There was not significant variation in the motor unit firing amplitude of the muscles, only seven out of twelve patients have shown the appreciable change in the motor unit amplitude i.e. stress behavior. Table 4.11 shows the rotor cuff and deltoid muscle contraction against the ROM on the ninth day of the subject 02 during abduction arm movement. The EMG test report of patient 02 has been attached in **Appendix VII**.

Table 4.11 Shoulder Muscles Contraction during Abduction Arm Movement

ROM in Degrees	Deltoid (μV)	Supraspinatus (μV)	Infraspinatus (μV)	Subscapularies (μV)	Teres Minor (μV)
45	0	0	0	0	0
50	0	0	0	0	0
55	125	125	0	100	0
60	0	0	75	50	0
65	50	75	50	50	25
70	225	125	75	0	25
75	325	175	75	75	25
80	300	225	75	25	25
85	200	125	0	50	50
90	75	0	0	0	25
95	0	0	0	0	25

Fig. 4.15 shows the amplitude variation against ROM of patient 02 in rotor cuff and deltoid muscles during SEMG testing.

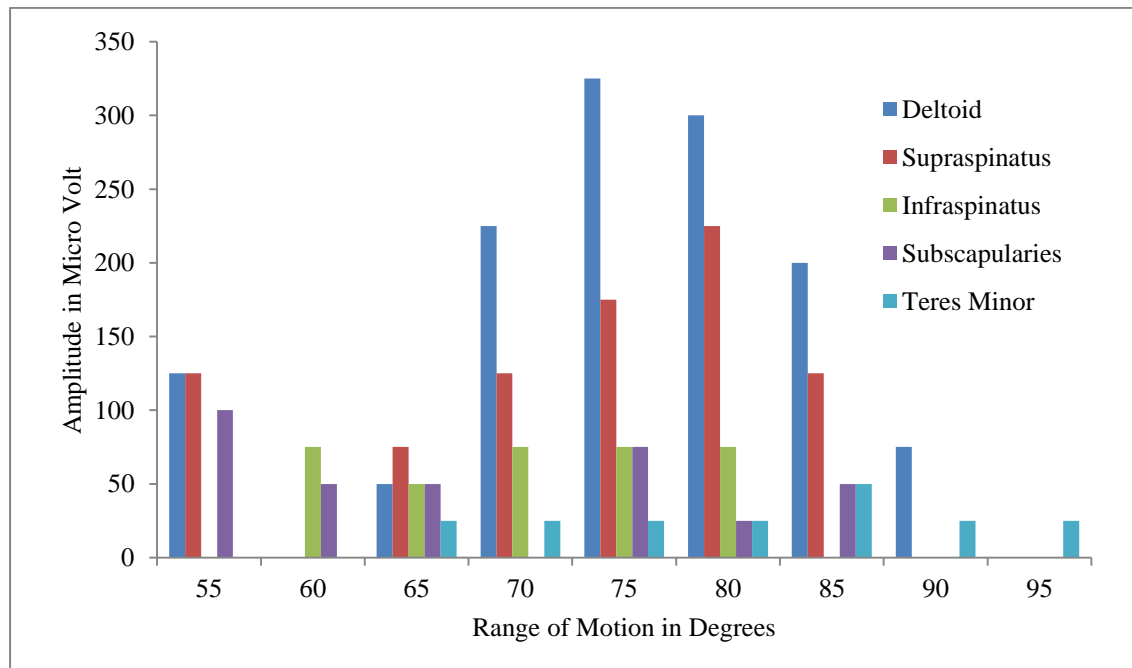


Fig. 4.15 Motor Unit Firing Against ROM in Shoulder Muscles

The maximum motor unit firing of deltoid muscle was observed in the range from 75° to 85° and that of supraspinatus muscle at 75°. The same trend was observed in the

test conducted on remaining subjects for deltoid and supraspinatus muscles. The plot of amplitude against ROM of deltoid and supraspinatus muscles for the remaining six SEMG tested subjects is as shown in Fig. 4.16 and Fig. 4.17.

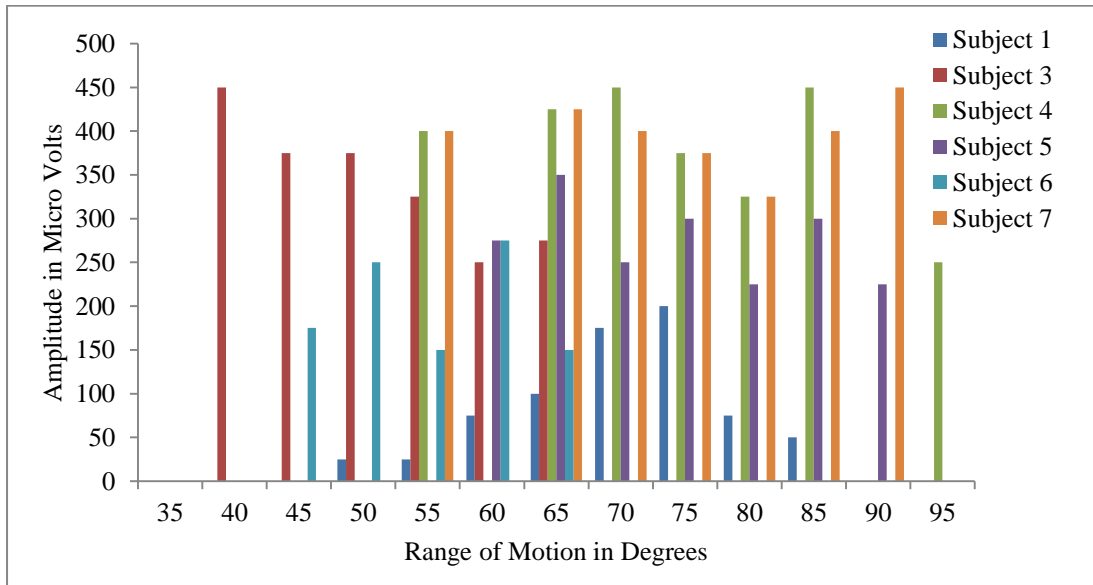


Fig 4.16 Motor Unit Firing against ROM in Deltoid Muscle during Abduction Arm Movement

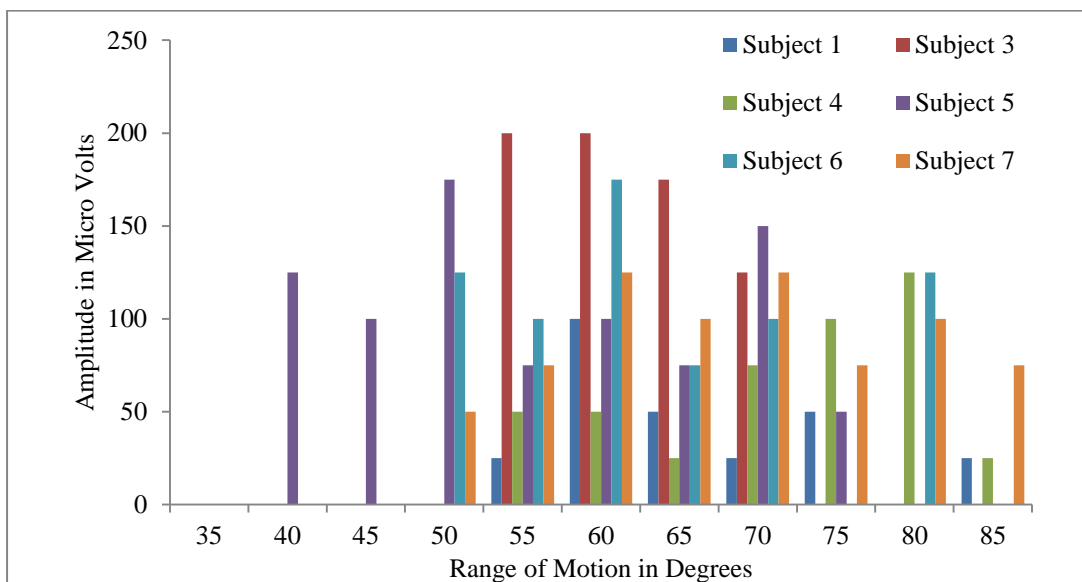


Fig. 4.17 Motor Unit Firing against ROM in Supraspinatus Muscle during Abduction Arm Movement

From the Fig. 4.16 and 4.17 , it can be observed that muscle contraction for all the subjects during abduction arm movement is maximum in the range of 70° to 90° (average 80°) of the ROM.

4.4 DISCUSSIONS

The primary aim of the present work was to analyze the stresses induced in different shoulder joint muscles during the abduction arm movement using 3D FEM model. Reverse modeling was used for fast and accurate 3D model generation and the shoulder muscle analysis. Modeling of bones in CATIA V5 without any background help was difficult and impracticable. The free form option in CATIA V5 was not useful for modeling the complicated and irregular objects such as human bones. The minute detailing required during the modeling of ligaments, tendons and muscles was not so easy in CATIA V5 which is good for surface modeling. Therefore scanning of the complicated shoulder bones was done by ATOS III 3D scanner to generate accurate and detailed contours. 3D multiple scanning of the bones to obtain a point-cloud model was finalized in the present work. 3D bone geometry of the shoulder model was done in CATIA V5 software from the scanned .stl file. The geometrical features of higher order (curve and surfaces) were designed by filtering and aligning number of cloud points, tessellation of polygonal model, recognition and defining the referential geometrical entities. According to quadratic dependency, a non-homogeneous bone constitutive law was implemented (Terrier et al., 1997, Rakotomanana et al., 1999).

Muscles were added on the shoulder joint model in CATIA V5. The 3D model was imported in .igs format into ANSYS 13 workbench for stress analysis. The kinematics for shoulder abduction arm movements were prescribed as an input to finite element simulations and the resulting muscles Von Mises stresses and an equivalent elastic strain were plotted. Careful alignment of the five muscles on humerus, scapula and clavicle were done. Muscle initialization and precise location on shoulder bones were done and was conferred by Blemker and Delp (2005). The efficacy of the glenohumeral joints model i.e. humerus, clavicle, scapula depends on the positioning, orientation and maintaining proper gap amongst the three bones during abduction arm movement. In the present FEM analysis there was no clash between bone to bone, muscle to muscle and muscle to bone during full ROM of shoulder joint. The muscle thickness varied from 2 mm to 6 mm along with its length to create a proper volume of tissue over the shoulder bones. This ensured the real time behaviour of the shoulder joint with the animated one.

During the individual deltoid muscle analysis, the Von Mises stresses induced in deltoid muscle was maximum (4.2175 MPa) compared to other individual four rotor cuff muscles and the results obtained are mentioned in table 4.12.

Table. 4.12 Von Mises Stresses Distribution in the Rotor cuff and Deltoid Muscle during Individual Muscle Analysis

Muscles	Deltoid	Supraspinatus	Infraspinatus	Teres Minor	Subscapularies
Stresses in MPa	4.2175	1.6205	0.95537	0.85448	1.3539

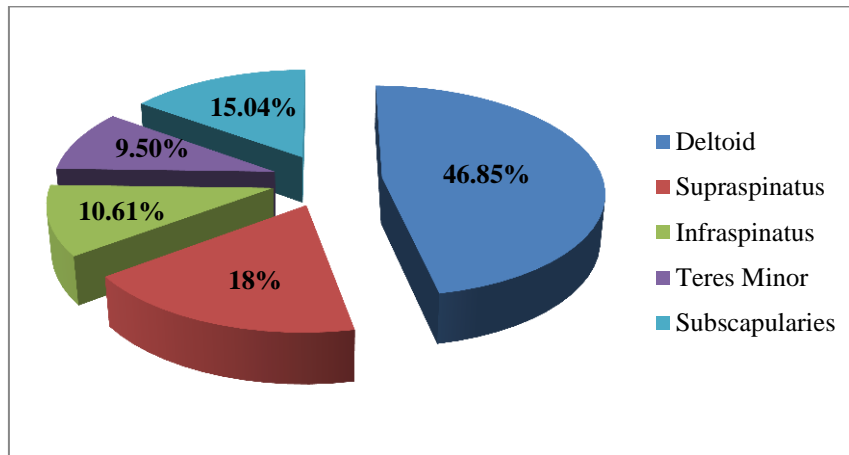


Fig. 4.18 Von Mises Stresses Distribution in the Rotor cuff Muscles and Deltoid during Individual Muscle Analysis

Fig. 4.18 shows the Von Mises stress distribution in shoulder joint muscles during individual muscle analysis. The percentage analysis of individual muscles contribution for abduction arm movement was found and 46.85% of the total Von Mises stresses were distributed in the single deltoid muscle only. Deltoid is the most sensitive muscle.

Table. 4.13 Von Mises Stresses Distribution in the Rotor cuff and Deltoid Muscle during Group Muscle Analysis

Muscles	Deltoid	Supraspinatus	Infraspinatus	Teres Minor	Subscapularies
Stresses in MPa	2.4127	1.216	1.0474	0.54826	1.083

During the group muscle analysis, Von Mises stresses obtained in deltoid muscle was maximum (2.4127 MPa) compared to other individual four rotor cuff muscles during abduction arm movement and the results obtained are mentioned in table 4.13. Fig. 4.19 shows the Von Mises stress distribution in shoulder joint muscles during group muscle analysis.

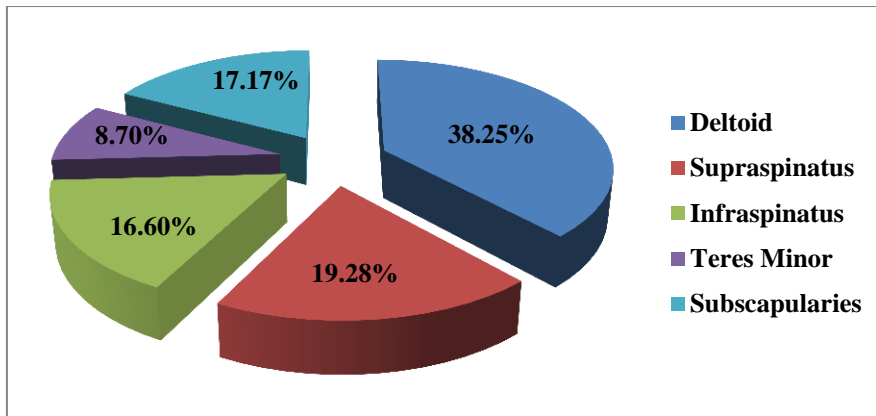


Fig. 4.19 Stress Distribution in the Rotor cuff Muscles and Deltoid during Group Muscle Analysis

There was 6.60 % of variation observed in Von Mises stresses distribution in the deltoid muscle during individual analysis (46.85%) and group muscle analysis (38.25%). These excess 6.60% stresses were distributed amongst the other four rotor cuff muscles during the group muscle analysis. The deltoid muscle was the most sensitive muscle in both the analysis during shoulder abduction arm movement. The maximum Von Mises stresses induced was at 80° abduction angle in both the analysis. The equivalent elastic strain analysis also predicted the same trend in shoulder muscles as mentioned in table 4.14.

Table. 4.14 Equivalent Elastic Strain (mm/mm) in the Rotor cuff and Deltoid during Group Muscle Analysis

Muscles	Deltoid	Supraspinatus	Infraspinatus	Teres Minor	Subscapularies
Strain (mm/mm)	3.5146	1.3504	0.79614	0.71206	1.1283

4.4.1 Comparison of FEM Analysis Results with SEMG Analysis

Presently SEMG is the only feasible method to analyse the muscle contraction (stress) levels in the living objects. SEMG is used to analyze the muscles behavior during the human arm movements. The current SEMG set up has quantified the muscle behaviour in the shoulder joint during the abduction arm movement on the developed CPM machine. SEMG is closely related to muscles contraction and is an indicator of the associated actions. In the present work two channel passive electrode surface electromyography (SEMG) was used to measure the muscle contraction during the abduction arm movements.

A case study of the patient 02 is considered for the analysis, the percentage variation in the muscle contraction of the deltoid and supraspinatus muscle was observed in the range of 75° to 85°. The variation in the muscle contraction in Micro volts and percentage variation in the muscle contraction of the rotor cuff and deltoid muscles during SEMG analysis is as mentioned in table 4.15 and table 4.16.

Table. 4.15 Muscles Contraction in the Shoulder Muscle during SEMG Analysis

ROM in Degrees	Deltoid (μV)	Supraspinatus (μV)	Infraspinatus (μV)	Subscapularies (μV)	TeresMinor (μV)
75	325	175	75	75	25
80	300	225	75	25	25
85	200	125	0	50	50

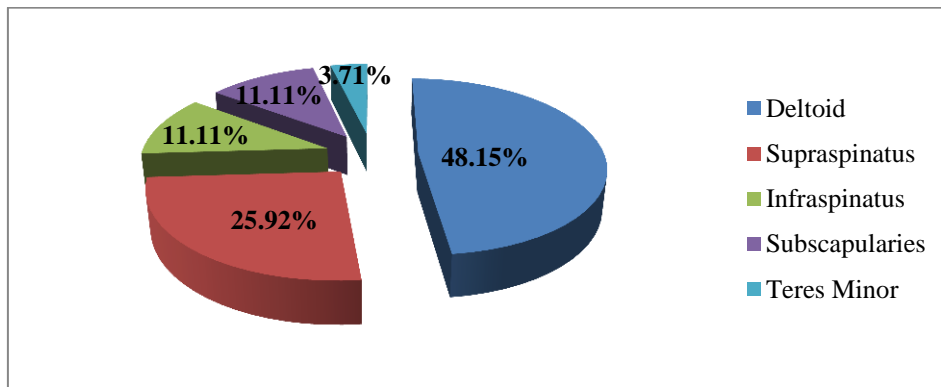


Fig. 4.20 Percentage Variation in the Muscle Contractions of Rotor cuff and Deltoid Muscles during Abduction Arm Movement by SEMG at 75°

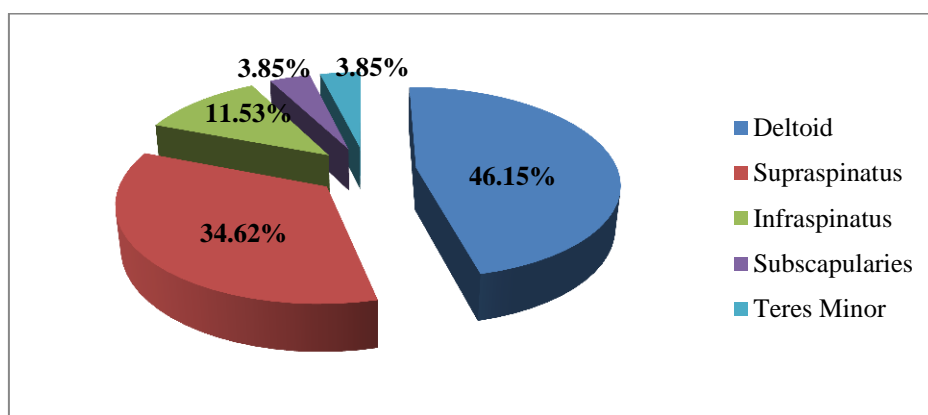


Fig. 4.21 Percentage Variation in the Muscle Contraction of Rotor cuff and Deltoid Muscles during Abduction Arm Movement by SEMG at 80°

Table. 4.16 Percentage Muscle Contractions of the Shoulder Joint Muscles at Different ROM

ROM Degrees	Deltoid %	Supraspinatus %	Infraspinatus %	Subscapularies %	Teres Minor %
75	48.15	25.92	11.11	11.11	3.71
80	46.15	34.62	11.53	3.85	3.85
85	47.05	29.41	0.00	11.77	11.77

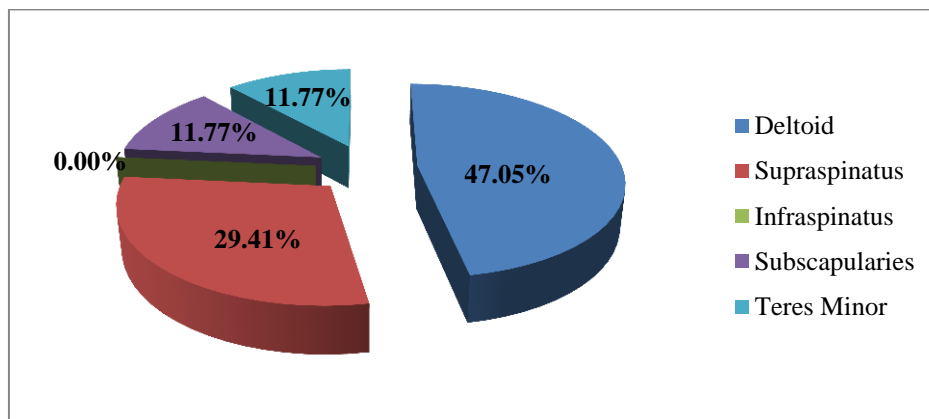


Fig. 4.22 Percentage Variation in the Muscle Contraction of Rotor cuff Muscles and Deltoid Muscle during Abduction Arm Movement by SEMG at 85°

During the SEMG muscle analysis, the muscle contraction (stress) obtained in deltoid muscle was maximum (325 μ V; 300 μ V and 200 μ V) as compared to other rotor cuff muscles at different ROM as shown in table 4.15.

The percentage analysis of individual muscles contribution for abduction arm movement predicted by SEMG analysis is 48.15%, 46.15% and 47.05% in the deltoid muscle. Deltoid is found to be the most stressed (contracted) muscle by the SEMG analysis as compared to other rotor cuff muscles during the abduction arm movement. The maximum muscle contraction has occurred in the range of 75° to 85° of the ROM. Fig. 4.20, Fig 4.21 and Fig.4.22 shows the percentage variations of shoulder joint muscle contraction for different ROM.

Though SEMG measures the electrical activity within a muscle; not the muscle force/stress directly. In the present work the maximum muscle contraction trends were considered for the comparison of the FEM analysis results on the shoulder muscle. The SEMG trends showed that maximum contraction during abduction arm

movement was in the deltoid muscle and then in supraspinatus muscle. The maximum motor unit firing (contraction; stress) during abduction was in the deltoid muscle probes of the SEMG machine. The maximum motor unit shoots were observed in the range of 75° to 85° during abduction arm movement.

Thus it can be concluded that the deltoid muscle is the most sensitive muscle in the shoulder joint during abduction arm movement. The maximum muscle contraction for all the patients during abduction arm movement was maximum in the range of 75° to 85° (average 80°) of the ROM. Deltoid and supraspinatus muscles are the initiator of the abduction arm movement. This will help the Orthopedic surgeon to develop and focus on the new therapy to strengthen the deltoid muscle during abduction arm movement. Different physiotherapy treatment on the deltoid muscle for expediting recovery process can be done for attaining the normal ROM.

4.4.2 Comparison of FEM Results with Previous Work

Comparing the FEM results is a complicated task as the model to be validated is dimensionally complex with many components involved in the analysis. It becomes more challenging in the joint like shoulder where the degree of asymmetry and the variation in the muscle functions are unpredictable.

Webb et al. (2014) has developed a 3D model of the deltoid muscle and rotor cuff muscles of the shoulder joint to study the muscle behavior during abduction, internal and external rotation exercises. The study was carried out to measure the maximum displacement in cm of the shoulder joint muscles. The results foreseen that the deltoid abduction moment arms range from 0 cm to 2.5 cm maximum; whereas the supraspinatus abduction moment arms range from 2 cm to 1 cm maximum and rest of the muscles had less moment arm than these two muscles during abduction arm movement from 0° to 90°. In the present work the stress sensitivity analysis is carried out amongst the five major muscles of shoulder joint in individual and group muscle analysis. The maximum muscles stress was at 80° in the deltoid muscle during abduction arm movement. As during the shoulder movement the muscle mass breaking is maximum than muscle synthesizing at 80°, therefore maximum stress will generate at 80° and the same trend was observed by Webb et al. (2014) in the displacement analysis.

A mathematical model was developed by J Dul, (1988) to quantify the shoulder muscle load, joint load and endurance time in work situations. This model was used to analyse the force acting on the shoulder during elevation arm movement. The input to the model was load on shoulder joint in kilograms and the output was deltoid force (F_d), supraspinatus force (F_s) and resultant of F_d and F_s (R). The results are plotted in Fig.4.23.

Matlab programming of the mathematical model was prepared in the present work for analyzing the behavior of the supraspinatus; deltoid and the glenohumeral joint during elevation arm movement for different loads (**Appendix VIII**). The graphical trends predicted that the maximum force was induced in supraspinatus muscle than the deltoid muscle. At 80° of arm elevation the maximum force calculated by the mathematical model was 94N on the deltoid muscle and 194N on the supraspinatus muscle. This study was carried out for the elevation arm movement in which the palm is facing forward, the arm raised straight up and away from the body at 175° angle as shown in Fig. 4.24.

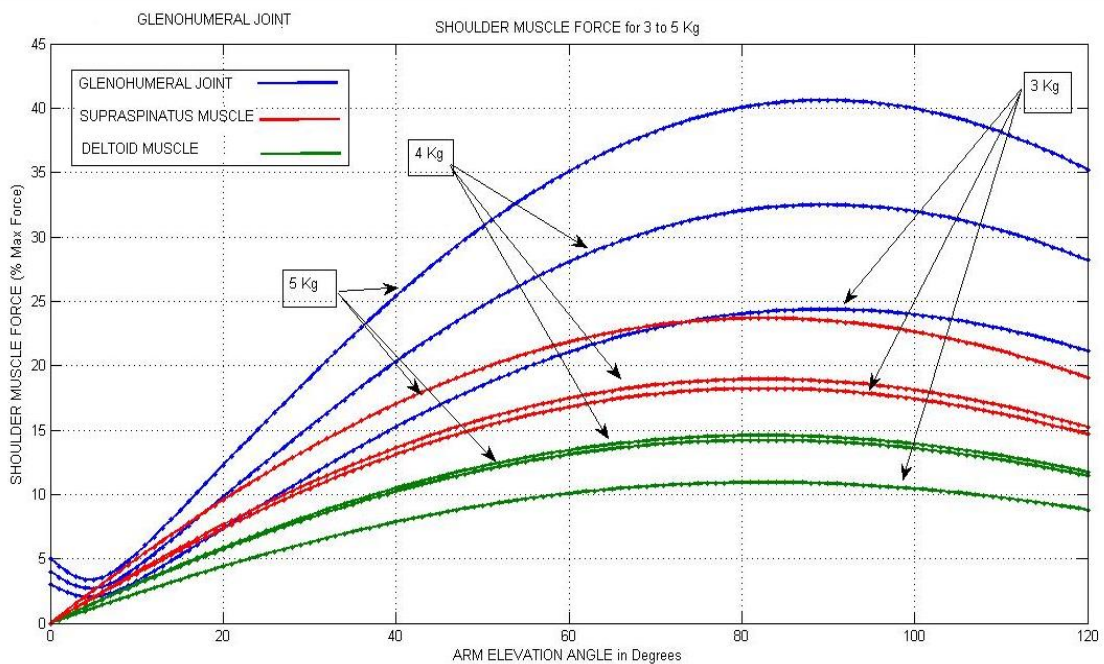


Fig. 4.23 Stress Distribution amongst the Rotor Cuff Muscles during Group Muscle Analysis

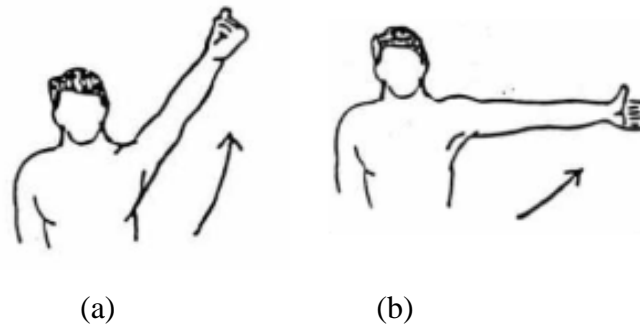


Fig 4.24 Arm Movement during (a) Elevation and (b) Abduction

The present work is focussed on the abduction arm movement in which the palm is facing inward (thumb out/ up) and the arm is raised out to the side and up toward the ear keeping arm straight at 175° angle as shown in Fig. 4.24. The present research results predicted that the maximum Von Mises stress were induced in the deltoid muscle during abduction arm movement. The deltoid muscle is the most sensitive muscle than the other four rotor cuff muscles in the abduction arm movement. Whereas the Supraspinatus muscle is the most sensitive muscle in elevation arm movement observed by Dul (1988).

The shoulder arm movement plane and the location of muscle are the two important parameters for the shoulder muscle analysis. As both the exercises (abduction and elevation) are done at the same point (shoulder joint) but in two different planes, therefore the maximum force/stress will be induced on the muscle which is opposite to the shoulder arm movement. Supraspinatus muscle is located opposite to the arm movement during elevation and deltoid muscle is located opposite to the arm movement during abduction. Therefore the maximum stress will get induced in the deltoid muscle during the abduction arm movement.

4.4.3 Remarks of Orthopedic Surgeons

Abduction is the range of movement, in which the arm is moving away from the midline of the body. Abduction arm movement is due to synergistic action of the three muscles; deltoid muscle contraction (initial ROM) followed by the supraspinatus contraction and then finally trapezius contraction. Deltoid is the only muscle in the arm having the fibers coming anteriorly, middle and posterior aspects and follows up

the shoulder arm movement. It is the initiator and follower of the abduction arm movement and is the most active shoulder muscle. The deltoid muscle is the most stabilizer muscle of the shoulder joint movement; especially the anterior deltoid provides the maximum stability than the posterior deltoid during abduction arm movement. During abduction arm movement the tension in the muscle will be maximum in the range of 70° to 80° and nullifies when reaches at the 90° . This is mainly due to the muscle mass breaking which is very high as compared to the synthesizing of the muscle mass in the range of 70° to 80° .

The present 3D FEM results of the shoulder joint muscles are in agreement with the the trends of SEMG tests conducted on the twelve patients. The results are also in agreement with the work done by Dul J et al. (1988), William Porter et al. (2010) and Webb et al. (2014). Deltoid muscle is the most sensitive muscle during the abduction arm movement. The present work will help researchers and orthopedicians for a better understanding of the shoulder joint mechanism and the most sensitive muscle during the abduction arm movement at different ROM. The orthopedic surgeons can take the corrective measures and focus their therapy to accelerate the healing process of the deltoid muscle by using various medication or physiotherapy techniques.

CHAPTER 5

RESULTS AND DISCUSSIONS: ANALYSIS OF KNEE JOINT

The previous chapter conferred about the different steps implemented to generate 3D FEM model for the knee joint. The post-processing was done in the ANSYS APDL software. The SEMG test conducted on eight patients during flexion movement was also discussed at length. The present chapter discusses the results of the 3D FEM analysis. Results of FEM analysis have been compared with the knee muscles test conducted by SEMG on a knee CPM machine and also with the previous work.

5.1 FEM ANALYSIS

The knee CAD model was imported in ANSYS APDL software for post-processing. Static analysis was done and the results of Von Mises stresses and an equivalent elastic strain were plotted and analyzed. The analysis was done for the rectus femoris and biceps femoris muscles of the knee joint. The maximum stressed muscle during flexion leg movement is analyzed and discussed in detail.

5.1.1 Analysis of Rectus Femoris and Biceps Femoris Muscles

Rectus femoris muscle was modelled on the knee bone from the patella; it is cylindrically shaped at the center, with its width narrowing at the ends and running straight down to the deep apo-neurosis and other end is connected to the hip. Similarly biceps femoris originates from the back side of the fibula and passes obliquely downward and lateral ward across covering the posterior surface of the femur bone to connect on the back end of the hip.

The results obtained from FEM analysis for the Von Mises stresses are mentioned in table 5.1. The simulation was done in nine steps for nine seconds and each second corresponds to 10° of rotations, the motion was chosen to be pure rotation along the knee joint in a single plane, required for flexion leg movement. Probes were added at six different locations in the knee muscles.

Table 5.1 Von Mises Stresses on Rectus Femoris Muscle

Rotation Angle (ROM)	Von Misses Stresses in MPa
10°	0.28535
20°	0.91502
30°	1.2942
40°	1.4137
50°	1.3443
60°	1.5579
70°	1.0498
80°	1.335
90°	0.82046

Fig. 5.1 shows the maximum Von Mises stresses in the rectus femoris muscle during flexion leg movement.

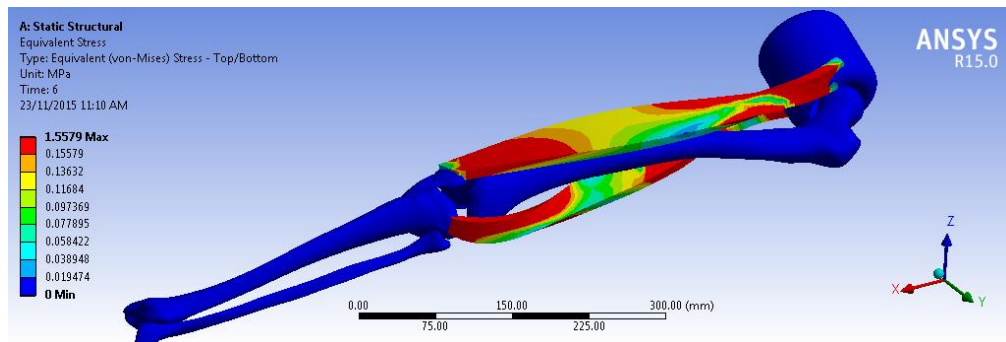


Fig. 5.1 Maximum Von Mises Stresses in Rectus Femoris Muscle

The muscle gets contracted as the knee joint is rotated from 0° to 90° during flexion leg movement. The muscle mass gets broken down and being synthesized with different rates during the movement of the leg. If the rate of breaking and synthesizing of the muscle mass is maintained (equal) then there will be no stresses induced in the knee muscles. If this rate is not maintained then the net effect will be the tissue formation around the joint and this induces the stresses in the knee muscle movement.

Maximum Von Mises stress is in the range of 55° to 65° during flexion leg movement and then it declined. The maximum Von Mises stresses in the rectus femoris muscle was 1.5579 MPa at 60° ROM during flexion leg movement.

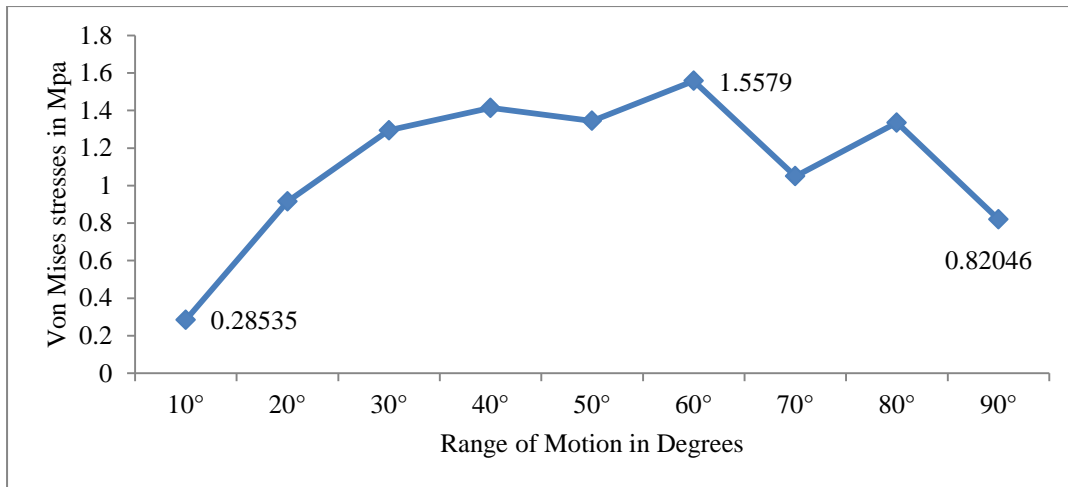


Fig. 5.2 Von Mises Stresses at Rectus Femoris Muscle during Flexion Leg Movement from 10° to 90°

As the flexion leg movement angle increases from 0° to 90°; the breaking down of the muscle mass increases and is maximum at 60° thus maximum Von Mises stresses gets induced in the knee muscle. The muscle mass breaking than synthesizing was more in the range of 50° to 70° ROM.

5.2 CPM MACHINE TEST

Fifty asymptomatic knee prone patients of different genders and age groups were tested on the developed knee CPM machine. The CPM machine was passed through series of motions for flexion and extension leg movement for 2 to 3 weeks. The test was conducted under the observation of the orthopedic surgeon. Table 5.2 shows the growth in the ROM of the patient during two weeks of the knee exercises on the developed knee CPM machine. (Appendix IX)

Table 5.2 Test Report of the Knee Joint Exercises on CPM Machine

Exercise	Range of Motion in Degrees															
	Day	01	02	03	04	05	06	07	08	09	10	11	12	13	14	%R
Flexion		45	50	55	60	65	65	70	70	75	80	85	85	95	95	79
Extension		40	50	55	55	60	65	70	75	75	80	90	90	95	100	83
Pain Scale		8.5	8.5	8	8	7.5	7.5	6	6	5.5	5	4.5	4	3.5	3.5	65

% R is the percentage recovery of the patient and it is calculated with respect to the normal range of motion of the knee joint and is mentioned in table 5.3.

Table 5.3 Normal Range of Motion for the Knee Joint Movement

Shoulder Exercise	Range of Motion in Degrees
Flexion	0 to 120
Extension	-120 to 0

Fig. 5.3 shows the improved ROM on the daily basis in the patients by using Knee CPM machine. This data will be useful for the orthopedic surgeon to understand the progress of the patients on regular basis and accordingly prescribe the medication and physiotherapy treatment to accelerate the healing and achieve the normal ROM. This % improvement is not compared to the normal range of motion. It is compared with the first day ROM of the subject.

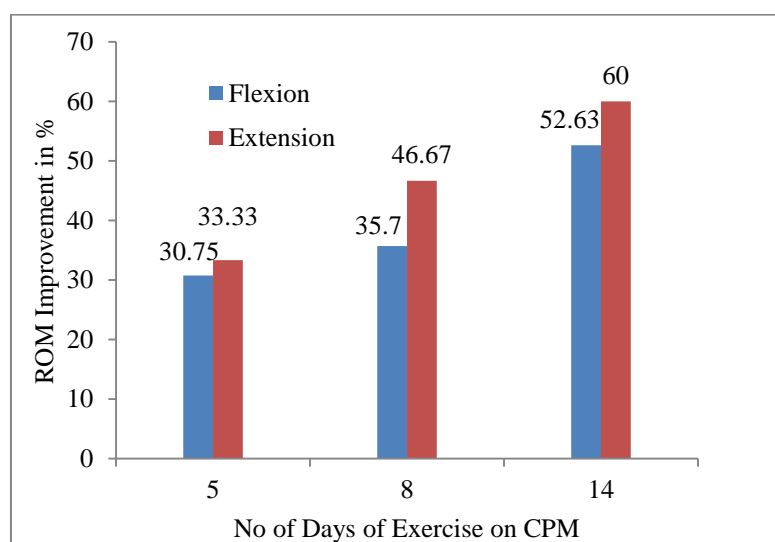


Fig. 5.3 Percentage Improvement in Knee ROM during Exercise on CPM Machine

Remarks of Orthopedic Surgeons: After two weeks of knee exercise on the CPM machine; subject's pain and range of motion improved by 79 % in flexion and 83% in elevation leg movements as compared to the normal range of motion. Two months ago the patient had met with a minor accident in which his left leg was injured. He needs further one week knee therapy on the CPM machine to get normal ROM. The progress is satisfactory. The reports attested that low cost knee CPM machine is full proof, comfortable and functioned satisfactorily for the knee leg movement. The cost

of the CPM exercise was also less and affordable for the knee joint patients. This tested CPM machine was further used to analyze the knee muscle behavior by using SEMG test on different patients.

5.3 MUSCLE ANALYSIS BY SEMG

Eight asymptomatic knee prone patients of different genders and age groups were tested by SEMG on the developed CPM machine. The SEMG machine was passed through series of motions for flexion leg movement for five days. The test was conducted under the observation of the Neurophysiotherapist surgeon in Talpallikar Physiotherapy center, Solapur, India.

Table 5.4 shows the maximum amplitude motor unit firing angle by SEMG test in the knee joint muscles during flexion leg movement.

Table 5.4 Maximum Motor Unit Firing Angle by SEMG Test on CPM Machine

	ROM in degrees for maximum amplitude display				
Movements	Day 1	Day 3	Day 5	Day 7	Day9
Flexion	60	65	70	80	90
Extension	65	70	75	85	90
Pain Scale	6	5.5	5	4	3

Table 5.5 shows the motor unit firing at different ROM in the rectus femoris and biceps femoris muscles during flexion leg movement by SEMG. The knee joint movement was very slow and continuous as the patients were under post-operative treatment; suffering from the knee pain and injuries. The exercise was done during the passive movement of the muscles; therefore the motor unit firing range was small. Due to pain the movement gets restricted, which causes shortening (contraction) of the muscle and the motor unit firing was observed. There was not significant variation in the motor unit firing amplitude of the muscles. Only five out of eight subjects have shown the appreciable change in the motor unit amplitude i.e. stress behavior. Table 5.5 shows the rectus femoris and biceps femoris muscles contraction against the ROM on the ninth day of the patients exercise on the CPM machine during flexion leg movement. The SEMG test reports of patient 01 are attached in **Appendix X**.

Table 5.5 Rectus Femoris and Biceps Femoris Contraction during Flexion

ROM in Degrees	Rectus Femoris (μV)	Biceps Femoris (μV)
15	0	0
20	75	0
25	70	75
30	175	75
35	200	100
40	250	175
45	275	75
50	225	100
55	50	25
60	0	125
65	0	75
70	0	0
75	0	0
80	0	0

Fig. 5.4 shows the motor unit firing against ROM of the subject 01 in rectus femoris and biceps femoris during SEMG testing on the developed knee CPM machine.

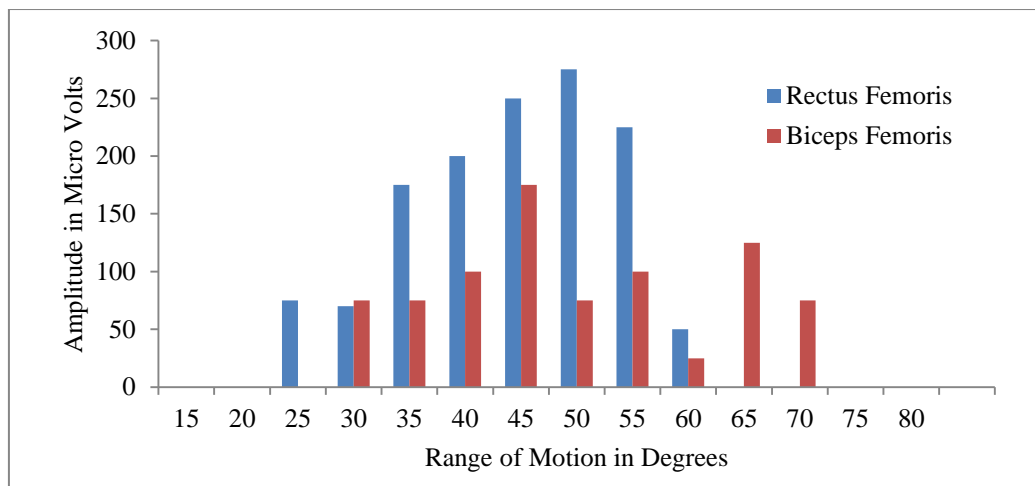


Fig. 5.4 Motor Unit Firing against ROM in Rectus Femoris and Biceps Femoris Muscles by SEMG

The maximum motor unit firing in the rectus femoris muscle was observed in the range of 40° to 60° and that of biceps femoris muscle at 45°. The same trend of motor

unit firing was observed in the test conducted on the remaining subjects for the rectus femoris and biceps femoris muscles. The plot of amplitude against ROM of the rectus femoris and biceps femoris muscle of the remaining four subjects is as shown in Fig. 5.5 and Fig. 5.6.

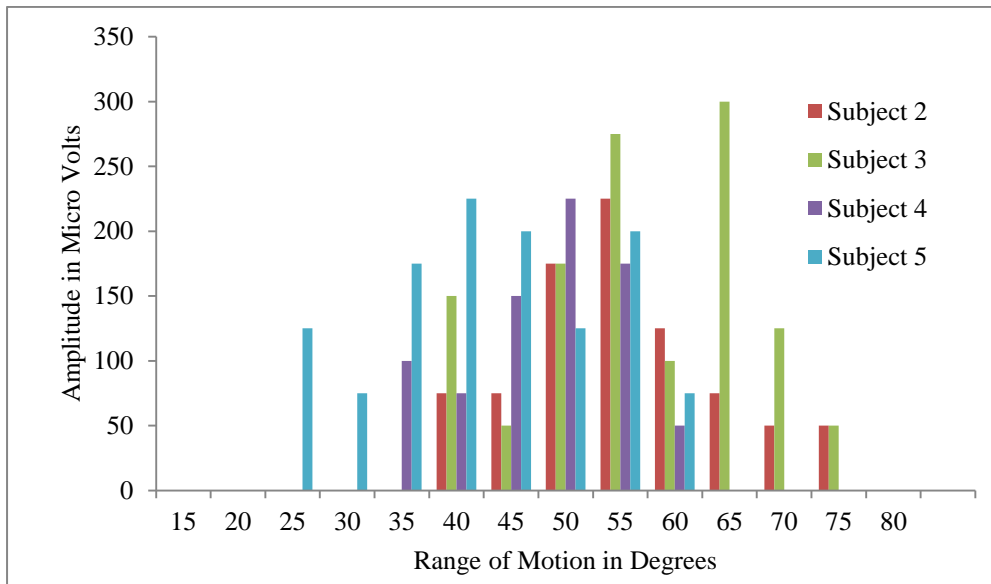


Fig. 5.5 Motor Unit Firing against ROM in Rectus Femoris Muscle during Flexion Leg Movement

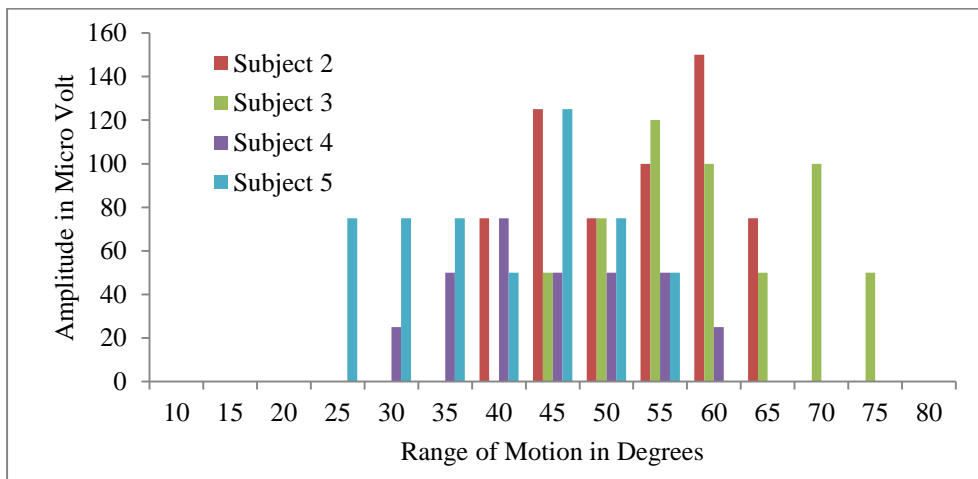


Fig. 5.6 Motor Unit Firing against ROM in Biceps Femoris Muscle during Flexion Leg Movement

From the Fig. 5.5 and Fig 5.6, it was found that the maximum muscle contraction of all the subjects during flexion leg movement was in the range of 45° to 65° of the ROM. As the flexion leg movement angle increases from 0° to 90°; the breaking

down of the muscle mass increases and is maximum in the range of 45° to 65°, thus maximum Von Mises stresses gets induced in the knee muscle.

5.4 DISCUSSIONS

The primary aim of the present work was to analyze the stresses induced in the major knee joint muscles during flexion leg movement by using 3D FEM model. Reverse modeling was used for the fast and accurate 3D model generation and the knee muscle stress analysis. Modeling of knee bones in CATIA V5 without any background help was very difficult and impractical. The free form option in CATIA V5 was not useful for modeling the complicated and irregular objects such as human bones. The minute detailing required during the modeling of ligaments, tendons and muscles was not so easy in CATIA V5 which is good for surface modeling. Therefore scanning of the complicated knee bones was done by ATOS III 3D scanner to generate accurate and detailed contours. 3D multiple scanning of the bones to obtain a point-cloud model was finalized in the present work. 3D bone geometry of the knee model was done in CATIA V5 software from the scanned .stl file. The geometrical features of higher order (curve and surfaces) were designed by filtering and aligning number of cloud points, tessellation of polygonal model, recognition and defining the referential geometrical entities. According to quadratic dependency, a non-homogeneous bone constitutive law was implemented.

Muscles were added on the knee joint models in CATIA V5. The model was imported in .igs format into ANSYS workbench for the Von Mises stress analysis. The kinematics for knee flexion leg movements were prescribed as an input to finite element simulations and the resulting muscles stresses were plotted. Careful alignment of the two muscles on fibula, patella, tibia and femur were done. Muscle initialization and precise location on knee bones were done (Blemker and Delp, 2005). The efficacy of the human joints model depends on the positioning, orientation and maintaining proper gap amongst the bones during flexion leg movement (Van der Helm, 1994). In the present FEM analysis there was no clash between knee bone to bone, muscle to muscle and muscle to bone during full range of motion. The muscle thickness varied from 5mm to 15mm along with its length to create a proper volume

of tissue over the knee bones. This ensured the real time behaviour of the knee joint with the animated one. During the muscle analysis, the Von Mises stresses induced in rectus femoris muscle was maximum (1.5579 MPa) compared to biceps femoris muscle. The maximum Von Mises stresses induced was in the range of 50° to 70° flexion angle during the FEM analysis.

5.4.1 Comparison of FEM Analysis Results with SEMG Analysis

Presently SEMG is the only feasible method to analyse the muscle contraction (stress) levels in the living objects. SEMG is used to analyze the muscles behavior during the human leg movements. The current SEMG set up has quantified the muscle behaviour in the knee joint during the flexion knee movement on the developed CPM machine. SEMG is closely related to muscles contraction and is an indicator of the associated actions. In the present work two channel passive electrode surface electromyography (SEMG) was used to measure the muscle contraction during the human leg movements.

Table 5.6 Maximum Contraction in Rectus Femoris and Biceps Femoris Muscle during SEMG Analysis at Different ROM in five Subjects

Subjects Number	ROM in Degrees	SEMG Amplitude (μ V)	
		Rectus Femoris	Biceps Femoris
01	40	250	175
	45	275	75
	50	225	100
02	50	175	75
	55	225	100
	60	125	150
03	50	175	75
	55	275	120
	60	100	100
04	50	225	50
	55	175	50
	60	50	25
05	45	200	125
	50	125	75
	55	200	50

Table 5.6 depicts the muscle contraction of the knee joint during the flexion leg movement by SEMG on the knee CPM machine. The maximum motor unit firing of the five patients is used for the rectus femoris and biceps femoris muscle analysis.

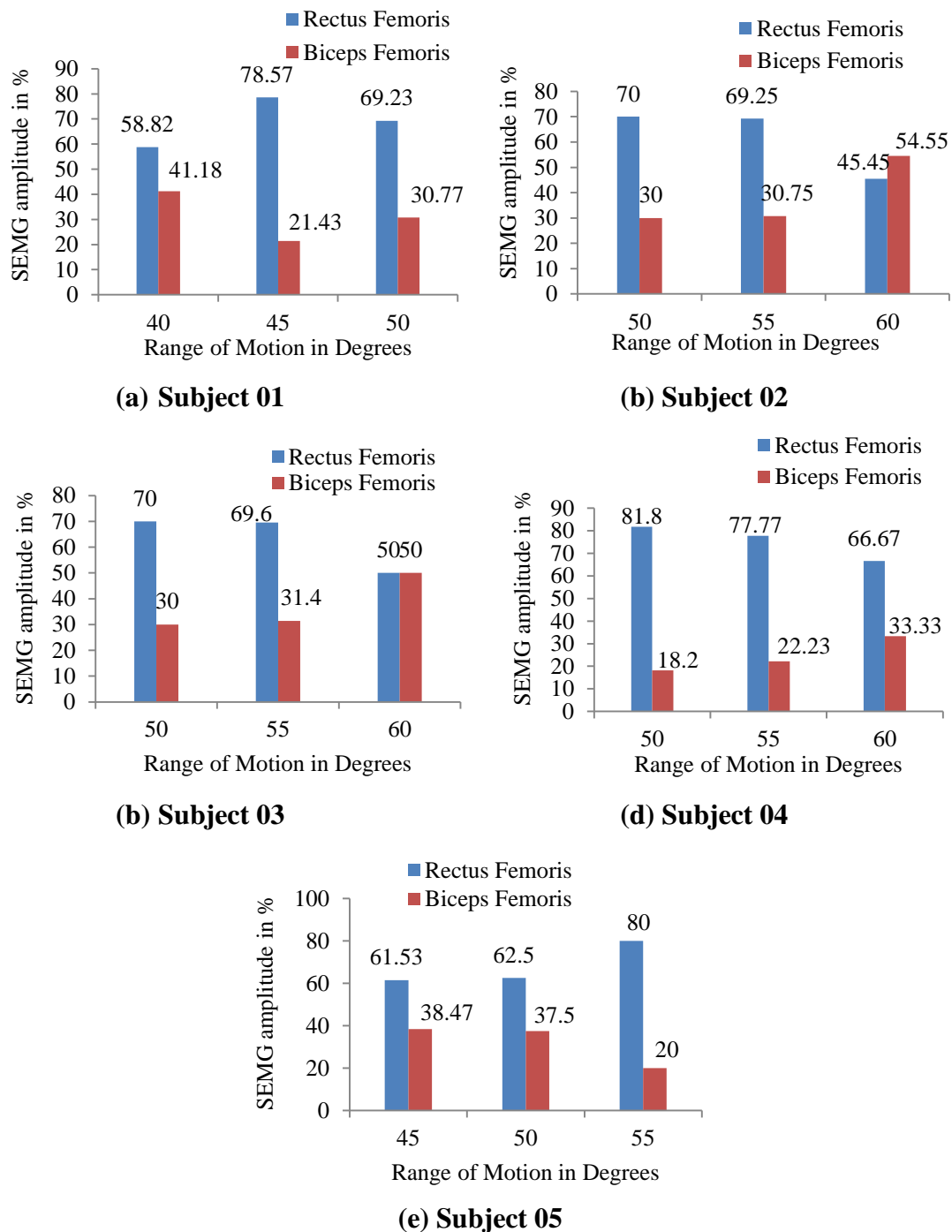


Fig. 5.7 Percentage Variation Muscle Contraction in the Rectus Femoris and Biceps Femoris Muscle during SEMG Test

It was found that during the SEMG analysis the maximum muscle contraction for all the subjects during flexion leg movement was in the range of 40° to 70° (average 55°). Fig. 5.7 shows the percentage variation in the muscle contraction of rectus femoris and biceps femoris muscle during SEMG analysis at different ROM of the five subjects.

During the SEMG muscle analysis of the five subjects, the muscle contraction (stress) obtained in rectus femoris muscle was maximum (275 μ V; 225 μ V; 275 μ V; 225 μ V and 200 μ V) compared to biceps femoris muscle (175 μ V; 150 μ V; 120 μ V; 50 μ V and 125 μ V) at different ROM during flexion leg movement and are mentioned in table 5.6. It was found that around 70% of the total Von Mises stresses were distributed in rectus femoris muscle during the flexion leg movement.

Though SEMG measures the electrical activity within a muscle; not the muscle force/stress directly. In the present work the maximum muscle contraction trends were compared with the 3D FEM analysis results of the knee joint muscle. The SEMG trends showed that maximum contraction during flexion leg movement is in the rectus femoris muscle than the biceps femoris muscle. The maximum motor unit firing (contraction; stress) was observed in the rectus femoris muscle probes in range of 50° to 70° during flexion leg movement. Thus rectus femoris muscle is the most stressed muscle in the knee joint during flexion leg movement. This will help the Orthopaedic surgeon to develop and focus on the new therapy to strengthen the rectus femoris muscle during flexion leg movement.

5.4.2 Comparison of FEM Results with Previous Work

Comparing the FEM results is a complicated task as the model to be validated is dimensionally complex with many components involved in the analysis. It becomes more challenging in the joint like knee where the degree of asymmetry and the variation in the muscle functions are unpredictable.

Edith et al., (2010) developed a knee 3D model to analyse the force and moment generation capacity of the lower limb muscle during walking. The maximum extension leg moment peaked in the biceps femoris muscle was 4.7 cm at 25° of the knee elevation compared to 3 cm at 55° of the knee flexion. The maximum force peaked in the biceps muscle was more during extension leg movement than during the

flexion leg movement. During the flexion leg movement, the maximum moment peaked was 13.9 cm in the rectus femoris muscle compared to 11.6 cm in the biceps femoris muscle. During flexion leg movement the peak force in rectus femoris muscle was 848.8 N compared to 705 N in biceps femoris muscle in the range of 40° to 70° of the ROM. During flexion leg movement the maximum force was generated in the rectus femoris muscle than the biceps femoris muscle.

In the present 3D FEM analysis the maximum Von Mises stresses are observed in the rectus femoris muscle during flexion leg movement is 1.5579 MPa. As during the knee joint movement the muscle mass breaking is maximum than muscle synthesizing at 60°, therefore maximum stress will generate at 60° in the rectus femoris muscle and the same trend was observed by Edith et al. (2010) in the lower limb muscle force and moment analysis during walking.

Mohsen et al., (2007) has developed 3-D finite element (FE) model for human buttocks to analyze the Von Mises stresses distribution in the skin, fat and thigh muscles. The model was validated for the soft tissue displacement with the MRI images of the buttock–thigh in a sitting posture for the same loading condition. The results predicted that the high compressive pressure in the soft tissue thigh muscle was in the range of 55–65 KPa.

In the present 3D FEM analysis the maximum Von Mises stresses are observed in the rectus femoris muscle during flexion leg movement is 1.5579 MPa. As during the knee joint movement the muscle mass breaking is maximum than muscle synthesizing, therefore maximum stress will generate at 60° in the rectus femoris muscle and the same trend was observed by Mohsen et al., (2007) during the Von Mises stresses distribution in the skin, fat and thigh muscles.

Ashutosh et al. (2014) have developed a 3D knee joint model to analyze the Von Mises stresses at the different loads conditions and weights. Scanning of the knee bones were done to get the correct dimensions, contours and profile of the bones. The 3D model is generated in Pro-Engineer Wildfire 4.0 modelling software. The FEM analysis was done in ANSYS software to get the Von Mises stresses at different loads. The results predicted that the maximum Von Mises stresses were in the range of 1.7MPa to 4.8 MPa acting on the knee joints muscles (upper femur part) when the femur part was fixed and load was applied on the tibial load during flexion leg

movement. The maximum Von Mises stresses were in the range of 12MPa to 30 MPa acting on the knee joints (upper femur part) when the femur part was fixed and load was applied on the tibial load during stair climbing (walking). The researcher has applied a load (490 N to 2448N) on tibial during the FEM analysis.

In the present 3D FEM analysis, external load is not applied on tibial, as the analysis is carried on the post-operative patients during flexion leg movement. Therefore the maximum Von Mises stresses in rectus femoris muscle during flexion leg movement (1.5579 MPa). In the present work due to passive motion condition, the stress values are less compared to the maximum Von Mises stresses in the range of 1.7MPa to 4.8 MPa observed by Ashutosh et al. (2014).

5.4.3 Orthopedic Surgeons Remarks

Flexion is the range of movement at the hip, in which the leg is moving around a knee joint such that angle between the femur and tibia goes on decreasing. It is a fusiform superficial fiber arranged in a twin-edged manner. It is the initiator and follower of the flexion leg movement and is the most active knee muscle. The rectus femoris and biceps femoris muscles are the most stabilizer muscle of the knee joint movement. During flexion leg movement the tension in the muscle will be more in the range of 50° to 70° and nullifies when it reaches at 80° ROM. This is mainly due to the rectus femoris muscle mass breaking is more compared to the synthesizing of the muscle mass in the range of 50° to 70°.

The present 3D FEM results of the knee joint muscles are in agreement with the trends of SEMG tests conducted on the eight patients. The results are also in agreement of the work done by Edith et al. (2010), Mohsen et al., (2007), Ashutosh et al. (2014). The rectus femoris muscle is the most stressed muscle during the flexion leg movement.

The present work will help researchers and orthopedicians for a better understanding of the knee joint mechanism and the most stressed muscle during the flexion leg movement at different ROM. The orthopedic surgeons can take the corrective measures and focus their therapy to accelerate the healing process of the rectus femoris muscle by using various medication or physiotherapy techniques.

CHAPTER 6

CONCLUDING REMARKS AND SCOPE FOR FUTURE WORK

This chapter concludes the findings of the present research work carried out to analyse the muscle behaviour in shoulder and knee joint during abduction and flexion movements and also present the scope for future work.

6.1 CONCLUDING REMARKS

Following objective conclusions are drawn from the present research work.

- 1) Finite Element Method (FEM) analysis was done to investigate the behavior of the shoulder muscles during the abduction arm movement. A 3D FEM shoulder joint model is developed for the five important shoulder muscles; deltoid, supraspinatus, subscapularies, teres minor and infraspinatus to evaluate the Von Mises stresses and an equivalent elastic strain for the shoulder abduction arm movement. The previous shoulder models developed by researchers have not considered the stress sensitivity analysis of the shoulder muscles during abduction arm movement. The Von Mises stresses from the FEM model has agreed well with the SEMG tests conducted on twelve subjects and the previous work in this area.
- 2) During the individual muscle FEM analysis, deltoid muscle was the maximum stressed muscle with 4.2175 MPa, amongst the five shoulder joint muscles. During abduction arm movement 46.85 % of the stress amongst these five muscles was distributed in the deltoid muscle. Hence, deltoid muscle is the most stressed muscle amongst these five shoulder muscles during the abduction arm movement.
- 3) During the group muscles FEM analysis also, deltoid muscle was the maximum stressed muscle with 2.4127 MPa, amongst the five shoulder joint muscles.

During abduction arm movement 38.25 % of the total stresses amongst these five muscles are distributed in the deltoid muscle.

- 4) Supraspinatus muscle was the next maximum stressed muscle after the deltoid muscle, with 1.6205 MPa (18%) in individual muscle analysis and 1.216 MPa (19.28%) in group muscle analysis. The rest of the three muscles namely: subscapularies, infraspinatus and teres minor muscles are stressed next to the supraspinatus muscle.
- 5) The shoulder joint muscle analysis was performed using SEMG test on twelve shoulder prone patients. As the test was conducted during the passive shoulder movement, there was no significant variation in the muscle contraction (motor unit firing amplitude) in three out of five muscles. The SEMG test was conducted on all four rotor cuff muscles and also on deltoid muscle to analyze the dominant muscle during abduction arm movement.
- 6) The maximum muscle contraction was observed in the deltoid muscle in the range of 70° to 90° of the arm movement. The same trend was observed in all the twelve SEMG tested patients.
- 7) During the SEMG study; 48.15 % of the muscle contraction was observed in deltoid muscle compared to 25.92% in supraspinatus, 11.11% in infraspinatus, 11.11% in subscapularies and 3.71% in teres minor muscle during the abduction arm movement. SEMG test results also revealed that deltoid is the most sensitive muscle amongst the five shoulder muscles during abduction arm movement.
- 8) The Von Mises stress FEM results of the present work were in agreement with the trends of the muscle behavior during SEMG analysis for all the eight patients. The stress results are also in agreement with the work done by Dul (1988), William et al. (2010) and Webb et al. (2014).
- 9) FEM analysis was done to investigate the Von Mises stresses in two important knee joint muscles; rectus femoris and biceps femoris during the flexion leg movement. The previous knee models developed by researchers have not considered the stress analysis of the knee muscles during the flexion leg movement. During 3D FEM muscle analysis rectus femoris muscle was the maximum stressed muscle with 1.5579 MPa.

- 10) The knee joint muscle analysis was conducted on eight knee prone patients by SEMG. As the test was conducted during the passive knee movement, there was no significant variation in the contraction (motor unit firing amplitude) of the knee joint muscles. The maximum muscle contraction was observed in the rectus femoris muscle in the range of 40° to 70° during flexion leg movement. A similar trend was observed in all the eight patients tested by SEMG.
- 11) During the SEMG study, 70 % of the muscle contraction was observed in the rectus femoris muscle compared to 30% in the biceps femoris muscle during the flexion leg movement. The SEMG test results also showed that the rectus femoris was the most stressed muscle amongst these two muscles for the flexion leg movement.
- 12) In the present study Von Mises stress results by FEM method are in agreement with the SEMG test results on knee prone five patients. The Von Mises stress FEM results of the present work are also in agreement with the work done by Edith Arnold et al. (2010), Mohsen et al. (2007) and Ashutosh et al. (2014).
- 13) The SEMG test was conducted on the developed shoulder and knee CPM machines and the CPM machine cost has been reduced to approximately 40% of the existing machines cost. The machine is foolproof, user friendly and meets all the functional requirements of the shoulder and knee exercises satisfactorily. The Orthopedic surgeon has certified the CPM machines for the shoulder and knee exercises (**Appendix III**).

6.2 MAJOR RESEARCH OUTCOMES

- 1) In case of shoulder joint, deltoid muscle is the most stressed muscle during the abduction arm movement.
- 2) In case of knee joint rectus femoris muscle is the most stressed muscle during the flexion leg movement.
- 3) Present research work provides researchers and orthopedic surgeons a better understanding of the behaviour of shoulder and knee joint muscles during the abduction arm and flexion leg movement at different ROM.
- 4) SEMG analysis was conducted on the passive movements of shoulder and knee joint muscles on the developed CPM machine and the use of developed low cost

CPM machine for the shoulder and knee joints is found to be a cost effective treatment for the rehabilitation of patients.

6.3 SCOPE FOR FUTURE WORK

The present work can be extended in number of directions as given below:-

- 1) In the present work, FEM analysis of the shoulder joint muscles is done for abduction arm movement. The same model can be utilised for adduction, elevation and flexion arm movement with some modification in the orientation and attachments of the muscles. The shoulder bone orientation and alignment should be done with utmost care and each bones axis and gap between them should be maintained.
- 2) FEM analysis for shoulder joint muscle is done for five major muscles; four rotor cuff muscles and deltoid muscle. As these muscles are the major shoulder joint muscles therefore these are considered for the present work. Shoulder joint consists of 20 muscles, adding theses muscles in the existing model would broaden the understanding of individual muscle behaviour during the abduction arm movement. However this will increase the computational cost and degrees of freedom.
- 3) FEM analysis for knee joint muscle is done for only two major muscles rectus femoris and biceps femoris for flexion leg movement in the present work. This work can be further extended by adding Vastus medial, Vastus lateralis Sartorius, semitendinosus, semimembranosus to analyse the Von Mises stresses during flexion and extension of leg movement. However this will increase the computational cost and degrees of freedom. Due to addition of these muscles the analysis time will increase considerably as in the present work for two muscles FEM analysis took eighteen hours.
- 4) As human joints are the over determined system having many more actuators than degrees of freedom, it will be better if the muscles functional analysis is done by using an optimization approach. The present 3D FEM analysis requires large functional evaluations and high computational time. Hybrid model which is simpler and time saving can be one of the possible approaches.

REFERENCES

- Adouni, M. and Shirazi-Adl, A. (2013). "Evaluation of Knee Joint Muscle Forces and Tissue Stresses-Strains during Gait in Severe OA versus Normal Subjects." *Wiley Periodicals, Inc. J Orthop Res*, 32, 69-78.
- Alexandre, Terrier., Vittoria, Brighenti., Dominique, Pioletti. (2012). "Importance of polyethylene thickness in total shoulder arthroplasty: A finite element analysis." *Clinical Biomechanics (Bristol, Avon)*, 27(5), 443-448.
- Alexandre, Terrier., Xabier, Larrea., Jonas, Guerdet., Xavier, Crevoisier. (2014). "Development and experimental validation of a finite element model of total ankle replacement." *Journal of Biomechanics*, 47, 742–745.
- Amirreza, Ziai. and Carlo, Menon. (2011). "Comparison of regression models for estimation of isometric wrist joint torques using surface electromyography." *Journal of Neuro Engineering and Rehabilitation*, 8, 56-62.
- Anitha, Oomen. (2010). "Basic Anatomy." *Ane Books Pvt Ltd*, ISBN: 978-93-8015-655-2, 1, 33-34.
- Ashutosh, Nayan, Nautiyal., P.K.S. Nain. and Pramod, Kumar. (2014). "Study of Knee-Joint Mechanism before Implanting a Knee Prosthesis by Modeling and Finite Element Analysis of Knee-Joint Bones." *International Journal of Advanced Mechanical Engineering*, 4(7), 721-727.
- Astier, V., Thollon, L., Pierre-Jean, A. and Frédéric M. (2007). "A finite element model of the shoulder for many applications: trauma and orthopaedics." *1st European Hyperworks Technology Conference, Berlin*.
- Blemker, S. S. and Delp, S. L. (2005). "Three-dimensional representation of complex muscle architectures and geometries." *Ann Biomed Eng*, 33(5), 661-673.
- Blemker, S, S. and Delp, S, L. (2006). "Rectus femoris and vastus intermedius fiber excursions predicted by three-dimensional muscle models." *Journal of Biomechanics*, 39, 1383–1391.

- Biçer, A. and Ankarali, H. (2010). "Shoulder Pain and Disability Index: a validation study in Turkish women." *Singapore Med J*, 51, 865-870.
- Bradley, D., Acosta-Marquez, C., Hawley, M., Brownsell, S., Enderby, P. and Mawson S. (2009). "NeXOS-The design, development and evaluation of a rehabilitation system for the lower limbs." *Mechatronics*, 19 (2), 247-257.
- Brooke, J. D., Cheng, J., Collins, D. F., Mcilroy, W. E., Misiaszek, J. E., and Staines, W. R. (1997). "Sensori-sensory afferent conditioning with leg movement: gain control in spinal reflex and ascending paths." *Progress in Neurobiology*, 51, 393-421.
- Burckhardt, S. Carol. and Jones, Kim. D. (2003). "Adult Measures of Pain." *Arthritis & Rheumatism (Arthritis Care & Research)*, 49(5S), S96- S104.
- Büchler, P., Ramaniraka, N. A., Rakotomanana, L. R., Iannotti J.P., Farron, A., (2002). "A finite element model of the shoulder: application to the comparison of normal and osteoarthritic joints." *Clinical Biomechanics*, 17 (10), 630- 639.
- Carel, G.M. Meskers., Jurriaan, H. Groot., Henk, J. Arwert., Piet, M. Rozing. (2004). "Reliability of force direction dependent EMG parameters of shoulder muscles for clinical measurements." *Journal of clinical Biomechanical*, 19 (9), 913-920.
- Carol, Oatis. (2009). "Kinesiology: Introduction to biomechanical analysis, The Mechanics and Path Mechanics of Human Movement." *Lippincott Williams & Wilkin*, 1, 115-122.
- Chandreshwar, Rao., Clare, K. Fitzpatrick., Paul, J. Rullkoetter., Lorin, P. Maletsky., Raymond, H. Kim., Peter, J. Laz. (2013). "A statistical finite element model of the knee accounting for shape and alignment variability." *Medical Engineering & Physics*, 35, 1450 - 1456.
- Christopher, J. Gat., Lisa, Case. Doro., Joseph, E. Langenderfer., Amy, G. Mell., Joseph, D. Maratt., Richard, E. Hughes., James, E. Carpenter. (2008). "Evaluation of three methods for determining EMG-muscle force parameter estimates for the shoulder muscles." 23(2), 166-174.
- Cram, Jeffrey. and Kasman, Glen. (2005). "The Basics of Surface Electromyography." *John & Brett Publication* ,1, 1-8.

- Dale, L. Rickert., Mark, Halaki., Karen, A. Ginn., Margaret, S. Barrett., Bronwen, J. Ackermann. (2013). "The use of fine-wire EMG to investigate shoulder muscle recruitment patterns during cello bowing: The results of a pilot study." *J Electromyogr Kinesiol*, 23(6), 1261- 1268.
- Daniel, Chen., Anish, Ravindran., Pradeep, Vishwa, Brahmana, Saraf. (2011). "Reverse Engineering Closely-Spaced Free-Form Shapes for a Fabric-over-Body Model." *Engineering*, 3, 1022-1029.
- Dao, Tuan., Tien. (2015). "Musculoskeletal Simulation for Assessment of Effect of Movement-Based Structure-Modifying Treatment Strategies." *Journal of Computational Medicine*, 1, 1-12.
- Dark, A., Ginn, K. A. and Halaki, M. (2007). "Shoulder muscle recruitment patterns during commonly used rotator cuff exercises: an electromyography study." *Phys Therapy*, 87(8), 1039-1046.
- David, G., Magarey, M.E., Jones, M.A., Devir, Z., Türker K.S. (2000). "EMG and strength correlates of selected shoulder muscles during rotations of the glenohumeral joint." 15(2), 95-102.
- Dew, Ashley. P., Moreau, Noelle. G., (2012). "A Comparison of 2 Techniques for Measuring Rectus Femoris Muscle Thickness in Cerebral Palsy." *Paediatric Physical Therapy*, 24(3), 218–222.
- Dinesh, Kant. Kumar., Dickstein, R.E., Arjunan, Sridhar. Poosapadi. and Singh, Vijay. Pal. (2013). "Towards identification of finger flexion's using single channel surface electromyography – able bodied and amputee subjects." *Journal of Neuro engineering and rehabilitation BioMed Journal*, 10, 41-50.
- Douglas, D. Robertson., Yuan, J., Bigliani, L. U., Flatow E. L., Ken, Yamaguchi. (2000). "Three-Dimensional Analysis of the Proximal Part of the Humerus: Relevance to Arthroplasty." *The Journal of Bone and Joint Surgery*, 82(11), 1594-1602.
- Dul, J. (1988). "A biomechanical model to quantify shoulder load at the work place." *Clinical Biomechanics*, 3, 124-128.

- Edith, M. Arnold., Samuel, R. Ward., Richard, L. Lieber. and Scott, L. Delp. (2010). "A Model of the Lower Limb for Analysis of Human Movement." *Annals of Biomedical Engineering*, 38(2), 269–279.
- Ellis, B.J., Debski, R.E., Moore, S.M., McMahon, P.J., Weiss, J.A. (2007). "Methodology and Sensitivity Studies for Finite Element Modeling of the Inferior Glenohumeral Ligament Complex." *Journal of Biomechanics*, 40(3), 603-612.
- Eriko, Kitamura., Roxana, Stegaroiu., Shuichi, Nomura., Osamu, Miyakawa. (2004). "Usage in application for preoperative planning in orthopedic." *Clin. Oral Impl. Res.*, 15, 401–412.
- Farhad, Nabhani., Martin, McKie., Simon, Hodgson. (2009). "Manufacture of a mechanical test rig to simulate the movements of forces within the shoulder." *Robotics and Computer - Integrated Manufacturing*, 25, 1008-1014.
- Fausto, Bernardini., Holly, E. Rushmeier. (2002). "The 3D Model Acquisition Pipeline." *Computer Graphics Forum*, 21 (2), 149–172.
- Fleishmann, P., Kosik, R., Selberherr, S. (1999). "Simple Mesh Examples to Illustrate Specific Finite Element Mesh Requirements." *8th Int. Meshing Roundtable*, 241–246.
- Garner, B. A. and Pandy, M. G. (2001). "Musculoskeletal model of the upper limb based on the visible human male dataset." *Comput Methods Biomech Engin, PubMed*, 4, 93-126.
- Gulshan, B.Sharma., Richard, E. Debski., Patrick, J. McMahon., Douglas, D. Robertson. (2010). "Effect of glenoid prosthesis design on glenoid bone remodelling: Adaptive finite element based simulation." *Journal of Biomechanics*, 43, 1653–1659.
- Gupta, Sanjay. and Frans, Vander, Helm. (2004). "Load transfer across the scapula during humeral abduction." *Journal of Biomechanics*, 37, 1001–1009.
- Gupta, S., van der Helm., Keulen, F. (2004). "Stress analysis of cemented glenoid prostheses in Total Shoulder Arthroplasty." *Journal of Biomechanics*, 37, 1777–1786.
- Hamill, Joseph. and Kuntzen, Kathleen. (2003). "Biomechanical Basis of Human Movement." *Lippincott Williams & Wilkins; Second edition, ISBN-13:, 978-0781734059*, 132–133.

- Henk, J. Arwert., Jurriaan, de. Groot., Wilbert, W. L., Woensel, M. Van. and Piet, M. Rozing. (1997). "Electromyography of shoulder muscles in relation to force direction." *J Shoulder Elbow Surg*, 6(4), 360-370.
- Holen, E. (1936). "Studies of the Yaqui Indians of Sonora, Mexico." *Lubbock Publication*, 12, 97-99.
- Huskisson, E.C., Jones, J., Scott, P.J. (1976). "Application of visual analogue scales to the measurement of functional capacity." *Rheumatol Rehabil*, 15, 185-187.
- Ingrassia, T., Nalbone, L., Nigrelli, V., Tumino, D., Ricotta, V. (2013). "Finite element analysis of two total knee joint prostheses." *Int. J Interact Des Manuf.*, 7, 91–101.
- Iwamoto, M., Nakahira, Y., Kimpara, H., and Sugiyama, T. (2009). "Development of a Human FE Model with 3-D Geometry of Muscles and Lateral Impact Analysis for the Arm with Muscle Activity." *Society of Automotive Engineers*, 01(22), 1-10.
- Jaspal, Sandhu., Shruti, Mahajan. and Shweta Shenoy.(2008). "An electromyographic analysis of shoulder muscle activation during push-up variations on stable and labile surfaces." *Int J Shoulder Surg.*, 2(2), 30- 35.
- Jeffrey, A. Weiss., John, C. Gardiner., Benjamin, J. Eriko., Trevor, J. Lujan., Nikhil, S. Phatak. (2005). "Three-dimensional finite element modeling of ligaments: Technical aspects." *Medical Engineering & Physics*, 27, 845- 861.
- Jesse, E. Bible., Andrew, K. Simphon., Debdut, Biswas., Richard, Pelker., Jonathen, Grauer. (2009). "Actual Knee Motion during continuous Passive Motion Protocols is Less than Expected." *Clin Orthop Relat Res*, 467(10), 2656- 2661.
- Yao, Jiang., Arthur, D. Salo., Jordan, Lee., Amy, L. Lerner. (2008). "Sensitivity of tibio-menisco-femoral joint contact behavior to variations in knee kinematics." *Journal of Biomechanics*, 41, 390- 398.
- Jinks, C., Jordan, K., Croft, P. (2002). "Measuring the population impact of knee pain and disability with the Western Ontario and McMaster Universities Osteoarthritis Index (WOMAC)." *Pain*, 100(1-2), 55-64.

John, J. Elias. Sonnissonsi. and Archana, Saranathan. (2013). “Discrete Element Analysis for Characterizing the Patellofemoral Pressure Distribution: Model Evaluation.” *J Biomech Eng*, 135(8), 111–116.

Johnson, C.A. (1992). “Comparison of postoperative analgesic effects of intra-articular bupivacaine and morphine following arthroscopic knee surgery.” *Medicine & Health & Social Sciences, the Journals of Gerontology*, 51(1), 24-29.

Shigle, Josef. Edward. (2003). “Mechanical Engineering Design.” *Mc Graw Hill Inc*, ISBN-10: 0071232702, 7, 1101-1146.

Kluess, Daniel. (2010). “Finite Element Analysis in Orthopedic Biomechanics, Finite Element Analysis.” *David Moratal (Ed.)*, ISBN: 978-953-307-123-7, 10-112.

Konrad, Peter. (2005). “The ABC of EMG: A practical introduction to kinesiological electromyography.” *Noraxon INC*, 1, 1-58.

Klyvia, Juliana, Rocha, de Moraes., Daniele, Andrade, da Cunha., Luciana, Ângelo, Bezerra., Renata, Andrade, da Cunha., Hilton, Justino, da Silva. (2012). “Surface Electromyography: Proposal of a Protocol for Cervical Muscles.” *Journal of CEFAC*, 14(5), 918-924.

Lacroix, D. and Prendergast, P. J. (1997). “Stress analysis of glenoid component designs for shoulder arthroplasty.” *Process Instrumentation Mechanical Engineers*, 211, 467- 477.

Lacroix, D., Murphy, L.A. and Prendergast, P.J. (2000). “Three dimensional finite element analysis of glenoid replacement prostheses: comparison of keeled and pegged anchorage systems.” *J Biomech Eng*, 122, 430-436.

Last, R. J. (1948). “Some Anatomical details of the Knee joint.” *The journal of bone and joint surgery*, 30, 683-688.

Laura, Tomatis., Masaru, Nakaseko., Thomas, Laubli. (2009). “Co-activation and maximal EMG activity of forearm muscles during key tapping.” *International Journal of Industrial Ergonomics*, 39, 749–755.

Lee, S. B., Kim, K. J., O'Driscoll, S. W., Morrey, B. F. and An, K. N. (2000). “Dynamic glenohumeral stability provided by the rotator cuff muscles in the mid-

range and end-range of motion. A study in cadavera.” *J Bone Joint Surg Am* 82(6), 849-857.

Lee, V. S. P., Gross, P., Spence, W.D., Solomonidis, S.E., and Paul, J. P. (1998). “Two Dimensional Finite element model of a transverse section of the trans-femoral amputees stump.” *Computer Methods in Biomechanics and Biomedical Engineering*, 2(2), 577-599.

Liu, J., Hughes R.E., Smutz W.P., Niebur, G., Nan-An, K. (1997). “Roles of deltoid and rotor cuff muscles in shoulder elevation.” *Clin Biomech*, 12(1), 32-38.

Liu, Danuta. Roman.,Tomasz, Tokarski., Joanna, Kamin, Iska. (2001). “Assessment of the Musculoskeletal Load of the Trapezius and Deltoid Muscles during Hand Activity.” *International Journal of Occupational Safety and Ergonomics*, 7(2), 179 - 193.

London, N. J., Brown, M. and Newman, R. J. (1999). "Continuous Passive Motion: Evaluation of a new portable low cost machine.” *Physiotherapy*, 85, 616- 618.

Lukáš, Zach., Lenka, Kunčická., Pavel, Růžička., Radim, Kocich. (2014). “Design, analysis and verification of a knee joint on ecological prosthesis finite element model.” *Computers in Biology and Medicine*, 54, 53- 60.

Magnus, K. Gislason., Benedict, Stansfield., David, H. Nash., (2010). “Finite element model creation and stability considerations of complex biological, articulation: The human wrist joint.” *Medical Engineering & Physics*, 32, 523- 531.

Marco, Viceconti., Cinzia, Zannoni., Luisa, Pierotti. (1998). “TRI2SOLID: an application of reverse engineering methods to the creation of CAD models of bone segments.” *Computer Methods and Programs in Biomedicine* , 56 (3), 211-220.

Marko, Veselinovic. Nikola, Vitkovic., Dalibor, Stevanovic., Miroslav, Trajanovic., Stojanka, Arsic., Jelena, Milovanovic. and Milos, Stojkovic. (2011). “Study on Creating Human Tibia Geometrical Models.” *Proceedings of the 3rd International Conference on E-Health and Bioengineering*, ISBN: 978-606-544-078-4,195-199.

- Masami, Iwamoto., Kauzo, Miki., King, H. Yang. (2001). “Development of Finite Element Model of the Human Shoulder to Investigate the Mechanical Responses and Injuries in Side Impact.” *JSME International Journal*, 44(4), 1072-1081.
- Maurel, N., Diop , A., Grimberg, J. (2005). “A 3D finite element model of an implanted scapula: importance of a multi parametric validation using experimental data.” *Journal of Biomechanics*, 38, 1865–1872.
- Melisa, M. B., Morrow, Kenton. R., Kaufman, Kai-Nan. An. (2010). “Shoulder model validation and joint contact forces during wheelchair activities.” *Journal of Biomechanics*, 43(13), 2487-2492.
- Mohsen, Makhsous., Dohyung, Lim., Ronald, Hendrix., James, Bankard., William., Rymer, Z. and Fang, Lin. (2007). “Finite Element Analysis for Evaluation of Pressure Ulcer on the Buttock: Development and Validation.” *IEEE Trans Neural System Rehabilitation Engineering*, 15(4), 517- 525.
- Murphy, L.A., Prendergast, P. J. and Resch, H. (2001). “Structural analysis of an offset-keel design glenoid component compared with a center-keel design.” *J Shoulder Elbow Surg*, 10, 568- 579.
- Ngoc-Bich, Le., Huu-Nghia, Nguyen., and Duy-Anh, Nguyen. (2013). “Study on Mechanical Adaptive Design, Construction and Control of Knee Continuous Passive Motion Machine.” *Journal of Automation and Control Engineering*, 1 (3), 227- 231.
- Onderko, Lynn. and Saqib, Rehman. (2013). “Treatment of Articular Fractures with Continuous Passive Motion.” *Orthopedic Clinics of North America*, 44 (3), 345–356.
- Pasquale, Farsetti., Roberto, Caterini.,Vito, Potenza.,Vincenzo, De. Luna., Fernando, De. Maio., Ernesto, Ippolito. (2009). “Immediate continuous passive motion after internal fixation of an ankle fracture.” *J Orthopaed Traumatol Springer-Verlag*, 10, 63–69.
- Pena, E., Calvo, B., Martinez, M.A., Doblare, M. (2006). “A three-dimensional finite element analysis of the combined behaviour of ligaments and menisci in the healthy human knee joint.” *Journal of Biomechanics*, 39, 1686–1701.

- Philippe, Favre., Christian, Gerber., Christian, Gerber. (2010). "Automated muscle wrapping using finite element contact detection." 43(10), 1931- 1940.
- Raja, S.N., Dickstein, R.E., Johnson, C.A. (1992). "Comparison of postoperative analgesic effects of intraarticular bupivacaine and morphine following arthroscopic knee surgery Medicine & Health & Social Sciences." *The Journals of Anesthesiology*, 77(6), 1143-1147.
- Raja,S.N., Dickstein, R.E., Johnson, C.A. (1992). "Comparison of postoperative analgesic effects of intraarticular bupivacaine and morphine following arthroscopic knee surgeryMedicine & Health & Social Sciences." *The Journals of Anesthesiology*, 77 (6), 1143-1147.
- Rakotomanana, L. R., Terrier, A., Ramaniraka, N. A. and Leyvraz, P. F. (1999). "Anchorage of orthopedic prostheses: influence of bone properties and bone- implant mechanics in Synthesis in bio solid mechanics." *Kluwer Academic Publishers*, 69, 55–66.
- Ring, D., Hotchkiss, R.N., Guss, D. B., (2005). "Hinged elbow external fixation for severe elbow contracture." *J Bone Joint Surg Am*, 87(6), 1293-1296.
- Romanes, G. J., (1986). "Cunninghams Manual of Anatomy, Upper and Lower Limb." *Oxford Press*, 1(15), 60-61.
- Ronald, L. Huston. (2013). "Fundamental of Biomechanics." *Taylor & Francis Group, CRC Press, ISBN 978-1-4665-1037-1*, 1, 22-277.
- Schmidutz, F., Agarwal Y., Müller, P.E., Gueorguiev, B., Richards, R.G., C.M. Sprecher. (2014). "Stress-shielding induced bone remodelling in cement less shoulder resurfacing arthroplasty: a finite element analysis and in vivo results." *Journal of Biomechanics*, 47, 3509–3516.
- Scott, E. Rand., Chris, Goerlich., and Kristina, Marchand. (2007). "The Physical Therapy Prescription." *Am Fam Physician*, 76(11), 1661-1666.
- Shawn, O'Driscoll. W. and Nicholas, J. Giori. (2000). "Continuous Passive Motion (CPM): Theory and Principles of Clinical Application." *Journal of Rehabilitation Research and Development*, 37, 179- 188.

- Shota, Miyaguchi., Kousei, Nojiri., Nobutomo, Matsunaga. and Shigeyasu, Kawaji. (2008). "An Effective Movement in CPM for Shoulder Joint." *IEEE International Conference on Systems, Man and Cybernetics, ICSMC.2008.4811331*, 530-534.
- Suman, Kanti. Chowdhury., Ashish, D. Nimbarte., Majid, Jaridi., Robert, C. Creese. (2013). "Discrete wavelet transform analysis of surface electromyography for the fatigue assessment of neck and shoulder muscles." *Journal of Electromyography and Kinesiology Elsevier*, 23, 995–1003.
- Tammy, L., Haut, Donahue., Hull, M. L., Mark, M. Rashid., Christopher, R. Jacobs. (2002). "A Finite Element Model of the Human Knee Joint for the Study of Tibio-Femoral Contact, *Journal of Biomechanical Engineering.*" 124, 273-280.
- Tenore, F., Ramos, A., Fahmy, A., Acharya, S., Etienne-Cummings, R., Thakor, N. V. (2009). "Decoding of individuated finger movements using surface electromyography." *IEEE Trans Biomed Eng*, 10(5), 1427–1434.
- Terrier, A., Rakotomanana, L., Ramaniraka, N., Leyvraz. 1997. "Adaptation models of anisotropic bone." *Computer Methods in Biomechanics and Biomedical Engineering*, 1, 47–59.
- Toby, O. Smith. and Leigh, Davies. (2007). "The efficacy of continuous passive motion after anterior cruciate ligament reconstruction: A systematic review." *Physical Therapy in Sport*, 8 (3), 141–152.
- Thollon, Lionel., Pierre-Jean, Arnoux., Frédéric Mouret., Christian Brunet. (2008). "Finite element simulation of humeral intramedullary nailing: case of torsion loading." *2nd European Hyperworks Technology Conference – Strasbourg*.
- Veeger, H.E.J. and Vander Helm, F.C.T. (2007). "Shoulder function: The perfect compromise between mobility and stability." *Journal of Biomechanic*, 40, 2119-2129.
- Venkatesh, Balasubramanian. and Srinivasan, Jayaraman. (2009). "Surface EMG based muscle activity analysis for aerobic cyclist." 13(1), 34–42.
- Vitković, N., Veselinović, M., Mišić, D., Manić, M., Trajanović, M., Mitković, M. (2012). "Geometrical Models of Human Bones and Implants, and their usage in Application for Preoperative Planning in Orthopaedics." *Journal of production Engineering*, 15(2), 87-90.

- Webb, Joshua. D., Silvia, S. Blemker. and Scott L. Delp. (2014). “3D Finite Element Models of Shoulder Muscles for Computing Lines of Actions and Moment Arms.” *Comput Methods Biomech Biomed Engin.*, 17(8), 829–837.
- William, Porter., Sean, Gallagher., Janet, Torma-Krajewski. (2010). “Analysis of applied forces and electromyography of back and shoulders muscles when performing a simulated hand scaling task.” *Applied Ergonomics*, 41, 411–416.
- Yesim, Akyol., Yasemin, Ulus., Dilek, Durmuş., Berna, Tander., Ferhan, Cantürk., Ayhan, Bilgici., Omer, Kuru., Yüksel, Bek. (2013). “Shoulder Muscle Strength in Patients with Sub acromial Impingement Syndrome: Its Relationship with Duration of Quality of Life and Emotional Status.” *Turk J Phys Med Rehab* , 59, 176-81.
- Yili, Fu., Fuxiang zhang.,Xin, Ma., Qinggang, Meng. (2005). "Development of CPM Machine for an injured finger." *IEEE Engineering and Medicine Journal*, 03, 8741-8744.
- Yoon, J.S. and Choi, H. (2014). “Development of continuous passive motion (CPM) devices using air pressure system.” *Physical therapy / Annals of Physical and Rehabilitation Medicine*, 57, 321–327.
- Yoshinari, Sakaki., Fuminari, Kaneko., Kota, Watanabe., Takuma, Kobayashi., Masaki, Katayose., Nobuhiro, Aoki., Eriko, Shibata., Toshihiko Yamashita. (2103). “Effects of different movement directions on electromyography recorded from the shoulder muscles while passing the target positions.” *Journal of Electromyography and Kinesiology*, 23(6), 1362-1369.
- Yunfeng, Niu. and Fuzhong, Wang. (2012). “A finite element analysis of the human knee joint: menisci prosthesis instead of the menisci and articular cartilage.” *International Conference on Biomedical Engineering and Biotechnology*, 5-8.
- Zach, L., Kuncicka, A., Machackova, A., Ruzicka, P., Pohludka, M., Jurica, J. (2015) “Finite element analysis of Ti-base Knee joint implant.”*Metalurgija*, 54(4), 691-694.
- Zwaan, Esther., Jules, G. Becher., Jaap, Harlaar. (2012). “Synergy of EMG patterns in gait as an objective measure of muscle selectivity in children with spastic cerebral palsy.” 35(1), 111–115.

APPENDICES

Appendix I

Specification of ATOS III 3D Scanner used for scanning the shoulder and knee bones.

System Configuration	Specifications
Camera	2 Mega pixels
Working Distance (mm)	490 – 2000
Point Spacing (mm)	0.01 - 0.61
Working Distance (mm)	490 – 2000
Measured points per scan	8 million points
Operating Temperature	5° to 40°C, non-condensing.
Triple Scan Capability	Yes
Sensor Controller	Integrated
Power Supply	90-230 V AC

Procedure followed during scanning of the bones:

1. The bones to be scanned were arranged under the scanning area/ location.
2. Bones were cleaned to avoid any dust, grease and oil presence during scanning.
3. Encoded markers were stuck on the component.
4. Bones were sprayed with very fine layer of developer spray; in order to make it dull faced.
5. Markers were used for cleaning the white color patches.
6. Scanner machine was assembled and calibrated for the required bone size with pixel adjustment.
7. Machine was switched ON for scanning of the bones. It was orientated in such a way that it should capture the entire bone configuration from all the sides.
8. After scanning was completed, then raw scanned data is processed to get a meshed ‘.stl’ data for further CAD modeling process.

Appendix II

Cost sheet for the shoulder CPM machine fabrication.

Major Mechanical fabrication parts	Amount in Rs.
1. Foldable chair (Fabricated in NKOCET college workshop and Irshad M/S Sholapur.)	6500/-
2. Arm linkages and covering box.	5500/-
3. Paint.	2000/-
4. Cushions.	1700/-
Major Electronics circuit parts	Amount in Rs.
5. Hybrid NEMA make high torque motors 0 To 6 rpm, 40 W, Special purpose Motor. (2 Nos.) with gear box (M1&M2).	31000/-
6. Tstep-087 Stepper Drive for NEMA motor.	6000/-
7. PLC: Delta Make DVP28SV11R , 8 Digital I/P & 6 Digital O/P, 24 volts.	16000/-
8. HMI DOP-B05S111 Delta 5.6 inch HMI touch screen panel with Programming Cable and software.	16000/-
9. Motor Drives.	1200/-
10. Electrical Cables and wires.	400/-
11. Power Supply: 24v D.C. / 48volt D.C.	800/-
12. Miscellaneous.	1100/-
Total Cost	Rs. 99000/-

Appendix III

SHOULDER PAIN AND DISABILITY INDEX (SPADI)

Patient Name _____ Date _____

Please read carefully:

Instructions: Please circle the number that best describes the question being asked.

Pain scale:

No pain at all 0 1 2 3 4 5 6 7 8 9 10 Worst pain Imaginable

How severe is your pain?

1. At its worst?
0 1 2 3 4 5 6 7 8 9 10
2. When lying on the involved side?
0 1 2 3 4 5 6 7 8 9 10
3. Reaching for something on a high shelf?
0 1 2 3 4 5 6 7 8 9 10
4. Touching the back of your neck?
0 1 2 3 4 5 6 7 8 9 10
5. Pushing with the involved arm?
0 1 2 3 4 5 6 7 8 9 10

Disability scale:

No difficulty 0 1 2 3 4 5 6 7 8 9 10 so difficult it requires help

How much difficulty do you have?

1. Washing your hair?
0 1 2 3 4 5 6 7 8 9 10
2. Washing your back?
0 1 2 3 4 5 6 7 8 9 10
3. Putting on an undershirt or pullover sweater?
0 1 2 3 4 5 6 7 8 9 10
4. Putting on a shirt that buttons down the front?
0 1 2 3 4 5 6 7 8 9 10
5. Putting on your pants?
0 1 2 3 4 5 6 7 8 9 10
6. Placing an object on a high shelf?
0 1 2 3 4 5 6 7 8 9 10
7. Carrying a heavy object of 10 pounds?
0 1 2 3 4 5 6 7 8 9 10
8. Removing something from your back pocket?
0 1 2 3 4 5 6 7 8 9 10

OTHER COMMENTS:

Examiner: Dr. V.S.Metan

Williams JW Jr., Holleman DR Jr., Simel DL: Measuring shoulder function with the Shoulder Pain and Disability Index. *J Rheumatol* 1995; 22 (4); 727-732

Appendix IV

Cost sheet for the knee CPM machine fabrication.

Major Mechanical and Electronics parts

Major components	Amount in Rs
1. A.C. Synchronous motor 60 RPM @ 50 Hz; 30W.	2800/-
2. Limit Switches (Mechanical).	360/-
3. Transformer Step down 230V to 12 V.	360/-
4. OMRON 4123 Relay 12V dc.	900/-
5. Paint for the machine.	500/-
6. Mechanical structure of the knee rest.	750/-
7. Cover plates of the machine and the knee rest.	450/-
8. SKF Deep Groove Ball Bearing 6005 25mm I.D, 47mm O.D.	540/-
9. Cushion for knee rest.	450/-
10. Lead screw and Nut assembly (Square thread and special purpose).	1200/-
11. IC, Filters, Pots, Connectors, switches.	1190/-
12. Miscellaneous.	500/-
Total Cost	10000/- Rs

Appendix V

KNEE PAIN AND DISABILITY INDEX (KPADI)

Patient Name _____ Date _____

Please read carefully:

Instructions: Please circle the number that best describes the question being asked.

Pain scale:

No pain at all 0 1 2 3 4 5 6 7 8 9 10
Worst pain Imaginable

How severe is your pain?

1. At its worst?
0 1 2 3 4 5 6 7 8 9 10
2. When lying on the affected side?
0 1 2 3 4 5 6 7 8 9 10
3. While Squatting?
0 1 2 3 4 5 6 7 8 9 10
4. While cross legging?
0 1 2 3 4 5 6 7 8 9 10
5. Getting up from chair?
0 1 2 3 4 5 6 7 8 9 10

Disability scale:

No difficulty 0 1 2 3 4 5 6 7 8 9 10
So difficult it requires help

How much difficulty do you have?

1. Standing on affected side?
0 1 2 3 4 5 6 7 8 9 10
2. During walking?
0 1 2 3 4 5 6 7 8 9 10
3. Climbing staircase?
0 1 2 3 4 5 6 7 8 9 10
4. Playing sports activity?
0 1 2 3 4 5 6 7 8 9 10
5. Putting on your pants?
0 1 2 3 4 5 6 7 8 9 10
6. Getting up from sitting position?
0 1 2 3 4 5 6 7 8 9 10
7. During morning walk?
0 1 2 3 4 5 6 7 8 9 10
8. While getting up early from your bed?
0 1 2 3 4 5 6 7 8 9 10

OTHER COMMENTS:

Examiner: (Dr.Vyanktesh Metan)

Williams JW Jr., Holleman DR Jr., Simel DL: Measuring Human joint function with the Pain and Disability Index. *J Rheumatol* 1995; 22 (4); 727-732.

Appendix VI

Dr. METAN HOSPITAL Orthopedic & Neurology Centre



Dr. Vyankatesh S. Metan
M.S. Orthopedics

Hospital Reg. No. : 113-A 24/1/2007

MMC Reg. No. 60784

Plot No 19, Jodbhavi Pet, Near Kanna Chowk, Solapur, 413002 Maharashtra State – INDIA

Phone: Hospital + 91 217 2742150; + 91 217 2631624;

E mail : metanv@yahoo.com

Website: www.drmetanhospital.org

SHOULDER CPM REPORT

Date: 1 /1 /14

OPD: 3886/14

Name : Shivkumar Patil
Age : 50
Gender : M
Address : Prabhakar nagar, Samrat Chowk, Solapur
Chief complaints : Pain in right shoulder (6 Days)
History : X-Ray (Right shoulder)

Exercise	Range of Motion in Degrees													
	01	02	03	04	05	06	07	08	09	10	11	12	13	14
Internal Rotation	45	45	50	55	60	60	65	65	70	70	75	75	80	80
External Rotation	40	40	45	45	45	50	50	55	55	60	65	65	70	75
Abduction	70	70	75	75	75	80	80	85	85	90	90	95	95	130
Adduction	60	65	65	70	70	75	75	80	80	85	85	90	95	120
Flexion	75	75	80	80	85	90	95	95	100	100	105	105	110	135
Elevation	75	75	80	80	85	85	90	95	100	100	105	110	115	135
Pain Scale	8	8	7.5	7.5	7	7	7	6.5	6.5	6	5.5	5.5	5	3.5

Dr. Vyankatesh Metan

Appendix VII

Dr. Manisha Talpallikar (PT)

*Talpallikar Physiotherapy
Sonya Maruti Mandir, Solapur
Phone Number: 0217-2328855*

B56 **Vijayalaxami L**

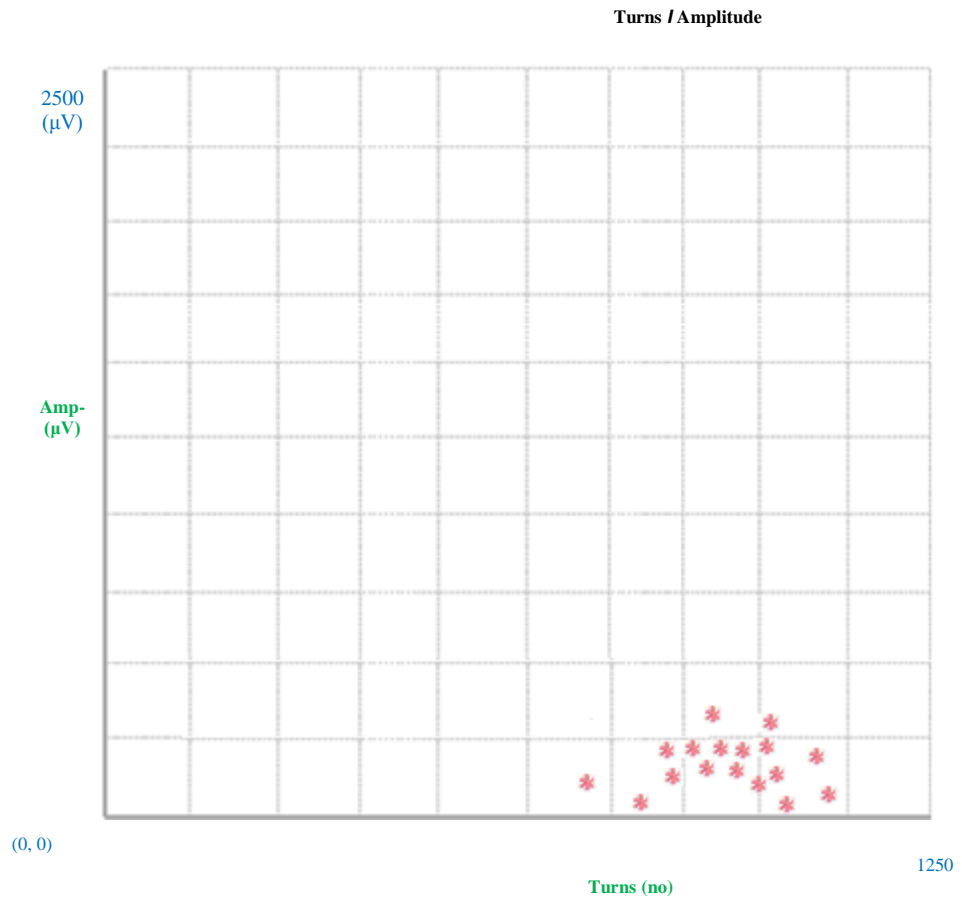
T&A

Thursday, May 28, 2015

6:16:32 PM



Muscle : Deltoid



Note: Amplitude (µV) per turn

Scale: One square box

X-Axis = 125 Turns

Y-Axis = 250 (µV)

Appendix VII

Dr. Manisha Talpallikar (PT)

*Talpallikar Physiotherapy
Sonya Maruti Mandir, Solapur
Phone Number: 0217-2328855*

B56 Vijayalaxami L

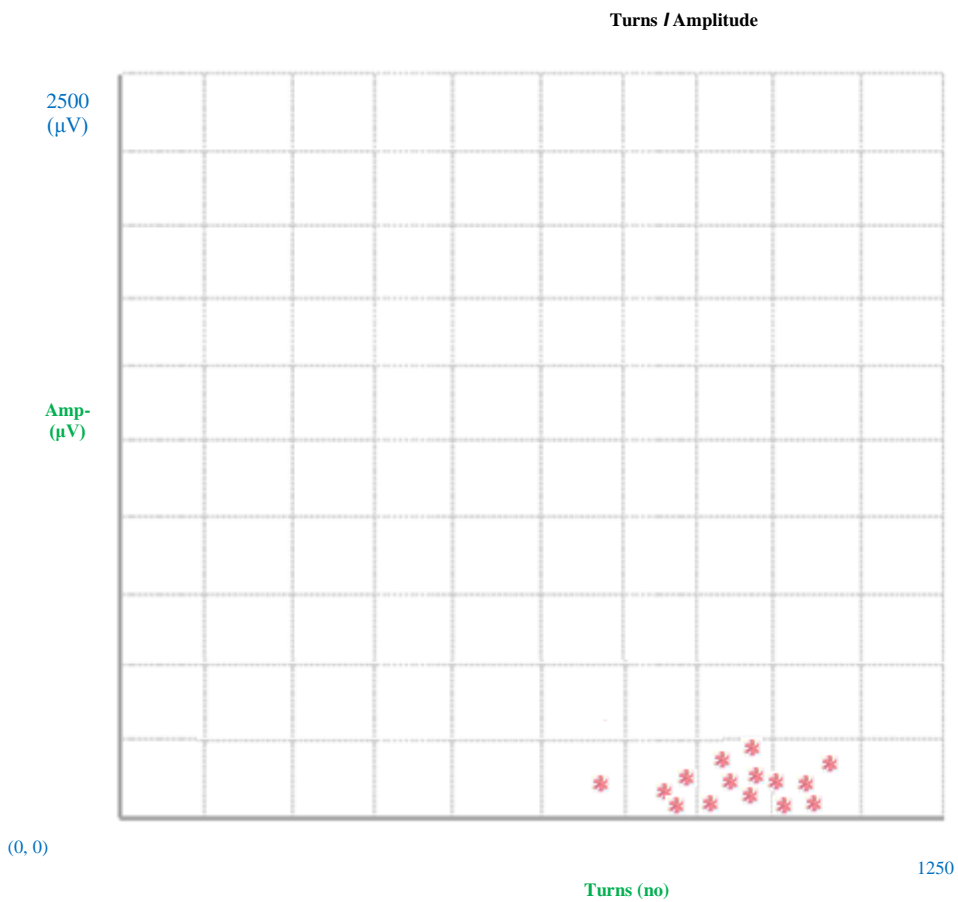
T&A

Thursday, May 28, 2015

6:16:48 PM



Muscle : Supraspinatus



Note: Amplitude (µV) per turn

Scale: One square box

X-Axis = 125 Turns

Y-Axis = 250 (µV)

Appendix VII

Dr. Manisha Talpallikar (PT)

*Talpallikar Physiotherapy
Sonya Maruti Mandir, Solapur
Phone Number: 0217-2328855*

B56 Vijayalaxami L

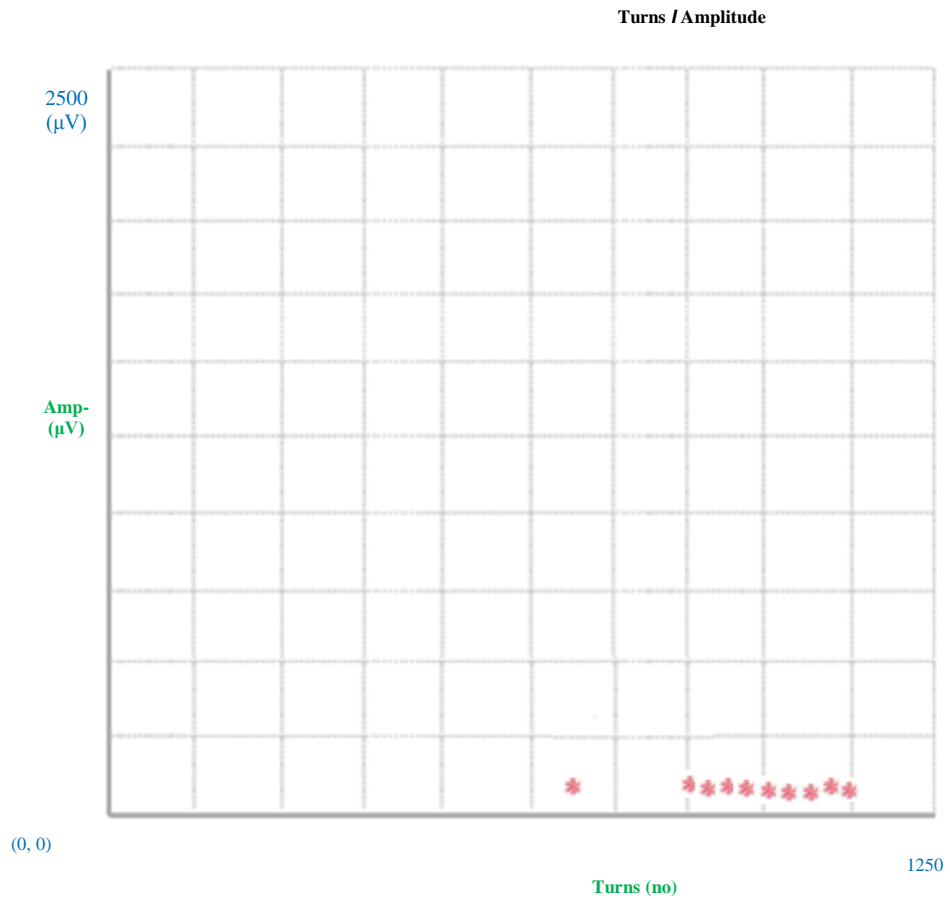
T&A

Thursday, May 28, 2015

6:17:18 PM



Muscle : Infraspinatus



Note: Amplitude (μV) per turn

Scale: One square box

X-Axis = 125 Turns

Y-Axis = 250 (μV)

Appendix VII

Dr. Manisha Talpallikar (PT)

*Talpallikar Physiotherapy
Sonya Maruti Mandir, Solapur
Phone Number: 0217-2328855*

B56 Vijayalaxami L

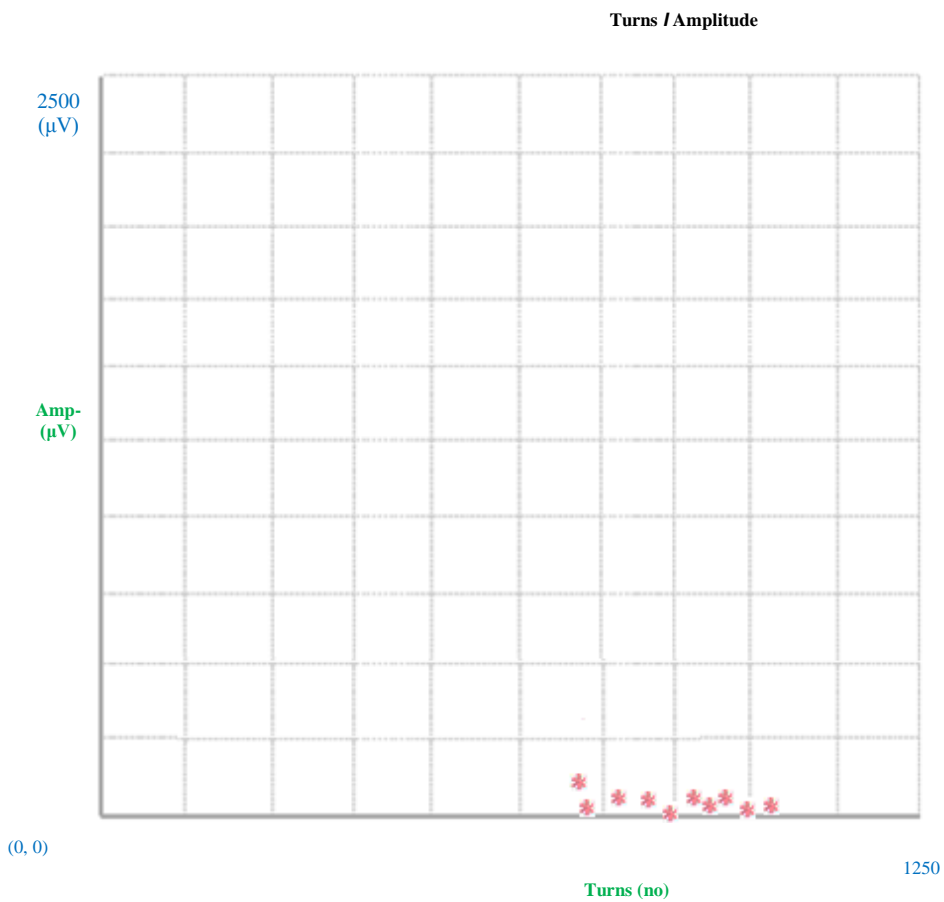
T&A

Thursday, May 28, 2015

6:16:56 PM



Muscle : Subscapularies



Note: Amplitude (µV) per turn

Scale: One square box

X-Axis = 125 Turns

Y-Axis = 250 (µV)

Appendix VII

Dr. Manisha Talpallikar (PT)

*Talpallikar Physiotherapy
Sonya Maruti Mandir, Solapur
Phone Number: 0217-2328855*

B56 Vijayalaxami L

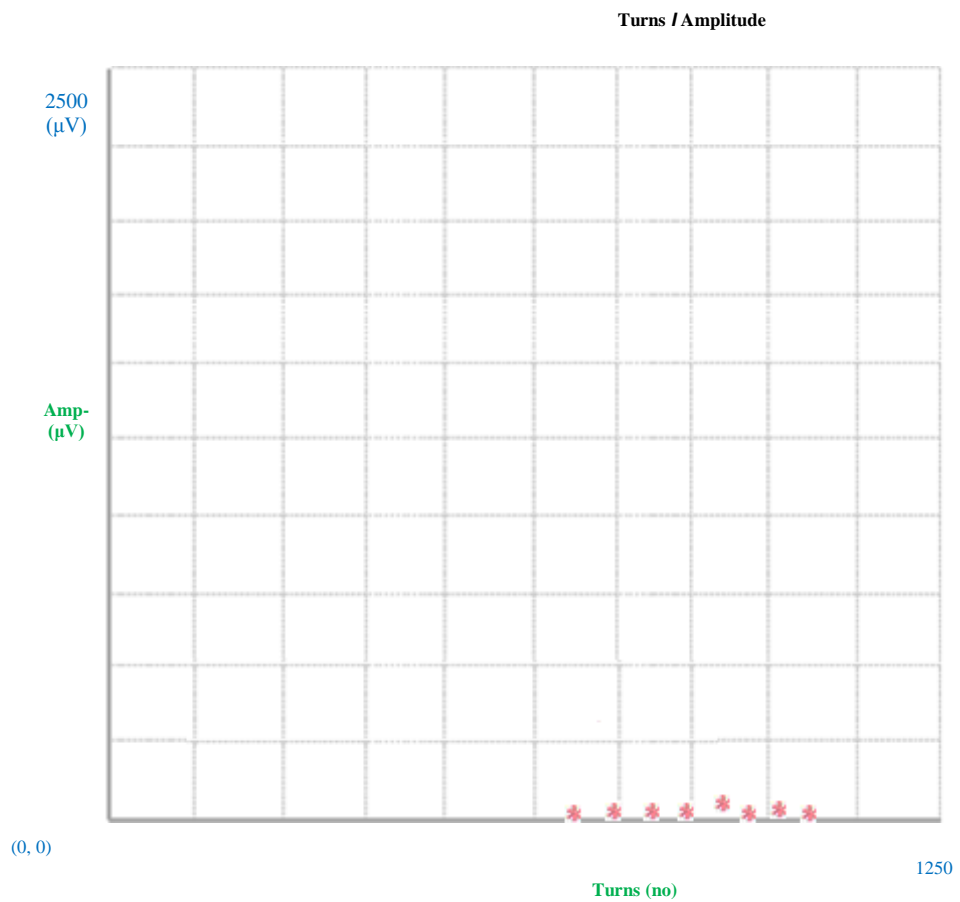
T&A

Thursday, May 28, 2015

6:17:06 PM



Muscle : Teres Minor



Note: Amplitude (µV) per turn

Scale: One square box

X-Axis = 125 Turns

Y-Axis = 250 (µV)

Appendix VIII

Matlab programing of the biomedical model to quantify the shoulder load.

Mainly two forces; deltoid force and supraspinatus force are acting on the shoulder joint during elevation arm movement in the analysis.

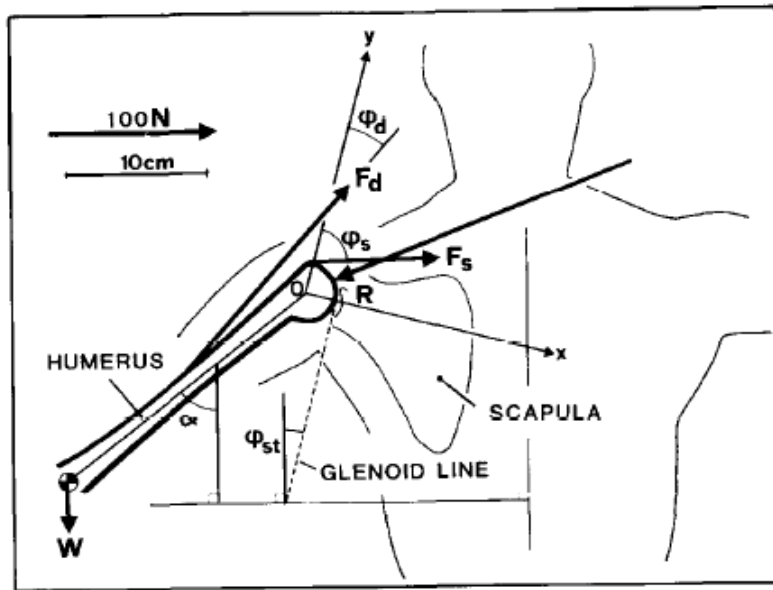


Fig. 8.1 Free body diagram of Glenohumeral joint

The mathematical model developed to analyze muscle behavior is given below.

F_d = deltoid force

F_s = supraspinatus force

R =resultant of F_d and F_s

α be the angle of elevation of arm

ϕ_{st} =angle between the trunk line and glenoid line of scapula

ϕ_d =angle made by F_d with Y-axis

ϕ_s =angle made by F_s with Y-axis

c = upper arm length. = 29 cm.

Where ϕ_{st} is given by the following equations:

$$\phi_{st} = 0 \quad (0^\circ \leq \alpha \leq 30^\circ)$$

$$\phi_{st} = 0.44\alpha - 12.4 \quad (0^\circ \leq \alpha \leq 150^\circ) \quad [1]$$

where a_d and a_s are the lever arms of the deltoid supraspinatus muscles. It is given by

$$a_d = 0.00976\alpha + 1.71 \text{ cm} \quad [2]$$

$$a_s = 2.2 \text{ cm} \quad [3]$$

And ϕ_d and ϕ_s is given by

$$\phi_d = 0.37\alpha + 15.8^\circ \quad [4]$$

$$\phi_s = 75^\circ \quad [5]$$

Above equations are standard and are used in the calculations of the forces of muscles by the author.

After solving the above equations to the shoulder system, results in an algebraic equation for the load sharing between the deltoid and supraspinatus muscles. The expression is as follows:

$$F_d = \mu(F_s)^{(1+d)} \quad [6]$$

Where $d=0$

R_x and R_y is the x and y components of joint reaction force.

The kinematic analysis is done on human with $W = 588.6 \text{ N} = 60 \text{ kg}$.

Weight of arm = 5% of body weight = 29.43 N (Cram and Kasman, 2005)

$$\alpha = 87^\circ$$

$$\phi_{st} = 25.88^\circ$$

$$\phi_d = 47.99^\circ$$

$$\phi_s = 75^\circ$$

$$a_d = 0.025 \text{ m}$$

$$a_s = 0.022 \text{ m}$$

Following are equations on which calculations are done: (Cram and Kasman, 2005)

$$F_d \times a_d + F_s \times a_s - W \times 0.7 \times c \times \sin\alpha = 0; \quad [7]$$

$$F_d \times \sin\phi_d + F_s \sin\phi_s + W \sin\phi_{st} - R_x = 0; \quad [8]$$

$$F_d \cos\phi_d + F_s \cos\phi_s - W \cos\phi_{st} - R_y = 0; \quad [9]$$

By calculating the mathematically we got

$$F_d = 316.89 \text{ N}$$

$$F_s = 88.746 \text{ N}$$

$$R_x = 471.65 \text{ N}, R_y = 162.67 \text{ N}, R = 498.99 \text{ N}, \Theta = 19.02^\circ.$$

The maximum force is shared by the deltoid muscle and then the supraspinatus

muscle.

Matlab programming is done for various loads of shoulder. The input was load in kilograms. The output was F_d , F_s and R (the resultant) against the shoulder arm movement angle α was plotted.

1. α vs. F_d
2. α vs. F_s
3. α vs. Glenohumeral joint force (R)

The program was written in MATLAB Works is as follows:

```
clc
clear all
w = input('enter the value of load')
alfa = 0:1:120;
for i = 1:1:29
    phist(i) = 0;
end
for i = 30:1:121
    phist(i) = 0.44*alfa(i)-12.4;
end
phid = 0.37*alfa+15.8;
phis =75;
Ad = 0.00976*alfa+1.75;
As =2.2;
c = 29;
Fs = (w*0.7*c*sind(alfa))./(1.3*Ad+As);
Fd = 1.3*Fs;
Rx = Fd.*sind(phid)+Fs*sind(phis)+w*sind(phist);
Ry = Fd.*cosd(phid)+Fs*cosd(phis)-w*cosd(phist);
R = sqrt(Rx.^2+Ry.^2);
plot(alfa,Fs);
hold on
plot(alfa,Fd);
plot(alfa, R).
```

Appendix IX

Dr. METAN HOSPITAL Orthopedic & Neurology Centre



Dr. Vyankatesh S. Metan
M.S. Orthopedics

Hospital Reg. No. : 113-A 24/1/2007

MMC Reg. No. 60784

Plot No 19, Jodbhavi Pet, Near Kanna Chowk, Solapur, 413002 Maharashtra State – INDIA

Phone: Hospital + 91 217 2742150; + 91 217 2631624;

E mail : metanv@yahoo.com

Website: www.drmetanhospital.org

KNEE CPM REPORT

OPD NO : 3994/13
DATE : 28/01/2014 12:30 pm
CASE : Pain in left knee. Night cry, restricted movement, minor injury 2 months old.
HISTORY : X- ray of left knee, overweight, trauma.

Exercise	Range of Motion in Degrees													
	01	02	03	04	05	06	07	08	09	10	11	12	13	14
Flexion	45	50	55	60	65	65	70	70	75	80	85	85	95	95
Extension	40	50	55	55	60	65	70	75	75	80	90	90	95	100
Pain Scale	8.5	8.5	8	8	7.5	7.5	6	6	5.5	5	4.5	4	3.5	3.5

Dr. Vyankatesh Metan

Appendix X

Dr. Manisha Talpallikar (PT)

Talpallikar Physiotherapy
Sonya Maruti Mandir, Solapur
Phone Number: 0217-2328855

F 35 **Rahul Panchal**

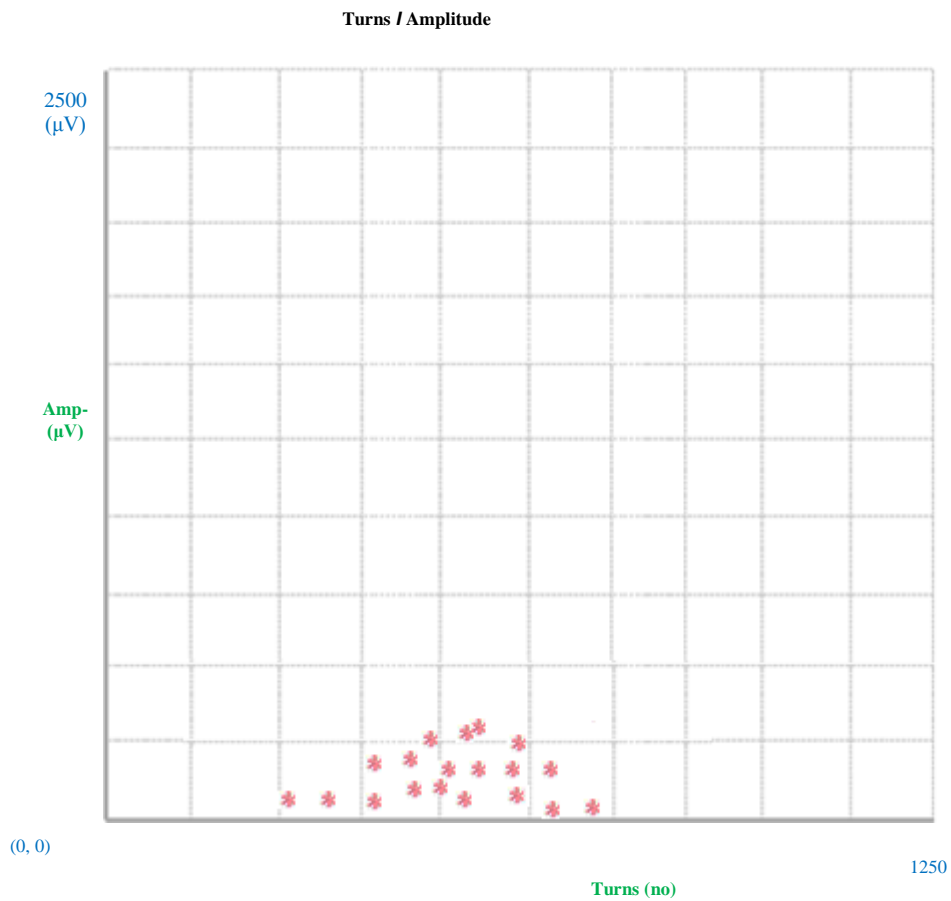
T&A

Tuesday, August 18, 2015

5:46:18 PM



Muscle : Rectus Femoris



Note: Amplitude (μV) per turn

Scale: One square box

X-Axis = 125 Turns

Y-Axis = 250 (μV)

Appendix X

Dr. Manisha Talpallikar (PT)

Talpallikar Physiotherapy
Sonya Maruti Mandir, Solapur
Phone Number: 0217-2328855

F 35 **Rahul Panchal**

T&A

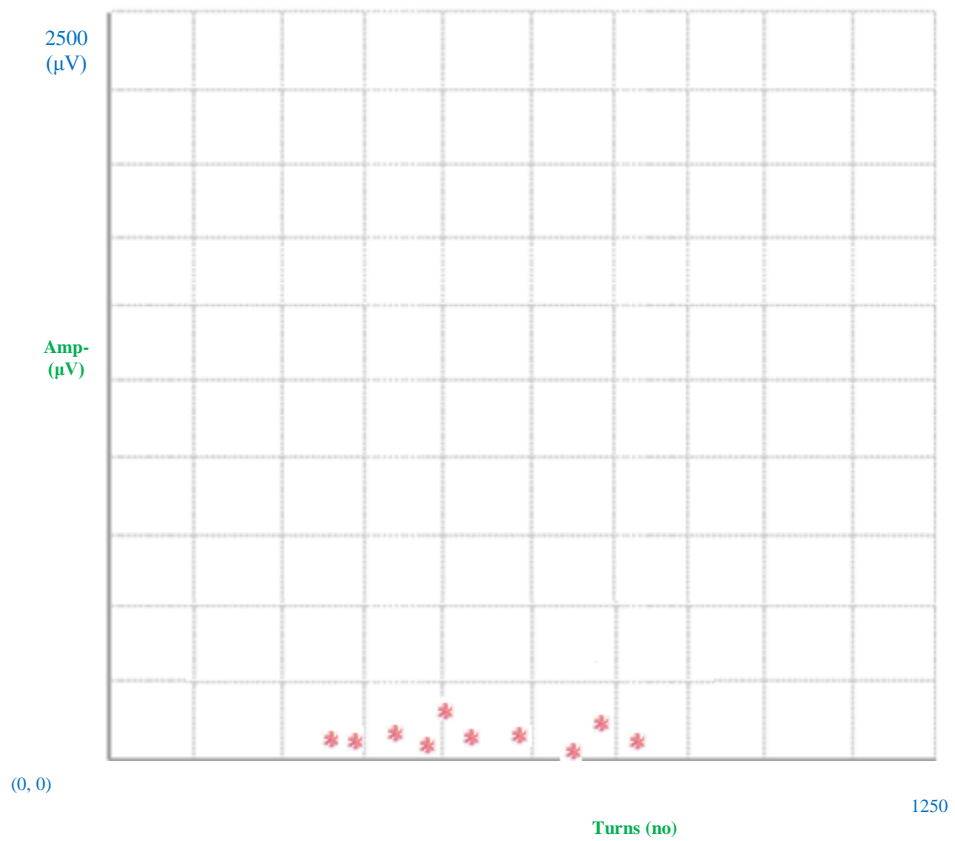
Tuesday, August 18, 2015

5:46:28 PM



Muscle : Biceps Femoris

Turns / Amplitude



Note: Amplitude (µV) per turn

Scale: One square box

X-Axis = 125 Turns

Y-Axis = 250 (µV)

Appendix XI

Dr. METAN HOSPITAL Orthopedic & Neurology Centre



Dr. Vyankatesh S. Metan
M.S. Orthopedics

Hospital Reg. No. : 113-A 24/1/2007

MMC Reg. No. 60784

Plot No 19, Jodbhavi Pet, Near Kanna Chowk, Solapur, 413002 Maharashtra State – INDIA

Phone: Hospital + 91 217 2742150; + 91 217 2631624;

E mail : metanv@yahoo.com

Website: www.drmetanhospital.org

CERTIFICATE

To whome so ever concern, it is to certify that the CPM machine developed by Prof. Shrinivas S Metan for shoulder exercise is working satisfactorily. The machine has been tested first on 50 normal subjects for different shoulder exercises (abduction, adduction, flexion, extension, internal rotation, external rotation) , then it is put on the 50 injured shoulders under the observation in Dr. Metan Hospital Orthopedic & Neurology Centre, Solapur, India. The machine was then used for the post-operative patients to improve their range of motion. The machine is successfully performing all the shoulder post-operative operations continuously , smoothly and without any jerks. The range of motion is calibrated and the functionality of the machine is foolproof and as per the orthopedic requirements. All the shoulder joint exercise are performed satisfactorily by using the CPM machine.

Dr. Vyankatesh Metan

Appendix XII

Dr. METAN HOSPITAL

Orthopedic & Neurology Centre



Dr. Vyankatesh S. Metan
M.S. Orthopedics

Hospital Reg. No. : 113-A 24/1/2007

MMC Reg. No. 60784

Plot No 19, Jodbhavi Pet, Near Kanna Chowk, Solapur, 413002 Maharashtra State – INDIA

Phone: Hospital + 91 217 2742150; + 91 217 2631624;

E mail : metanv@yahoo.com

Website: www.drmetanhospital.org

CERTIFICATE

To whome so ever concern, it is to certify that the CPM machine developed by Prof. Shrinivas S Metan for knee exercise is working satisfactorily. The machine has been tested first on 50 normal subjects for different knee exercises (flexion and elevation) , then it is put on the 50 injured knee under the observation in Dr. Metan Hospital Orthopedic & Neurology Centre, India. The machine was then used for the post-operative patients to improve their range of motion. The machine is successfully performing all the knee post-operative operations continuously , smoothly and without any jerks. The range of motion is calibrated and the functionality of the machine is foolproof and as per the orthopedic requirements. All the knee joint exercise are performed satisfactorily by using the CPM machine.

Dr. Vyankatesh Metan

PUBLICATIONS

1. Metan, S.S., Prasad, Krishna., Mohankumar, G.C. (2012). "Low Cost CPM for knee joint." *Applied Mechanics and Materials*, 215 (216), 125-132.
2. Metan, S.S., Prasad, Krishna., Mohankumar, G.C. (2014). "FEM model an effective tool to evaluate Von Mises stresses in shoulder joint and muscles for adduction and abduction." *Procedia Material Science Elsevier*, 5, 2019-2098.
3. Metan S.S., Mohankumar, G.C., Prasad, Krishna. (2014). "Shoulder put into effect by means of developed low cost CPM machine." *European Scientific Journal*, 10 (27), 242-254.
4. Metan, S.S., Mohankumar, G.C., Prasad, Krishna. (2016). "FEM an Effective Tool to Analyze the Knee Joint Muscles during Flexion." *American Journal of Biomedical Engineering*, 6(2), 43-52.
5. Metan, S.S., Mohankumar, G.C., Prasad, Krishna. (2016). "Sensitivity Analysis of Shoulder joint muscles by using FEM model." *Biomaterials and Biomedical Engineering*, Techno Press. (Communicated)

CURRICULUM VITAE

Name and Designation : **SHRINIWAS S METAN**
(Head of Department, Associate Professor)
Address for Communication : “Tirumala Niwas”, Plot No 58, Ramrajya Nagar,
Shelgi, Solapur, Maharashtra, India 413006.
Email: shrinims@gmail.com
Date of Birth : 25th April 1973
Organisation : NK Orchid Engineering and Technology, Solapur.
Academic Qualifications :

Degree	University	Division	Year	Specialisation
B.E. (Mech)	Shivaji University, Kolhapur	Distinction	1994	Mechanical Engineering
M.S.	Aachen University, Germany.	Distinction	2008	Mechatronics
Ph.D.	N.I.T.K. Surathkal	CGPA: 9.5	(Pursuing)	

Industrial Experience :

Sr.No.	Industry	Period of Service	Designation
1	Patheja Forging and Stamping Ltd, Pune.	May 1995 to Jan. 1997	Senior Production Engineer
2	R.M.Page Consultancy, Pune.	Jan 1997 to Feb. 1999	Mechanical Design Engineer
3	Hindustan Dorr Oliver Ltd, Mumbai.	March 1999 to Dec 1999	Piping Design Engineer

Academic Experience :

Sr.No.	Institution	Period of Service	Designation
1	Walchand Institute of Technology, Solapur.	Jan 2000 to Sept 2006	Senior Lecturer
2	NK Orchid Engineering and Technology, Solapur.	Dec 2008 to till date	H.O.D., Associate Professor.

I hereby declare that the above information is true to the best of my knowledge.

Date :

Place : NITK Surathkal, India

Mr. Shrinivas S Metan